

ABSTRACT

CALDERON, VICTOR ALEJANDRO. Condition Dependent Performance Based Seismic Design.
(Under the direction of Dr. Mervyn Kowalsky.)

Structures located in seismic regions are often subjected to multiple earthquakes. Multiple earthquakes can accumulate damage resulting in a deterioration of the seismic performance of a structure. In addition, aging of the structure can lead to corrosion that further propagates the deterioration. Past research has shown that the Park and Ang damage index (DI)(a demand parameter that quantifies damage) increases as damage aging conditions in the structures worsen or multiple seismic events are included in the analysis. The accumulation of damage increases the probability of structures collapsing. This research studied the effects of multiple earthquakes and damage accumulation in RC structures by developing strain-based fragility functions for different aging conditions. It was also vital to develop limit states representing corroded reinforcing steel to achieve this goal. Therefore, an experimental program was developed to perform accelerated corrosion in passivated reinforcing steel rebars. These corroded rebars were subjected to tension and buckled bar tension tests. The results from the experimental program showed the degradation in the performance of corroded reinforcing steel bars. The results also showed that the drop in the performance after mass loss corrosion level of 10% was very significant. In addition, A framework incorporating corrosion models developed from the experimental program into a nonlinear time history analysis (NLTHA) was developed. In this analytical program, a series of SDOF cantilever columns was subjected to a sweep of earthquakes. The results show an increase in the probability of reaching a limit state when the corrosion level increases. The results from the analytical program corroborated that a limiting corrosion level of 10% is ideal since the probability of reaching a strain limit state increased. Finally, this research proposed a new design and assessment methodology which will enable 1) to design structures that remain at a desired level of performance and 2) more accurately assess structures that have sustained a given level of corrosion. These methodologies are proposed for up to a maximum corrosion level of 10%.

© Copyright 2022 by Victor Alejandro Calderon

All Rights Reserved

Condition Dependent Performance Based Seismic Design

by
Victor Alejandro Calderon

A thesis submitted to the Graduate Faculty of
North Carolina State University
in partial fulfillment of the
requirements for the Degree of
Doctor of Philosophy

Civil, Construction, and Environmental Engineering

Raleigh, North Carolina

2022

APPROVED BY:

Dr. James Nau

Dr. Mohammad Pour-Ghaz

Dr. Rudolf Seracino

Dr. Thomas Birkland

Dr. Mervyn Kowalsky
Chair of Advisory Committee

DEDICATION

To God, “How much better it is to get wisdom than gold! And to get understanding is to be chosen above silver” (Prov 16:16).

To my parents Victor M. Calderon and Roxana P. de Calderon, for all their love and support throughout the years and across the miles.

To my wife Aubrey, “If it takes doing a Ph.D. for us to meet it will have been worth it.”

Thank you for your love, support, patience, and for filling my days with joy. I love and cherish every moment, every laugh and everything we do. Te Amo Aubrey.

To all my friends and family, thank you for your support in this adventure.

BIOGRAPHY

Victor A. Calderon was born in San Salvador, El Salvador. He obtained his Bachelor's in Civil Engineering at the Universidad Centroamericana José Simeón Cañas. Subsequently, he worked for the structural engineering consulting firm JEP Ingenieros y Arquitectos. He gained experience designing commercial buildings, schools, and residential buildings. While still part of JEP, he graduated with a Master's in Civil Engineering at NC State in 2016. That same year, he became part of a team that designed the facilities for a large dam project in El Salvador. In the spring of 2018, Victor decided to return to NC State for his Ph.D. program. In 2021, he became a registered Professional Engineer in North Carolina. He plans to continue his career as a structural engineer in the industry and serve his community.

ACKNOWLEDGEMENTS

I would like to thank Dr. Kowalsky for his help. The staff and students at the Constructed Facilities Lab (CFL), the Analytical Instrumentation Facility (AIF), the Sensing and Materials Research Team (SMART) Lab, and the Center for Additive Manufacturing and Logistics (CAMAL) at NC State. Special thanks to the Alaska Department of Transportation and Public Facilities (AKDOT P&F).

TABLE OF CONTENTS

LIST OF TABLES	viii
LIST OF FIGURES	ix
Chapter 1 Introduction	1
1.1 Scope and layout	3
Chapter 2 Literature Review	4
2.1 Corrosion	4
2.1.1 Time to corrosion	5
2.1.2 Rate of corrosion	6
2.1.3 corrosion modified properties of reinforcing steel bars	7
2.1.4 Physical test on corroded RC Structures	8
2.2 Steel strain aging	10
2.2.1 Metallurgical process	11
2.2.2 Strain aging effects in structures	11
2.3 Damage Indexes	13
2.4 Multiple earthquake loading	15
2.4.1 Mainshock-aftershock sequences loading	15
2.4.2 Mainshock sequences loading	18
2.5 Aging of structures	20
2.6 Research Gap	22
2.6.1 Objectives	22
Chapter 3 Experimental Program	24
3.1 Specimen Preparation	24
3.1.1 Preparation of Rebar Ends	25
3.1.2 Passivation of Rebar Specimens	26
3.1.3 Accelerated Corrosion of Rebars	27
3.2 Tension Tests	29
3.2.1 Tension Test Procedure	30
3.2.2 Testing Parameters	30
3.2.3 Test Matrix	31
3.3 Buckled Bar Tension (BBT) Tests	32
3.3.1 Test Procedure	32
3.3.2 Testing Parameters	35
3.3.3 Test Matrix	35
3.4 3D Scanning	35
3.5 SEM observations	37
3.5.1 SEM imaging	38
3.5.2 EDS Spectrum Analysis	38
3.6 Turned Down Corroded Rebars Tests	39
3.6.1 Test Matrix	39

3.6.2	Testing Parameters	40
Chapter 4 Experimental Results from Corroded Rebar Specimens	41
4.1	Measurement of Corrosion Level	42
4.1.1	Mass loss method	42
4.1.2	3D Scanning Method	42
4.1.3	Comparison of Corrosion Level (CL) Measurements Mass Loss vs 3D Scanning Methods	45
4.2	Tension Tests	46
4.2.1	Effective Yield Strength as a Function of the Corrosion Level	46
4.2.2	Ultimate Strength as a Function of the Corrosion Level	49
4.2.3	Effect of Corrosion on Uniform Elongation	49
4.3	Buckled Bar Tension (BBT) Tests	50
4.3.1	Summary of BBT Procedure	50
4.3.2	Effect of Corrosion on Critical Bending Strain	52
4.3.3	Effect of Corrosion at the Micro-structural Level	54
4.4	Tests on Turned Down Corroded Rebars	57
4.5	Discussion of Results	59
Chapter 5 Analytical Program	61
5.1	Modeling of Corrosion for Structural Analysis	61
5.2	Multiple Seismic Events	62
5.2.1	Earthquake Selection	63
5.2.2	Modeling of Mainshock-Aftershock Series for Corrosion	63
5.3	Analytical Model	65
5.3.1	SDOF System: Cantilever Column	65
5.3.2	Strain Penetration	67
5.3.3	Design Limit States	68
5.4	Comparison with Existing Physical Tests	69
5.4.1	Pristine Condition Column	70
5.4.2	Accelerated Corrosion Column	71
5.5	Intensity Measure: $Sd(T_{eff}, \xi)$	73
5.5.1	Effective Period Calculation	73
5.5.2	Calculate $Sd(T_{eff}, \xi)$	74
5.6	Analysis of Results Using MSA	75
5.7	Analytical framework	76
5.7.1	Analysis Algorithm	78
5.8	Results from Analytical Program	79
5.8.1	Structural Response at Different Corrosion Levels	79
5.8.2	Effect of Ground Motion Sequences	86
5.8.3	Effect of Corrosion Level on Strain Demands	86
5.8.4	Discussion of results	89
Chapter 6 Condition Dependent Performance Based Design and Assessment	93
6.1	Design of new structures for condition dependent PBD	93

6.1.1	Acceptable level of corrosion for new designs	94
6.1.2	Life Service Design Existing methodologies	94
6.1.3	Direct Displacement Based Design (DDBD) Methodology	97
6.1.4	Proposed Condition Dependent DDBD Methodology	99
6.1.5	Condition Dependent DDBD application example: SDOF Bridge Pier RC Column	100
6.2	Assessment of existing structures considering aging conditions	106
6.2.1	Recommendations from the experimental and analytical programs	106
6.2.2	Existing methodologies	106
6.2.3	Direct Displacement Based Assessment (DDBA) Methodology	108
6.2.4	Proposed Condition Dependent Performance Based Seismic Assessment .	111
6.2.5	Condition Dependent DDBA application Example: SDOF Bridge Pier RC Column	112
6.3	Discussion of results	116
6.4	Future Work	117
Chapter 7 Conclusions and recommendations	118
7.1	Conclusions	118
7.1.1	Experimental Program	118
7.1.2	Analytical Program	119
7.1.3	Condition Dependent Performance-Based Design and Assessment	122
7.2	Recommendations	122
BIBLIOGRAPHY	123
APPENDICES	129
Appendix A	Standard Operation Procedure for Accelerated Corrosion	130
Appendix B	Code for NLTHA	152
Appendix C	Records of Mainshocks used for NLTHA	177

LIST OF TABLES

Table 2.1	Damage index level classification [75]	14
Table 3.1	Accelerated corrosion times for the total length in parent specimen of a 19 mm (0.75 in) rebar	29
Table 3.2	Tension test matrix	31
Table 3.3	BBT test matrix	36
Table 3.4	Test matrix for turned down specimens	39
Table 4.1	Corroded Level measured from mass loss in gauge length	42
Table 4.2	Corrosion levels (CL) measured from 3D scans in gauge length	44
Table 5.1	Design limit states	69
Table 5.2	Analysis matrix	78
Table 5.3	Detailing of columns for NLTHA	78
Table 6.1	Detailing of structure for design	103
Table 6.2	Detailing of structure for design	114

LIST OF FIGURES

Figure 2.1	Corrosion process in reinforcing steel bar [42]	5
Figure 2.2	Concrete water to cement ratio vs rate of corrosion	6
Figure 2.3	Diameter decrease due to corrosion	7
Figure 2.4	Corrosion level vs time (years)	8
Figure 2.5	Force displacement response of RC corroded columns [41]	9
Figure 2.6	Corrosion process for RC column [41]	9
Figure 2.7	Corroded rebars stress-strain curves [41]	10
Figure 2.8	Strain aging effect on yield strength vs time (days)	12
Figure 2.9	Park and Ang conceptual scheme	13
Figure 2.10	Mainshock-aftershock sequence train of ground motions [56]	17
Figure 2.11	Mainshock-aftershock sequence selection at T=0.4s for crustal earthquakes in Vancouver, British Columbia [67]	18
Figure 2.12	Mainshock-aftershock sequence results for story displacement [60]	19
Figure 2.13	Mainshock sequence selection at Eureka, CA [66]	19
Figure 3.1	Rebar Specimen Geometry	25
Figure 3.2	Rebars Ends Protection	25
Figure 3.3	Large specimen containing three subset of specimens	26
Figure 3.4	As received rebars anodic polarization immersed in pore solution for different times[21]	27
Figure 3.5	Assembly for rebar preparation for the development of passive layer in pore solution	28
Figure 3.6	Accelerated corrosion process	28
Figure 3.7	Tension test setup	30
Figure 3.8	BBT test sequence[7]	32
Figure 3.9	a) Picture of buckled bar; (b) Position of optical markers and adjustment to neutral axis; (c) Calculation of curvature [6]	34
Figure 3.10	(a)Ductile rebar fracture; (b) Brittle rebar fracture	34
Figure 3.11	BBT results for pristine rebars [6]	35
Figure 3.12	3D scan probe	37
Figure 3.13	VPSEM used in observations at AIF	38
Figure 3.14	Turned down sample from CL=20% corroded rebar	39
Figure 4.1	Sample of 3D scans obtained for CL=15% and CL=20%	43
Figure 4.2	Corrosion level (CL) measured using mass loss method vs 3D scans	45
Figure 4.3	Tension test setup and fracture observations	46
Figure 4.4	Tension test results at different corrosion levels	47
Figure 4.5	Yield strength as a function of corrosion level	48
Figure 4.6	Comparison of proposed model and Du et al. model [14] for effective yield strength as a function of corrosion level	48
Figure 4.7	Ultimate strength as a function of corrosion level	49
Figure 4.8	Comparison of proposed model and Du et al. model [14] for uniform axial elongation (ε_u) as a function of the corrosion level (CL)	50

Figure 4.9	General procedure of buckled bar tension (BBT) test	51
Figure 4.10	Type of failures in BBT tests	52
Figure 4.11	Obtaining critical bending strain	53
Figure 4.12	Bending strain at different corrosion levels	53
Figure 4.13	Maximum bending strain as a function of corrosion level	54
Figure 4.14	Basic features analysis of fracture surfaces in metals	55
Figure 4.15	SEM observations for brittle and ductile failure at different positions of the fracture surface	56
Figure 4.16	SEM cyclic loading features on fracture surface at 500x magnification . .	57
Figure 4.17	Spectrum analysis of back scatter electrons (BSE) imaging of fracture surface for brittle and ductile failures	58
Figure 4.18	Tension tests on turned down specimens	59
Figure 4.19	BBT tests on turned down specimens	60
Figure 5.1	Mainshock selection from PEER NGA West2 database	64
Figure 5.2	Mainshock selection from PEER NGA West2 database	64
Figure 5.3	Mainshock selection from PEER NGA West2 database	65
Figure 5.4	Structural Model: a) SDOF Column b) Fiber Model Representation . .	66
Figure 5.5	End point plastic hinge method [61]	67
Figure 5.6	Section of the RC Column	67
Figure 5.7	Force-Displacement results from experimental results [26] and analytical model	70
Figure 5.8	Strain hysteresis from experimental RC column in pristine condition . .	71
Figure 5.9	Force-Displacement results from experimental RC column with corrosion in longitudinal bar (CL=9.5%) [35] and analytical model results (shown in light blue)	72
Figure 5.10	Strain hysteresis from experimental RC column with corrosion in longitudinal bar (CL=9.5%) results from analytical model	73
Figure 5.11	Calculation of effective stiffness (k_{eff})	74
Figure 5.12	Calculation of spectral displacement at effective period at 5% damping $Sd(T_{eff}, 5\%)$ and at equivalent damping $Sd(T_{eff}, \xi)$	75
Figure 5.13	MSA analysis	77
Figure 5.14	Main Flow-Chart	80
Figure 5.15	NLTHA Flow-Chart	81
Figure 5.16	Post-processor Flow-Chart	82
Figure 5.17	Post-processor Flow-Chart continued	83
Figure 5.18	Force-Displacement results	84
Figure 5.19	Stress strain response for extreme rebar location	85
Figure 5.20	Strain hysteresis	85
Figure 5.21	Non Linear Time History Analysis (NLTHA) results showing no increase in the strain demands due to as recorded sequence of mainshock and aftershock	86
Figure 5.22	Non Linear Time History Analysis (NLTHA) results for Strain demands vs Spectral Displacement at Effective Period (T_{eff}), and Equivalent Damping (ξ)	87

Figure 5.23 Cumulative Distribution Function (CDF) for steel strain limit states and different Axial Load Ratios (ALR)	88
Figure 5.24 Analysis of mean values ($P = 0.5$) for the performance limit states	90
Figure 5.25 Analysis of the 84 th percentile ($P = 0.84$) for the performance limit states	91
Figure 6.1 Philosophy of Condition Dependent Performance Based Design	94
Figure 6.2 Life 365 corrosion level for 100 years of life service in different environments	95
Figure 6.3 Example of identification of exposure zones according to SHRP-R19A [62].	96
Figure 6.4 Reliability for structure with fly ash for 100 years of service life using the FIB-34 full probabilistic method [62].	97
Figure 6.5 Direct Displacement Based Design (DDBD) methodology [55].	98
Figure 6.6 Proposed Condition Dependent DDBD Methodology flowchart	101
Figure 6.7 Column Elevation	102
Figure 6.8 Column cross-section	102
Figure 6.9 Calculating corrosion level at 100 years of service life	103
Figure 6.10 Force displacement response for structure considering CL=5%	104
Figure 6.11 Spectral displacement for $\xi = 5\%$, and at the equivalent damping $\xi_{eq} = 15\%$	105
Figure 6.12 SLaMA %NBS calculation for assessment [48].	108
Figure 6.13 SLaMA flowchart for the assessment of existing buildings [48].	109
Figure 6.14 Column Elevation	113
Figure 6.15 Column cross-section	113
Figure 6.16 Force-Displacement response for assessment of column	115
Figure 6.17 Spectral displacement Demands versus displacement capacity of coulumn	116
Figure 7.1 Bending strain at different corrosion levels	119
Figure 7.2 Tension tests on turned down specimens	120
Figure 7.3 BBT tests on turned down specimens	120
Figure 7.4 Analysis of mean values ($P = 0.5$) for performance limit states	121

Chapter 1

Introduction

Structures are designed assuming their original condition remains intact through their service life. However, as structures age, they suffer various forms of degradation. In addition, they may be subjected to multiple discrete seismic events. Both of these items may impact structural performance. For example, consider an RC column and the limit state corresponding to bar buckling. The limit state displacement (Δ) to achieve bar buckling for a pristine column is different from a column subjected to corrosion. Similarly, multiple small seismic events may predispose the column to suffer longitudinal bar buckling for a lower seismic intensity level. This research aimed to incorporate the effects of aging and multiple ground motions into the definition of performance limit states. This research can potentially serve two purposes: a) for existing structures, assessment can consider likely current conditions, and b) for new structures, changes could be proposed to the initial design that could mitigate the effect of future condition degradation.

Structures subjected to multiple events and aging conditions should be considered in Performance Based Earthquake Engineering (PBEE). Recent earthquake sequences such as the Christchurch 2010, Umbria-Marche Earthquake 1997, and more recently the Puerto Rico Earthquakes 2020, have shown that structures after sustaining damage during a mainshock have then collapsed or sustained increased damage after being subjected to a large magnitude aftershock[1][9][43]. Researchers have used the Park and Ang damage index (DI) to quantify damage, expressed as a two-term expression. The first term relates to the maximum displacement, and the second term relates to the inelastic energy dissipation [75]. The second term is associated with the inelastic cyclic behavior of structural components. In addition, the calibration factor is minimal and contributes little to the damage index. If the damage index renders the inelastic cyclic behavior negligible, it cannot accurately represent damage. Further, this damage index uses calibrated data to determine the strength degradation parameter that has a degree of arbitrariness, which is undesirable [72]. In addition to the Park and Ang damage index, other

measures of damage such as drift ratio-based limit states have been incorporated into the PEER Performance-Based Design Probabilistic Framework[53][24][64]. The majority of these studies show an increase in the probability of damage or even collapse of a structure due to repeated loading or aging conditions, such as high corrosion levels (CL). However, these results are based on the limitations presented by these damage measures [64]. In this study, strain limits are used as damage indicators for RC bridge columns. Specifically, concrete compressive and reinforcing steel tensile strain limits are used as damage measures [25]. These strain limits have been correlated to observed damage in large-scale column tests. Therefore, we believe that our research will provide a realistic measure of the increase in damage for different limit states due to aging conditions and multiple earthquake loadings.

In addition, structures can have an existing condition such as corrosion that further deteriorates the structure's performance. Corrosion is one of the aging conditions that more significantly deteriorates the seismic response of a structure. Thus, it is crucial to determine the limit states of corroded reinforcing steel. Currently, the literature has developed expressions that correlate the level of corrosion to the decrease in strength of the reinforcing steel[76][14]. However, these studies have utilized an accelerated corrosion process that does not consider the protective film that is developed on the reinforcing steel surface when it is embedded in concrete, a process known as passivation of the reinforcing steel [42][21]. The protective film on the reinforcing steel bar must erode to enable the corrosion process. This process is known as depassivation. Depassivation of the reinforcing steel dramatically affects the behavior of reinforcing steel and can significantly modify the measured properties of the corroded reinforcing steel. Furthermore, no study has presented performance limit states on corroded reinforcement. Therefore, this research aims to close this gap by performing an experimental campaign. This experimental campaign consists of a series of tension tests and buckled bar tension tests to help define the performance limit states of corroded reinforcement. These results will then inform the computational model.

Moreover, there is a high likelihood for structures in a high seismic region to be subjected to a mainshock-aftershock sequence during their service life. Therefore, it is vital to consider the effects of mainshock-aftershock sequences. A series of condition-dependent nonlinear time history analyses are performed on a cantilever RC bridge column. The analysis applies a series of MS-AS sequences for different structure ages. The structure's material properties are changed due to the aging conditions (e.g., corrosion). At the end of each analysis, the main variables of the study are the limit state that was reached, the controlling mode of response (flexural or shear controlled), the equivalent viscous damping, and the accumulated deformations. This research considered the likely future condition of a structure in defining strain-based performance limit states.

1.1 Scope and layout

This document describes the main components, objectives, and results of the graduate studies of the author of this document. Chapter 2 contains the literature review, which summarizes state of the art in damage measurements and performance-based design framework. Chapter 3 covers the experimental program in corroded reinforcing steel, and Chapter 4 presents the experimental results. Chapter 5 shows the analytical program to analyze the change in the structural demands due to corrosion and discusses the results. Chapter 6 shows the application of the results from this study to new designs and assessment of existing structures that consider corrosion. Finally, Chapter 7 presents the main results of this research.

Chapter 2

Literature Review

Bridges are designed based on discrete events assuming that the initial material and structure properties remain constant through the bridge's life. The purpose of the research described is to study condition-dependent performance-based design that considers the material and geometric properties as the structure ages and the effects of multiple and discrete events on the achievement of prescribed limit states.

This chapter presents the current knowledge of the aging of structures, damage indexes, corrosion, and multiple earthquake loading. Then the study gap and the objectives of this research are defined.

2.1 Corrosion

Corrosion is one of the main aging effects in RC structures. In RC structures, after the concrete is cast, a protective layer forms on the surface of the reinforcing steel. This process is known as the passivation of the reinforcing steel. However, the protective film can be broken under conditions such as chloride attack. This process is known as depassivation. The depassivation process leads to corrosion. Corrosion reduces the steel area and modifies the effective strength of the reinforcing steel. If corrosion degrades the structural performance of the reinforcing steel, it will certainly degrade the overall strength of the system. The incidence of corrosion in RC structures in earthquake-prone areas could trigger the earliest onset of limit states, such as bar buckling or fractures (compared to pristine conditions). Therefore, it is important to incorporate corrosion mechanics in this condition-dependent performance-based seismic design. The general chloride attack corrosion process can be explained using three main parameters such as (1) time to initiation of corrosion, (2) corrosion growth in reinforcing steel, and (3) the mechanical properties of corroded reinforcing steel. Figure 2.1 schematically shows the corrosion process.

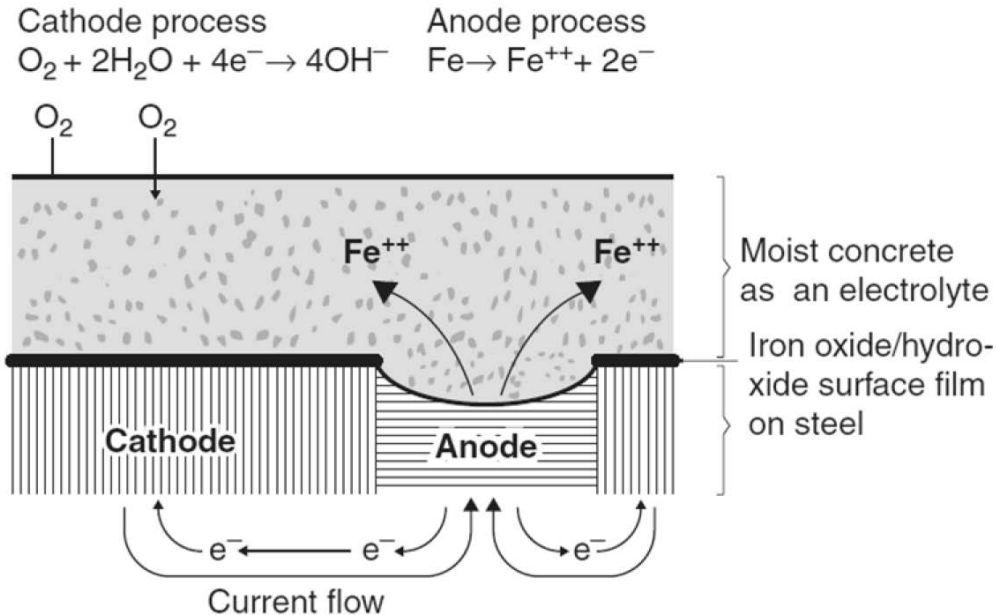


Figure 2.1 Corrosion process in reinforcing steel bar [42]

2.1.1 Time to corrosion

Jensen et al. performed a series of experiments to measure the chloride ingress in the cement and mortar paste [29]. In their study, it was determined that the ingress of chlorides follows Fick's law of diffusion, shown in Eq. 2.1. Stewart et al solved Eq. 2.1 in terms of the chloride ion concentration ($C(x, t)$), distance from concrete surface (x), time of exposure to chloride ions (t), and the chloride diffusion coefficient (D_c). The solution rendered equation Eq. 2.2 which describes the time to initiation of corrosion [65][73][68]. Mean values for C_0 and C_r have been previously defined for environments that are controlled by deicing salts [23][71][16].

$$\frac{\partial C(x, t)}{\partial t} = D_c \frac{\partial C(x, t)}{\partial x^2} \quad (2.1)$$

$$T_{corr} = \frac{x^2}{4D_c} \left[\operatorname{erf}^{-1} \left(\frac{C_0 - C_r}{C_0} \right) \right]^{-2} \quad (2.2)$$

2.1.2 Rate of corrosion

Vu et al. developed an empirical model to evaluate the corrosion rate [70][65]. In their study, a constant corrosion rate was assumed. However, it is known that the corrosion rate is not constant over time because it is dependent on factors such as the quality of concrete, the amount of oxygen available in the environment, and relative humidity. Nonetheless, for long-term studies, this approximation is valid. The underlying assumptions of this model are a relative humidity of 75% and a temperature of 20°C. The model developed by Vu et al. is shown in Eq. 2.3. Figure 2.2 shows the corrosion rate for different concrete covers (d_c), as a function of the water to cement ratio (w/c). In general, for large values of cover depth, the rate of corrosion decreases rapidly, and as the water to cement ratio (i.e., lower quality concrete) increases, the rate of corrosion increases.

$$i_{corr} = \frac{37.5(1 - w/c)}{d_c} \quad (2.3)$$

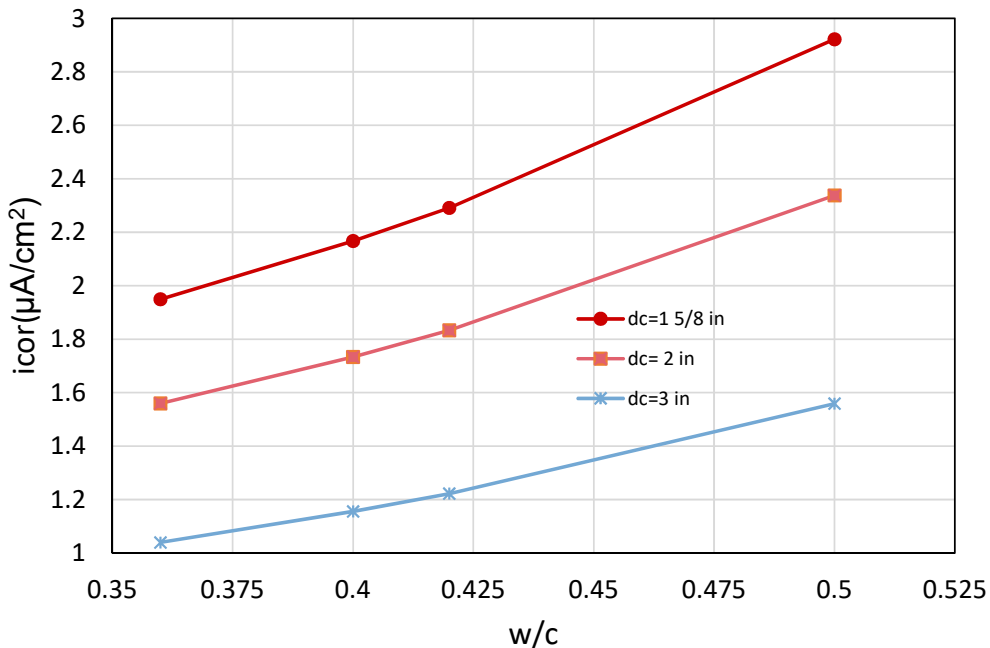


Figure 2.2 Concrete water to cement ratio vs rate of corrosion

In addition, Vu et al further improved the model of corrosion growth in reinforcing steel developed by Stewart et al [70][65][11][23]. Their proposed model describes the reduction in diameter of reinforcing steel ($d_{corr}(t)$) as a function of time described in Eq. 2.4. Figure 2.3

shows this model applied to a rebar with an initial diameter (d_{bi}) of 3/4 inch, a concrete cover of 1-1/2", and water to cement ratios ranging from 0.36-0.50.

$$d_{corr}(t) = d_{bi} - \frac{1.0508(1 - w/c)}{d_c}(t - t_{corr})^{0.71} \quad (2.4)$$

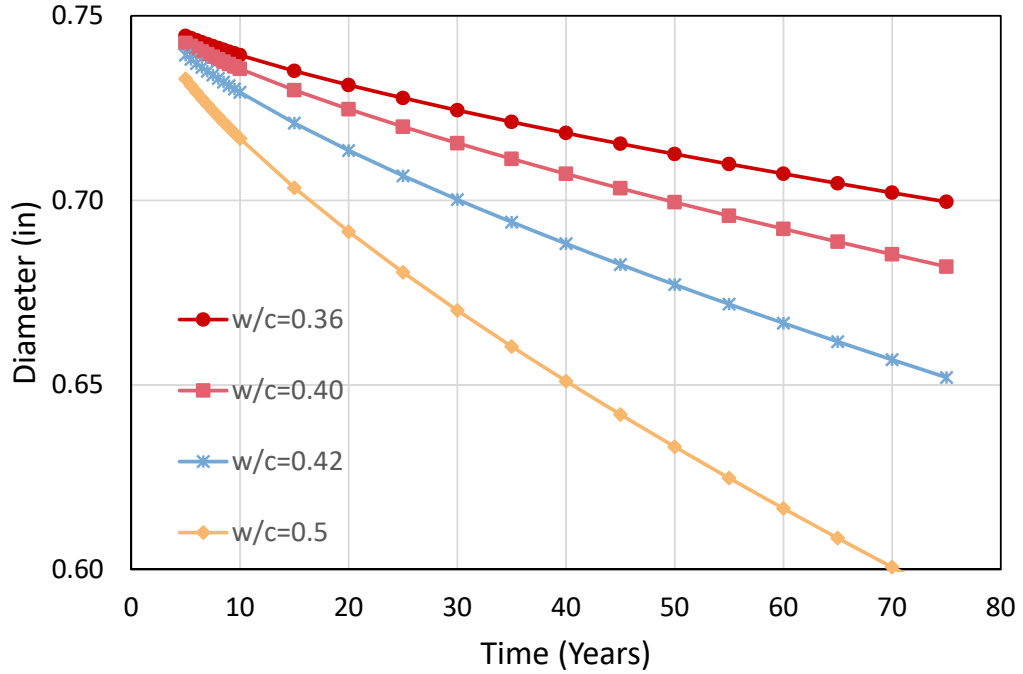


Figure 2.3 Diameter decrease due to corrosion

Further, the evolution of corrosion in reinforcing steel can be expressed in the percent loss of mass of rebar. If uniform corrosion is assumed, this can be expressed as the percentage of diameter reduction. The corrosion level can be expressed as shown in Eq. 2.5.

$$CL = \frac{d_{bi} - d_{corr}(t)}{d_{bi}} * 100 \quad (2.5)$$

Combining Eq. 2.4 with Eq. 2.5, the variation of the corrosion level can be described as a function of time. Figure 2.4 shows the results of this process.

2.1.3 corrosion modified properties of reinforcing steel bars

Du et al. [14][15] performed tension tests on corroded rebars and determined that the mechanical properties of steel change with the level of corrosion. In general, as corrosion increases, the

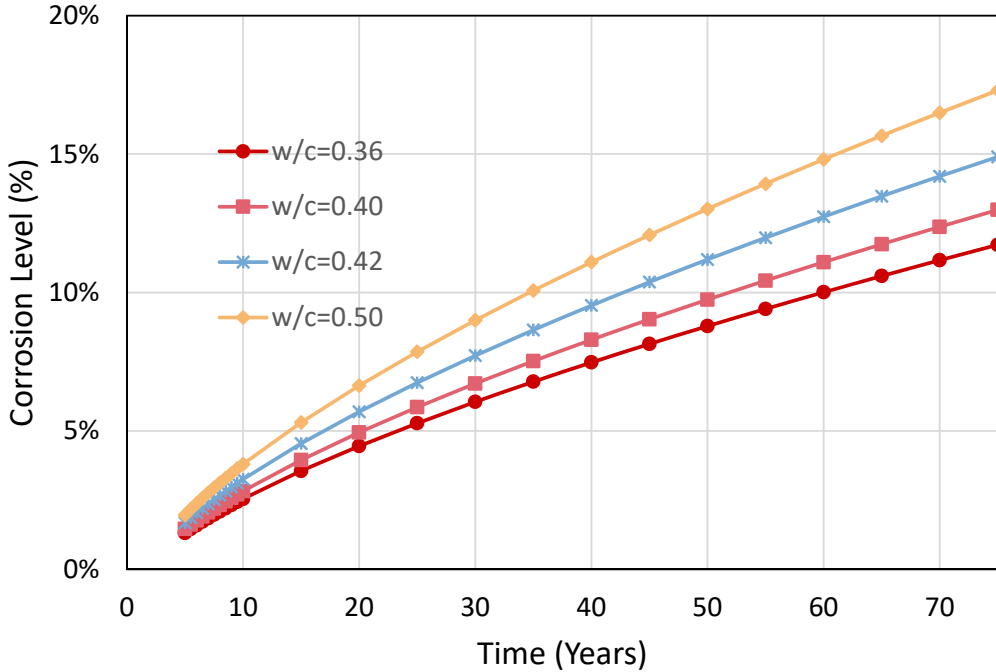


Figure 2.4 Corrosion level vs time (years)

reinforcing steel's yield strength, and ultimate strength decrease. The variation of the mechanical properties is shown in Eq. 2.6 for the yield strength and ultimate strength of the reinforcing steel.

$$f_{y,CL} = f_{yo}(1 - 0.005CL) \quad (2.6)$$

$$f_{u,CL} = f_{uo}(1.018 - 0.005CL)$$

One of the limitations of their study is that the accelerated corrosion process used to develop the corrosion in the rebars did not account for the depassivation process that naturally occurs in rebars embedded in concrete. Chapter 3 shows a proposed experimental assessment that will provide an accurate evaluation of the mechanical properties of corroded reinforcing steel.

2.1.4 Physical test on corroded RC Structures

Recent studies [35], [41] and [74] have been developed to assess the effect of corrosion on the structural performance of cantilever RC columns. These columns were subjected to accelerated corrosion to obtain different levels (CL). The range of CL for these studies corresponds to $CL = 0\%-20\%$. In these studies, the accelerated corrosion was performed via an electrochemical process directly applied to the reinforcing steel as shown in Fig. 2.5.

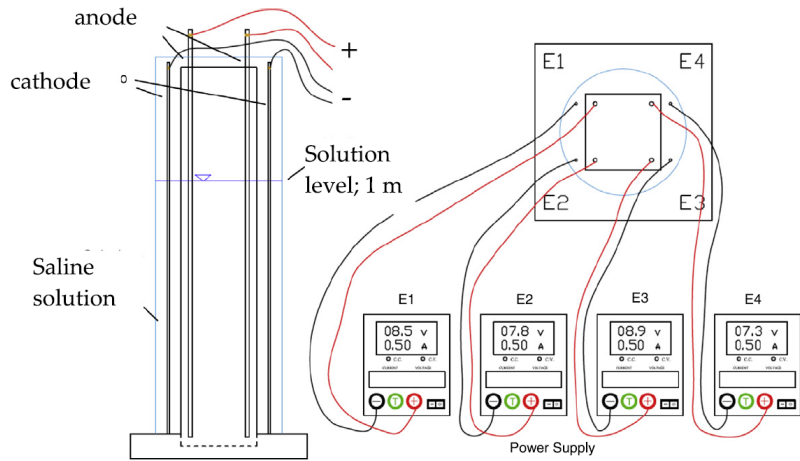


Figure 2.5 Force displacement response of RC corroded columns [41]

The corroded RC columns were then subjected to a quasi-static loading protocol. The resulting force-displacement response of one of these experiments is shown in Fig. 2.6. Again, it can be seen that there is a reduction in the strength and displacement capacity of the system.

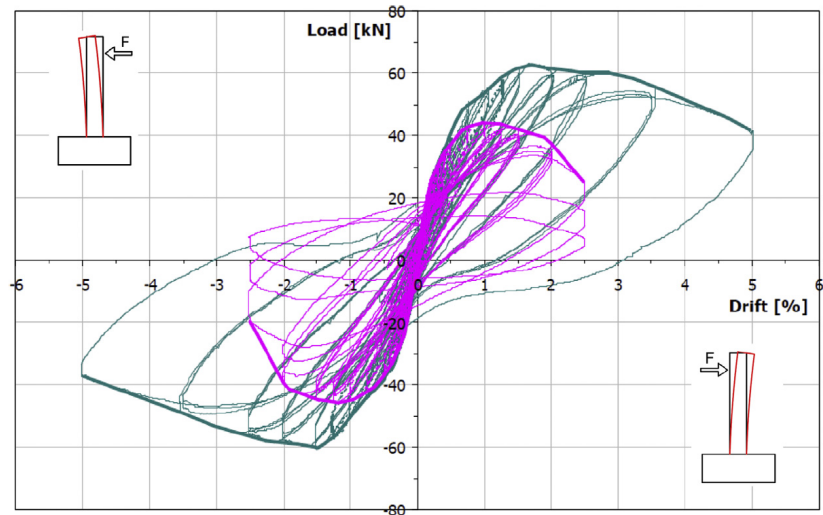


Figure 2.6 Corrosion process for RC column [41]

As stated in the previous section, the mechanical properties of steel are affected by corrosion. Therefore, in the previous studies [41] the authors performed tension tests on corroded reinforcing steel. In these tests, a reduction in the mechanical properties of steel was observed

as well as a reduction in the rupture strain ε_{srupt} , see Fig. 2.7.

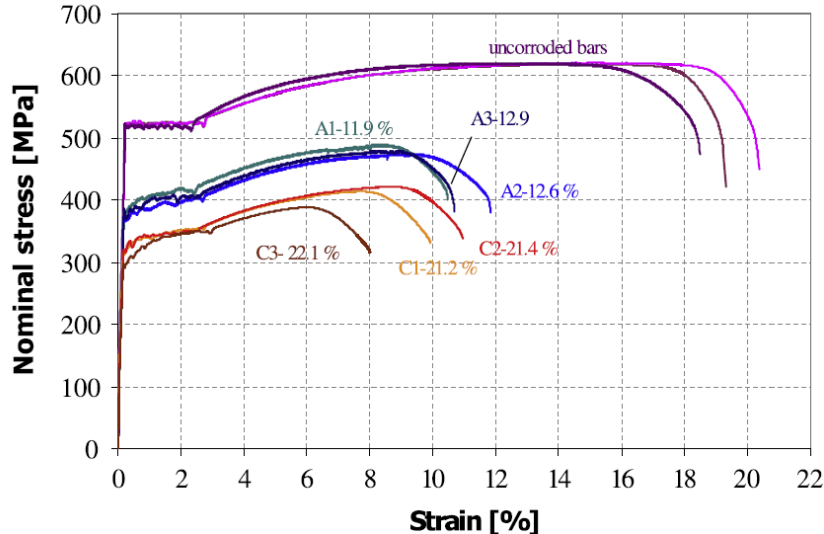


Figure 2.7 Corroded rebars stress-strain curves [41]

While these studies show how corroded RC columns behave under cyclic loading, they did not consider the protective film's generation due to the concrete's alkaline environment. This film can modify the mechanical properties of corroded steel. In addition, the accelerated corrosion process used a 3% *NaCl* concentration solution, while the chloride attack in concrete usually has a 1.0% - 1.5% concentration of the same chloride. Therefore the results obtained from these studies do not accurately represent the actual conditions of corroded RC columns. Thus, an experimental campaign is proposed to provide results on the mechanical behavior of corroded reinforcing steel inside concrete. The experimental campaign is discussed in Chapter 3.

2.2 Steel strain aging

While corrosion is an important parameter that affects steel in structures, strain aging is a phenomenon that affects mild steel, which is common in older structures. Strain aging is when steel, after being subjected to large strains and an amount of time passes after the loading, when the steel is reloaded. As a result, it presents a higher strength and reduced ductility than before the first loading. Therefore, incorporating this parameter in this research will help evaluate this effect in older structures when subjected to repeated earthquake loading. This process is explained in more detail in this section.

2.2.1 Metallurgical process

It is generally accepted that strain aging is due to the diffusion of carbon and nitrogen atoms in solution to dislocations that have been generated by plastic deformation. Initially, an atmosphere of carbon and nitrogen atoms is formed along the dislocation length, immobilizing it. Extended aging, however, results in sufficient carbon and nitrogen atoms for precipitates to form along the length of the dislocation[52][28].

These precipitates impede the motion of subsequent dislocations and result in some hardening and loss of ductility. The extent of strain aging, a thermally activated process, depends primarily on aging time and temperature. In general, extended aging results in a saturation value above which further aging has no effect [57].

A second strengthening mechanism occurs when cold deformation (alone) is applied to steels. When dislocations break away from their pinning interstitial atoms and begin the movement causing slip, they begin to intersect with each other. A complex series of interactions between the dislocations occur, causing them to pin each other, decreasing their mobility and resulting in higher strength, lower ductility, and lower toughness. As a result, cold deformed steels already have lowered ductility and toughness before any strain aging occurs. When heating follows cold deformation, the loss in ductility and toughness is more significant. It is this combination of events that is the most damaging to the toughness of structural steels [44].

2.2.2 Strain aging effects in structures

Strain aging is how steel subjected to large strains develops an increased strength and reduced ductility with time. Large earthquakes can cause this effect on structures built with mild steel. Therefore, it is vital to include strain aging in a time-dependent analysis. Furthermore, strain aging will cause an increase in the strength of the plastic hinge, and as a consequence, plastic hinges may form in regions of the structures that have not been designed for such demands. The effects of strain aging may also alter the transverse reinforcement due to cold bending, making them susceptible to brittle failure[44].

According to Restrepo-Posada[57], most strain aging occurs in the first 37 days. In addition, Monahan et al. [44] studied strain aging effects concerning the time at different levels of pre-strains. The pre-strains ranged from $2\varepsilon_y$ to $10\varepsilon_y$, for 3 days to 50 days. Their results determined that a significant effect of strain aging took place from pre-strains $5\varepsilon_y$ and on. Strains higher than $15\varepsilon_y$ indicate a performance level in which substantial damage has been induced in the structure such that it is deemed unrepairable and therefore pre-strains higher than $15\varepsilon_y$ are impractical and were not studied [44].

Monahan et al correlated the increase in yield strength as a function of time and the pre-strain in reinforcing steel bars. The proposed equations are shown below:

For $10\varepsilon_y$

$$\frac{f_y}{f_{yi}} = 0.0026t + 0.9838 \quad (2.7)$$

For $5\varepsilon_y$

$$\frac{f_y}{f_{yi}} = 0.0008t + 0.996 \quad (2.8)$$

For $2\varepsilon_y$

$$\frac{f_y}{f_{yi}} = 0.0004t + 0.9979 \quad (2.9)$$

It is proposed to limit the increase in yield strength obtained at 50 days, which was the limit of the scope of their study. Equations 2.7 to 2.9 are plotted in Fig. 2.8

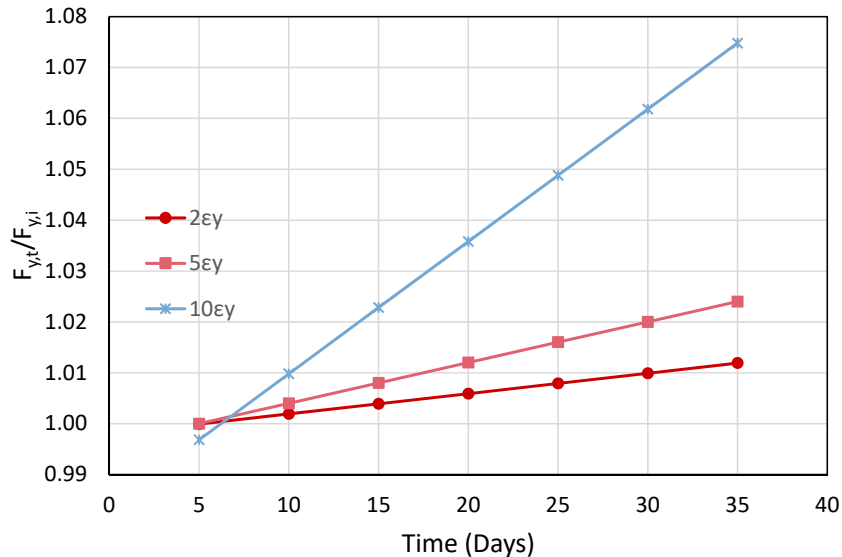


Figure 2.8 Strain aging effect on yield strength vs time (days)

2.3 Damage Indexes

The use of damage indexes has dominated the research related to damage accumulation. While these methods are practical in that they can be easier to deploy in probabilistic analyses and appear to have a logical basis, they are based on empirical relationships and need to be correlated for each structure case to be of any significance. An example is shown in this section that demonstrates this inconsistency. The literature review presented here is to understand what has been done previously to study the effect of damage accumulation. However, this research's purpose is that strain limit states are an improved measure of damage over empirical methods.

Park et al. studied the effect of cumulative damage in structures [75]. They proposed the damage index as shown in Eq. 2.10. The damage index was used to quantify damage in terms of the maximum experienced earthquake and the absorbed hysteretic energy.

$$D = \frac{\Delta_m}{\Delta_u} - \beta \frac{E_h}{F_y \Delta u} \quad (2.10)$$

Δ_m : Maximum deformation under earthquake

Δ_u : Ultimate deformation under monotonic loading

F_y : Calculated yield strength

E_h : Total hysteretic energy

β : Dimensionless constant

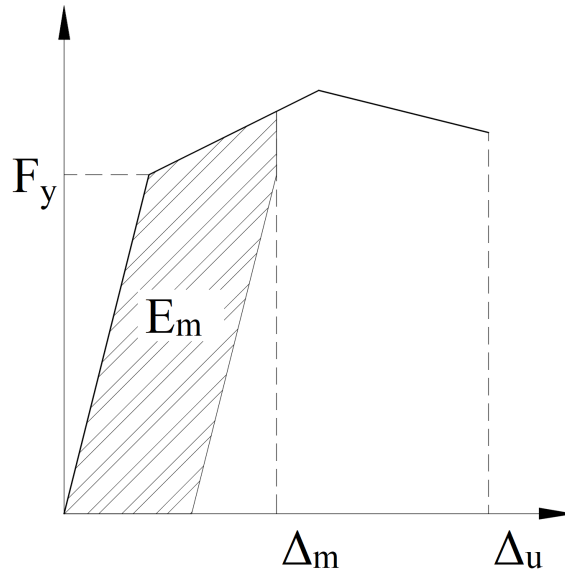


Figure 2.9 Park and Ang conceptual scheme

Equation 2.10 was derived for concrete elements. The first term here is a simple, pseudo-static displacement measure. The second term accounts for cumulative damage. This concept is shown in Fig. 2.9. The advantages of this model are its simplicity and flexibility in adapting the model to correlate with experimental data. After calculating the damage index, this can be classified according to the damage index level defined by Park and Ang [75]. The damage index level classification is shown in Table 2.1.

Table 2.1 Damage index level classification [75]

Level	Damage index (DI)	Damage measure
I	DI<0.1	No damage; localized minor cracking
II	0.1<DI<0.25	Minor damage; light cracking throughout
III	0.25<DI<0.4	Moderate damage; severe cracking; localized spalling
IV	0.4<DI<1.0	Severe damage; crushing of concrete; reinforcement exposed
V	D>1.0	Loss of elemental load resistance

However, this model has several limitations. Firstly, the calibration of the β coefficient with observed damage has proven to be very low ($\beta = 0.05 - 0.15$) [75] [24], rendering the second term relatively inconsequential compared to the contribution of the first term. A sample result is taken from Gosh et al. [24], which applied a modified version of the Park and Ang damage index in terms of the moment (M_y), the rotation (θ_y), and curvature ductility (μ). The modified model is expressed in Eq. 2.11.

$$D = \frac{\mu_m}{\mu_u} - \beta \frac{E_h}{M_y \theta_y \mu u} \quad (2.11)$$

Using the following values: $\mu_m = 4.93$; $\mu_u = 17.02$; $M_y = 8751.375$; $\theta_y = 0.0042$; $E_h = 119.07$; $\beta = 0.05$

And substituting in equation Eq. 2.11:

$$D = \frac{\mu_m}{\mu_u} - \beta \frac{E_h}{M_y \theta_y \mu u} = 0.3$$

First term:

$$\frac{\mu_m}{\mu_u} = \frac{4.93}{17.02} = 0.2897$$

Second term:

$$\beta \frac{E_h}{M_y \theta_y \mu u} = 0.05 \frac{119.07}{8751.375 * 0.0042 * 17.02} = 0.0103$$

It can be seen that 97% of the damage index comes from the first term, which is the elastic

term, and the inelastic part is only 3% of the total.

Despite its limitations, several studies have used or modified this model to study cumulative damage effects for different structures. Those of relevant importance are those performed by Kunnath et al. [33], who used a modified Park and Ang model to account for damage at the local level for elements in the structural analysis program IDARC 3.0. In this software, for the case of multiple degrees of freedom buildings, they also added parameters to consider the damage at the inter-story level and the global model. In addition, Ghosh et al. [24] developed a damage accumulation framework to estimate the probability of exceeding a damage index for multiple ground motions. Other regressions have been proposed [30], [17], [58] but show no improvement in assessing the damage state of a structure. While these studies provide an insight into some of the characteristics of damage accumulation, they still rely on the Park and Ang model and carry the same limitations.

Krawinkler (1987) [31] proposed a method that considered damage as a function of low cycle fatigue parameters. The form of the Krawinkler damage index for steel components, weldments, and local buckling has a general shape to the Miner model. This model relies on the accumulation of plastic deformations. While this model has proven to work well for evaluating individual steel structure elements, it does not provide a way to generalize damage for other types of structures.

2.4 Multiple earthquake loading

The evaluation of multiple seismic events has been scarcely studied; however, they have been felt in numerous earthquake sequences such as the Christchurch 2010, Umbria-Marche Earthquake 1997 and the Puerto Rico Earthquakes 2020. The hypothesis is that the accumulation of damage will restart in a minor seismic event to achieve a prescribed limit state, similar to how corrosion and other aging phenomena might impact the intensity needed to achieve a future limit state.

In the literature, the study of multiple earthquake loading can be classified into two groups:

- Mainshock-aftershock sequences
- Mainshock sequences

These studies have shown some of the effects of multiple earthquake loading for different structures.

2.4.1 Mainshock-aftershock sequences loading

Strong aftershocks can increase the state of damage to a building or even collapse an already damaged structure. Therefore, it is crucial to quantify the increase of seismic demands in struc-

tures due to aftershock loading. In recent years different studies have been carried out to develop methodologies that consider these effects.

Tesfamariam et al. [67] investigated the increase in the demands for multiple degrees of freedom systems (MDOF). They conducted a parametric study of RC bare frame buildings and RC frames with infill masonry buildings. The main parameter of the study focused on the thickness of the infill frames ranging from 75mm - 125 mm. In addition, a series of mainshock-aftershock sequences were applied, selected for the area of Vancouver, BC. The mainshock-aftershock sequence was selected using the conditional mean spectra (CMS) over the period range of the structures. The motions considered in their study were different for the bare frame and the infill frames. The bare frame was subjected to a mainshock followed by three aftershocks, while those of the infilled frame consisted of one mainshock followed by one aftershock each. Their results showed an increase of 10% in the inter-story drift demands for the RC basic frame structures. For the case of infill frames, the inter-story drift did not significantly increase. Their study used FEMA 356 [19] to define the performance limit states. FEMA 356 drift performance limit states are based on linear regression on observed damage to drift level obtained from experimental tests. The linear regression compared to the experimental results have high dispersion. Therefore, it is possible that in the study by Tesfamariam et al., while a drift limit state did not increase after applying an MS-AS sequence, a higher strain was reached in some of the components due to the MS-AS sequence, and as a consequence, a higher strain performance limit state could have been reached. Their results emphasized the importance of using strain performance limit states. Similarly, Raghunandan et al. [56] studied the vulnerability of RC frame structures. Their study showed that depending on the level of interstory drift achieved during the mainshock, the additional damage experienced during the aftershock would be different. For example, the authors showed that for an RC frame that experiences 4% or more interstory drift in the mainshock, the median capacity to resist aftershock shaking is reduced by about 40%. Furthermore, other studies have focused on the behavior of single degree of freedom (SDOF) systems response to mainshock-aftershock (MS-AS) sequences [27][38]. Hatzigeorgiou et al. focused on determining the inelastic displacement coefficient variation due to the MS-AS sequence. Their study concluded that there is an increase in the inelastic displacement demands. However, the limitations in their study did not report what happens to the performance limit states. Further, Manafpour et al. studied the seismic drift behavior of structures to MS-AS sequences for far-field earthquakes and near-field earthquakes. Their study concluded that for SDOF structures, near-field earthquake sequences were the most damaging, increasing the drifts by as much as 45% compared to a structure subjected to the mainshock only.

Researchers have applied three earthquake selection procedures for mainshock-aftershock sequences. The first method, incremental dynamic analysis (IDA), consists of 1)subjecting the nonlinear building model to a ground motion having a particular intensity, 2) recording the

response of the structure [69], 3)in subsequent analyses, the ground motion is incrementally scaled to a higher intensity measure (IM), and 4)the structural response is recorded in each analysis. The IDA procedure was extrapolated for MS-AS sequence as follows: 1)Apply the IDA to the mainshocks to obtain 11 drift damage levels ranging from 0.5% to 5.5% of interstory drift in the structure, 2) after each mainshock, include an incrementally scaled aftershock with a 4 seconds gap between the mainshock and the aftershock, and 3)Change the polarity of the aftershock, which refers to the direction of the aftershock variation to the mainshock. Fig. 2.10 shows one of the resulting MS-AS sequences using the IDA methodology. Due to scaling factors, the IDA methodology uses artificial mainshock-aftershock sequences. Therefore, the IDA analysis can be computationally expensive. For instance, the authors reported 9900 ground motion sequences per structure.

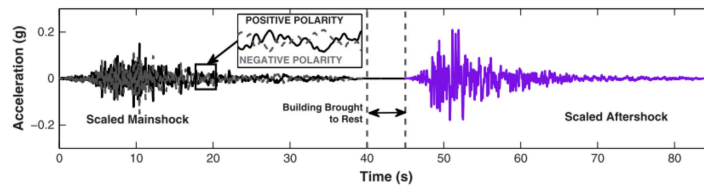


Figure 2.10 Mainshock-aftershock sequence train of ground motions [56]

The second method matches the MS-AS sequences to a site seismic hazard curve obtained from a probabilistic seismic hazard analysis (PSHA). Tesfamariam [67] used conditional mean spectra (CMS) to match and select mainshock-aftershock sequences for structures located in Vancouver, BC. Their study selected MS-AS sequences from two databases of ground motions, NGA-West2 [3], and the K-NET//KiK-net [49]. The CMS process consists of computing the expected response spectrum associated with a target spectral acceleration (S_a) value at a single period, using the known values from the PSHA such as the magnitude, distance, and ϵ values. The authors used CMS to select the MS-AS sequences for different earthquake scenarios a)Crustal earthquake, b) Interface, and c) Inslab. They hypothesized that different earthquake scenarios would have different MS-AS sequence characteristics, such as higher spectral acceleration (S_a) values at short periods for interface earthquakes and high S_a values at more extended periods for crustal earthquakes. They argue that using the CMS method makes the selection of ground motion consistent with the seismological features of the study area. Fig. 2.11 shows this selection for a structure with a 0.4s period for crustal earthquakes. The CMS method adapts to the site conditions. No scaling of MS-AS is required since the selection is optimized to ground motion sequences stored in the databases. Since the CMS method uses site-specific data, it can be a part of an analytical framework that can be adapted to different seismic regions.

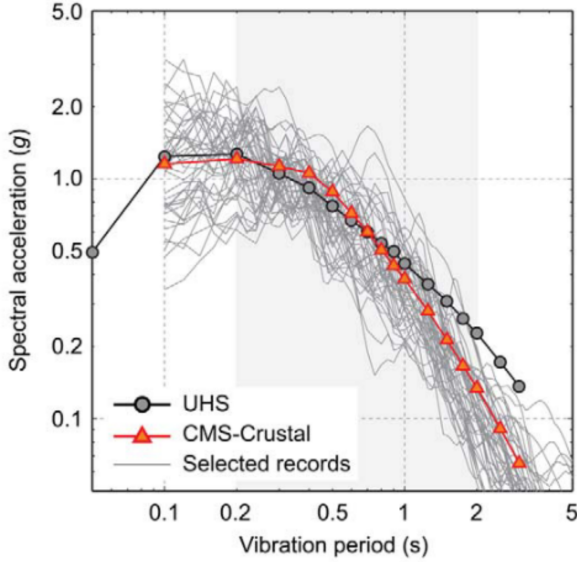


Figure 2.11 Mainshock-aftershock sequence selection at $T=0.4\text{s}$ for crustal earthquakes in Vancouver, British Columbia [67]

Finally, the third method consists of unscaled ground motion sequences. Ruiz Garcia et al. [59] examined the response of 9 typical low-height reinforced concrete highway bridges under 26 as-recorded mainshock–aftershocks sequences gathered in the subduction zone of the Mexican Pacific Coast. They found that aftershocks do not significantly increase drift demands due to the inherent overstrength in the study-case low-height highway bridges[59]. In addition, Ruiz Garcia et al. [60] in another study determined that Non-Degrading Systems are unaffected by recorded MS-AS sequences for steel-frame models, which did include p-delta effects but not the degradation of the hysteresis of the connections. The study by Ruiz-Garcia also demonstrated that the effect of the aftershock is not substantial due to the different frequency contents of the ground motion as shown in Fig. 2.12. However, they also noted an apparent increase in the demands if the sequences are altered. The limitations of these studies are that the degradation of the structural systems was not included, and only shallow crustal earthquakes were considered.

2.4.2 Mainshock sequences loading

Reliable temporal prediction of earthquakes is currently impossible. However, earthquake recurrence time can be modeled reasonably well as a Poisson process for a large region. Sunasaka [66] developed mainshock sequences that followed a Poisson process. Their study focused on the accumulation of damage due to mainshock sequences and mainshocks-aftershocks sequences. Damage accumulation was accounted for by the Park and Ang index. The authors used ground

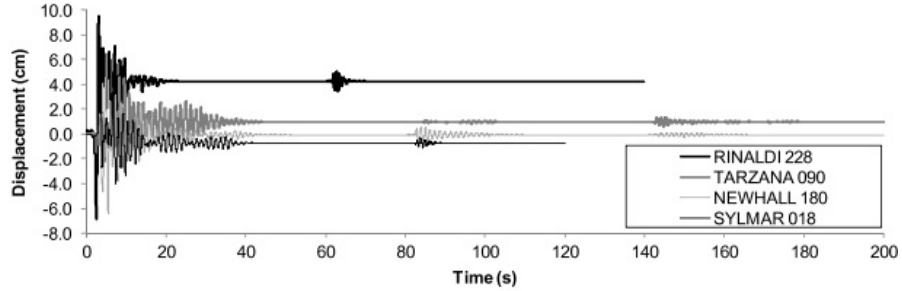


Figure 2.12 Mainshock-aftershock sequence results for story displacement [60]

motion prediction equations to develop artificial mainshock sequences. Their study calculated each mainshock's recurrence period, magnitude, location, and peak ground acceleration. Finally, the author subjected an SDOF bridge in Eureka, CA, to the mainshock sequence shown in Fig. 2.13. While the results show a significant increase in the damage index due to mainshock sequences, the conclusions are limited by the assumption that a Poisson process can be applied to single faults, which has not shown a good correlation with observed events[63]. While this study shows what could be possible if mainshocks were predictable in small regions, more seismology advances are needed to apply the proposed methodology confidently.

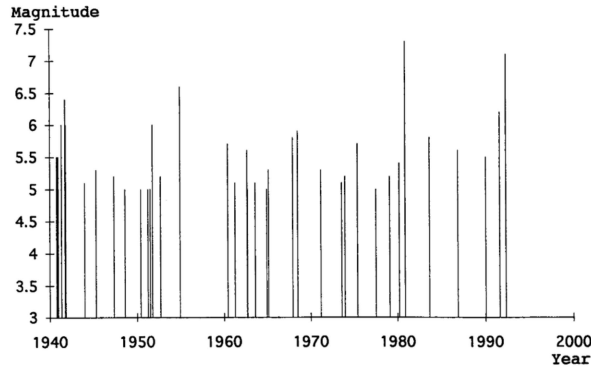


Figure 2.13 Mainshock sequence selection at Eureka, CA [66]

Other studies have used three equally spaced mainshocks [27]. The three equally spaced mainshocks can be deployed without much computational effort. However, there is no seismological basis for using three equally spaced mainshocks. Therefore, the use of this methodology would be limited to scenario analysis and not valid for analysis and design since the probabilities of three equally spaced in time mainshocks on any given structure are very low.

2.5 Aging of structures

There have been attempts by many researchers to characterize the aging of structures.

In recent years studies have focused on the effect of cumulative damage. These studies have focused on assessing the damage accumulation considering multiple earthquakes, corrosion, and service life of the structure. Two fields of study have been observed:

- Probabilistic framework
- Fragility curves

Probabilistic Framework

One of the most widely used probabilistic frameworks is the Pacific Earthquake Engineering Research Center (PEER) Performance Based Design (PBD). PEER PBD can be expressed by the following equation:

$$\nu_{DM}(dm^{LS}) = \iint D_{DM|EDP}(dm|edp)|, dG_{EDP|IM}(edp|im)|| d\nu_{IM}(im)| \quad (2.12)$$

Mackie et al. [36] using the PEER PBD, developed the performance-based damage design (PBDD) and performance-based loss design (PBLD) by defining the probabilistic demand, damage, and loss model parameters in terms of reinforced concrete column damage. The RC column damage was defined as mean drift ratios obtained from the PEER structural performance database (<http://nisee.berkeley.edu/spd/>). The drift limit states considered in their study were concrete spalling, bar buckling, and failure. In their study, failure was defined as the first occurrence of the database fields for reinforcing bar fracture and loss of axial load-carrying capacity

The authors show that for a given intensity measure (IM) and a confidence level of achieving a limit state, it is possible to define the probability of exceeding that limit state. The authors used peak ground velocity (PGV) as their intensity measure. While this methodology was able to define the damage and incorporate it into the PEER PBD framework, the authors did not consider strain to define the limit states. In a PEER report, Mackie et al. studied seismic demands for the performance-based design of bridges. In the report, they performed a design parameter sensitivity analysis to evaluate different intensity measures. Their analysis showed that the optimal IM to predict most engineering demand parameters (EDP) is the first mode spectral displacement $Sd(T_1)$ [37]. However, at the time their report was written, the $Sd(T_1)$ did not show a good correlation with strain as the EDP , and as a consequence, they did not recommend using strain as a predictor of structural performance. Nonetheless, a recent study presented by Krish et al. showed that new advancements in the modeling of plastic hinge forming

members could more accurately relate strain and $S_d(T_1)$. Therefore, they concluded that the use of these parameters is well suited to predict the performance of structures [32].

Fragility Curves

Another common trend in this subject is the use of fragility curves to estimate the effect of damage on structures. Two main approaches were found in the literature. One relied on the Park and Ang Model damage index to define damage, while the second approach related damage to drift.

Ghosh et al. [24] formulated a damage accumulation framework. Their study relied on the Park, and Ang Damage index explained in the previous section. In addition, the study performed a series of nonlinear time history analyses for two cases:

- Using a constant main shock hazard occurrence rate (3 main shocks in a 50-year period)
- Mainshock - Aftershock series using a time-dependent aftershock hazard occurrence rate

The results from their study showed regression equations that statistically predict the damage index as a function of earthquake intensity and damage history. This study revealed that for both mainshock and aftershock scenarios, there was a significant increase in the probability of damage index exceeding a damage index level (as defined in Table 2.1) under repeated shock scenarios. While this study shows the importance of considering damage accumulation, these results have to be taken with caution since they present the same disadvantages as the Park and Ang damage index.

Ghosh et al [23] also studied the effects of corrosion on time-dependent seismic fragility curves. Their study characterizes corrosion in concrete columns as a continuous phenomenon that occurs as a function of time. The authors also considered the effects of corrosion on steel bridge bearings. The authors then ran a series of NLTHA analyses for different aging times of the structures. Based on their analysis, time-dependent fragility curves were presented. The results showed that as time increases and corrosion increases, the probability of exceeding a limit state increases. In their study, limit states were defined based on inter-story drifts, which were obtained from experimental results and field observations [53]. It is essential to mention that the limit states used in their study were not defined based on strains or other structural properties. Instead, the limit states came from a survey performed in central and southeastern United States departments of transportation on the premise of a range of experienced inter-story drifts and the time is taken to repair them. In addition, assuming that corrosion is a continuous process has to be cautiously taken as valid since site information such as temperature, water to cement ratio, the addition of cementitious materials such as silica fume, and the environment (e.g., coastal vs. inland) affect the rate of propagation of corrosion[68].

While these studies provide a general view of how damage increases the likelihood of observing collapse or deterioration of the seismic performance, the methods used to arrive at those

conclusions can be misleading since the definition of damage as either a Damage Index or Drift is not the best parameters to quantify the damage. Therefore, we believe that strain-based limit states will better understand the implications of damage accumulation.

2.6 Research Gap

Many studies have tried to show the importance of quantifying the effects of accumulated damage and multiple shocks throughout the lifetime of a structure. Therefore, it is essential to develop a model that establishes the likelihood of achieving a limit state as the structure ages. In addition, it is crucial to understand the impacts of aging on bridge seismic performance. Furthermore, bridges in seismic areas can be subjected to mainshock and aftershocks. Therefore, a methodology that incorporates aging and multiple seismic events is needed.

Damage accumulation is a topic gaining momentum in the engineering community. This study will better inform the potential future conditions of a structure to stakeholders such as state DOTs, building owners, and practicing engineers. The literature observed that damage accumulation had been studied using the Park and Ang damage index or drift-based limit states to measure damage accumulation. Different researchers have also included corrosion in their scope of analysis, which shows that aging conditions play an essential role in the deterioration of a structure. In addition, Krish [32] determined that spectral displacement at the first effective period is an improved intensity measure (IM), while the past literature used the peak ground acceleration (PGA) as the controlling IM. This research will develop a parametric study using a single degree of freedom (SDOF) systems, subjecting them to different conditions such as corrosion and steel strain aging. The SDOF structures will be subjected to a sweep of ground motions using nonlinear time history analysis to obtain maximum strain demands. With the results from NLTHA, fragility functions will be used to show the increase in the likelihood of reaching a performance limit state due to the aging of the structure. In addition, this research will provide the engineering community with a design framework to account for damage accumulation in their analysis and guide decisions on the resiliency of a structure. In addition, this study will provide a methodology in which the Direct Displacement-Based Design (DDBD) is modified to consider the effects of the damage and aging conditions.

2.6.1 Objectives

The main goal of this research was to provide a design methodology to consider damage for performance-based seismic design of structures. In addition, this study demonstrated the implications of aging conditions and multiple earthquakes for the design of bridge RC columns.

- Incorporate different aging conditions and develop fragility curves that consider strain

limit states as a measure of damage

- Establish limit states for corroded rebars
- Describe the methodology to appropriately mimic the real corrosion process in material experiments of corroded rebars, which can later be extrapolated to large scale testing of RC columns subjected to corrosion
- Consider the effects of multiple earthquakes for two cases: (1) Mainshock-Aftershock sequence and (2) Mainshock-Aftershock sequence with the effects of time (corrosion and strain aging) between the mainshock and the aftershock.
- Incorporate these results into the Direct Displacement Based Design (DDBD) methodology.

Chapter 3

Experimental Program

Corrosion is the main aging condition that affects structures. Therefore, the success of this study relies on the most accurate representation of the corrosion process in the analytical model. As mentioned in Chapter 2, previous studies developed accelerated corrosion rebar specimens with high current densities, but did not account for the depassivation process of the reinforcing steel. A main objective of this study was to verify the mechanical properties of corroded rebars while considering the depassivation process. The experimental process was divided into the following main components: (1) corroded specimen preparation, (2) tension tests on corroded rebars, (3) buckled bar tension (BBT) tests on corroded rebars, (4) 3D scans of corroded rebars, (5) SEM observations of fracture surfaces from BBT tests, and (6) tension and BBT tests on turned down corroded rebars. The results obtained from the tension and BBT tests were used in the analytical model presented in Chapter 5, and more broadly provide accurate mechanical properties of corroded rebars.

3.1 Specimen Preparation

Rebars embedded in concrete generate a protective film that protects the rebars against corrosion, due to the alkaline environment of the cement paste. The most common form of corrosion occurs via chloride attack. During a chloride attack, the chloride diffuses in the concrete cover and comes into contact with the surface of the reinforcing steel. This initiates the process of depassivation, in which the protective film on the surface of the rebar is eliminated. The depassivation of the rebar enables the process of corrosion to occur. The proposed experimental campaign described in this chapter aimed to simulate the process of corrosion as it would occur in rebars embedded in concrete. Using “as received rebars”, that is, no special treatment to the surface of the rebar, the specimen preparation procedure consisted of (1) protecting the rebar ends that will be used as grips during the tension and buckled bar tension (BBT) tests,

(2) generating the passive layer on the rebars, and (3) performing accelerated corrosion of the rebars until the specified levels of corrosion.

3.1.1 Preparation of Rebar Ends

First, it was necessary to protect the areas of the rebar that functioned as grips during the tension and BBT tests against corrosion, to prevent a failure inside the grips. Therefore, the ends of the rebars were protected with three layers. The first layer consisted of two-part epoxy, the second layer consisted of electroplater tape, and the third layer consisted of shrink-tube. These layers ensured minimal corrosion in the grip areas of the rebar. Fig. 3.1 and Fig. 3.2 show the specimen geometry and the protective layers at the ends of the rebars.

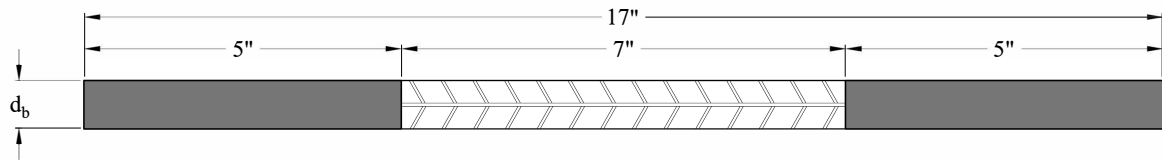


Figure 3.1 Rebar Specimen Geometry

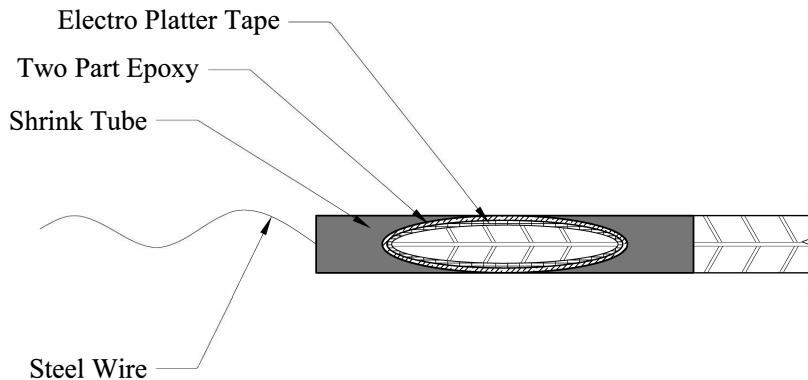


Figure 3.2 Rebars Ends Protection

To optimize the space and time it takes to prepare the rebars for corrosion, a large parent rebar that contains three specimens was prepared. This ensured that the parent specimen, placed in a corrosion cell, provided the same level of corrosion to all the specimen subsets. After each parent specimen had the specified level of corrosion, the large specimen was cut into the three smaller specimens shown in Fig. 3.3.

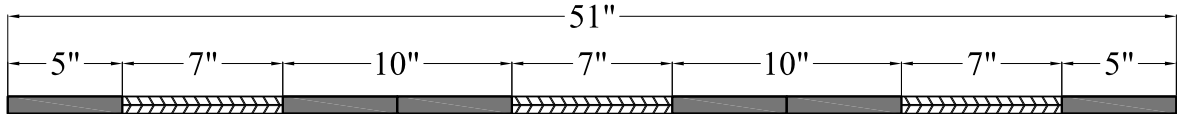


Figure 3.3 Large specimen containing three subset of specimens

3.1.2 Passivation of Rebar Specimens

In order to simulate the conditions of rebars embedded in concrete, it was necessary to generate the passive layer on the surface of the rebars. There are two ways to generate the passive layer: (1) embed rebars in concrete and wait for the passive layer to generate, or (2) submerge the reinforcing steel in a synthetic pore solution that mimics the cement paste environment. The second option is more suited for material testing, since it does not involve demolishing the concrete. To this regard, Ghods et al [22] developed ten different pore solutions to generate the passive film on the surface of rebars. The pore solutions that were developed in their study intended to mimic the cement paste. Their study used 10 solutions designed to encompass concentrations of Ca^{+2} , Na^+ , K^+ , and $(SO_4)^+$ found in the cement paste. The solution that generated the passive layer with the best quality of protective film, based on passive current density, was used in this study. To achieve the desired concentration of the Ca^{+2} , Na^+ , K^+ , and $(SO_4)^+$ ions, the following concentration of chemicals recommended in [22] was used in the pore solution:

- Saturated calcium hydroxide $Ca(OH)_2$ (approx. 1.7 g/L)
- Sodium hydroxide $Na(OH)$ (4.00 g/l)
- Potassium hydroxide (KOH) (11.22 g/l)
- Calcium sulfate dehydrate $Ca(SO_4) + 2H_2O$ (13.77 g/l)

The rebars were placed in the pore solution without any special surface preparation in the gauge length. Since, any form of special surface preparation affects the quality of the passive

layer [4], [13], [46], and [54]. In addition, Ghods et al. showed no significant change in the anodic polarization of the rebar surface after being placed in the pore solution for 8 days or 14 days. Their results are shown in Fig. 3.4. Therefore, the rebars were placed in the pore solution for 8 days.

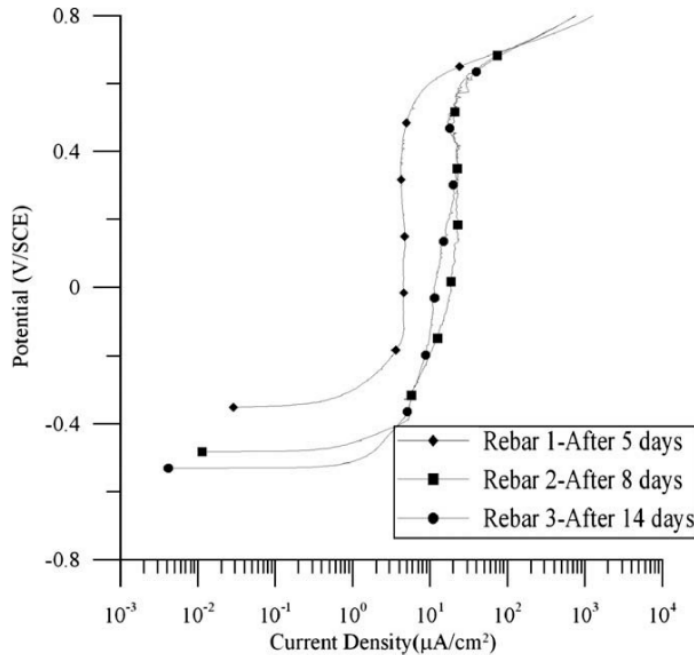


Figure 3.4 As received rebars anodic polarization immersed in pore solution for different times[21]

A specimen preparation assembly was constructed to prepare the rebars for the development of the passive layer. The assembly consisted of placing the rebar inside a PVC pipe, closing the ends of the pipe with a 90° PVC elbow, and closing the open ends with PVC pipe plugs. The assembly is shown in Fig. 3.5. This assembly ensured that the pipe remained airtight and prevented the carbonation of the calcium hydroxide ($Ca(OH)_2$) in the pore solution.

3.1.3 Accelerated Corrosion of Rebars

Four components are required for corrosion to occur: (1) the anode, (2) the cathode, (3) an electrolytic connection, and (4) an electrical path. The corrosion cell deployed in this study used this concept in the following way: the anode consisted of the rebar, the cathode consisted of a stainless steel mesh, the electrolytic connection was made with a sodium chloride solution, and the electrical path was forced via an electric circuit. The corrosion cell uses the assembly

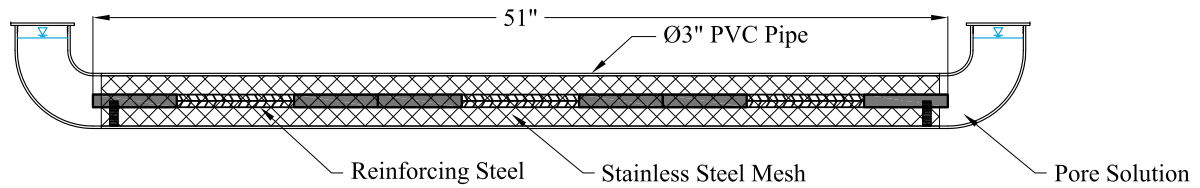


Figure 3.5 Assembly for rebar preparation for the development of passive layer in pore solution

developed to generate the passive layer with the components needed for corrosion as shown in Fig. 3.6. The circuit was designed so that the current in the specimen was $150mA$, equivalent to $340\mu A/cm^2$ on the gauge length surface of the rebar. To the author's knowledge this is the lowest current density ever used on an accelerated corrosion process for corroded rebars subjected to tension and BBT tests. Since the rebar and stainless steel mesh have a low resistance, a 100Ω resistor was added to the circuit, such that it stabilized the current and kept it constant at $150mA$.

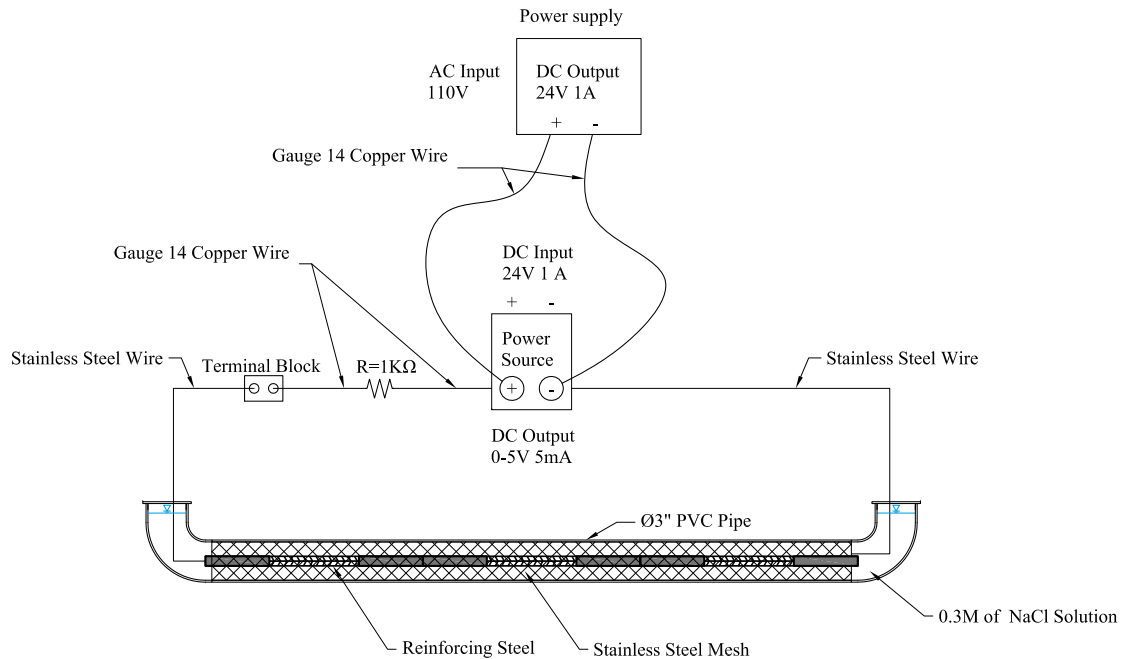


Figure 3.6 Accelerated corrosion process

Ghods et al [22] determined that for rebars with passive films, a concentration of 0.3 Moles of sodium chloride ($NaCl$) will start the depassivation process on the rebars. Accordingly the same sodium chloride solution was used in this study. To estimate the time to apply the current and obtain the desired level of corrosion, Faraday's law shown in Eq. 3.1 was used.

$$m_{loss} = \frac{it(AM)}{nF} \quad (3.1)$$

In Eq. 3.1, m_{loss} corresponds to the mass loss, i is the current in amperes ($i = 5mA$), t is the time the current is sustained in seconds, and (AM) is the atomic mass of the oxidizing component. For this study the oxidizing component is the iron (Fe) in the rebars, hence $(AM) = 54.845g/mol$, n is the number of electrons lost per atom oxidized, for iron (Fe) the number of electrons is equal to 2, and F is Faraday's number ($F = 96485C$). Solving Eq. 3.1 for t and assuming uniform corrosion for different corrosion levels, the time of application was calculated for the total gauge length in the parent rebar specimen. The estimated times to achieve the corrosion levels are shown in Table 3.1.

Table 3.1 Accelerated corrosion times for the total length in parent specimen of a 19 mm (0.75 in) rebar

Corrosion Level (CL)	Mass loss (g)	time (days)
5%	57.6	16
10%	115.3	31
15%	172.9	47
20%	230.5	63
25%	288.1	78

After the accelerated corrosion is performed, the corrosion products from the bar are removed via a hydrochloric acid application. The acid removes imperfections on the surface and allows the placement of the instrumentation on the surface of the reinforcing steel bar.

3.2 Tension Tests

The tension tests were performed to evaluate differences in the stress-strain behavior of corroded reinforcing steel with those found in the literature. In addition, the data obtained from these tests served as an input to the analytical model. The tension tests were performed in accordance with the ASTM A370 standard, which specifies the loading procedure and the gauge lengths.

3.2.1 Tension Test Procedure

The tension tests consisted of:

1. Placing the rebar in the universal testing machine
2. Pulling the rebar in tension
3. Recording the load and the strain on the rebar

The strains were captured through the use of LED markers from the Optotrack Certus HD system. The gauge length between the LED markers was 2 inches as is specified in the ASTM A370 standard. Fig. 3.7 shows an example of the test setup. The stress was calculated based on the load reading from the UTM machine and divided by the measured area of the corroded rebars.



Figure 3.7 Tension test setup

3.2.2 Testing Parameters

The results obtained from the tension tests were valuable to understanding the change in the stress-strain relationship, the yield strength, and ultimate strength of corroded rebars. These values were obtained as outlined in ASTM A370, and are summarized below.

Yield Strength: Yield strength is the stress at which a material exhibits a specified limiting deviation from the proportionality of stress to strain. To determine the yield strength, the offset method was used to obtain this value.

Ultimate Strength: Ultimate strength is calculated by dividing the maximum load the specimen sustains during a tension test by the original cross-sectional area of the specimen.

Uniform Axial Elongation: The uniform elongation is the increase in length of the gauge length, expressed as a percentage of the original gauge length. The uniform elongation must be measured away from the necked region of the rebar.

Regression analysis of the results helped update the equations that correlate these parameters to the corrosion level, and yielded an updated form of Eq. 2.6. The outcomes of the tension tests were used as input for the analytical model in Chapter 5.

3.2.3 Test Matrix

A total of 3 tension tests per corrosion level were envisioned for each corrosion level from 0% - 20%. The specimens were labeled in accordance with the following format:

CL- (Corrosion level in %) *-T-* Subset specimens (initial specimen_final specimen)

It must be noted, as will be shown in the results in Chapter 4, that a specimen for CL=15% did not reach the intended corrosion level, mainly due to a faulty weld between the stainless steel wire and the specimen. The intended test matrix is presented in Table 3.2.

Table 3.2 Tension test matrix

Parent specimen label	Target CL (%)	Initial mass (g)	Subset specimen label
CL5-T-1_3	5	1260.8	CL-5-T-1
			CL-5-T-2
			CL-5-T-3
			CL-10-T-1
CL10-T-1_3	10	1244.0	CL-10-T-2
			CL-10-T-3
			CL-15-T-1
CL15-T-1_3	15	1251.2	CL-15-T-2
			CL-15-T-3
			CL-20-T-1
CL20-T-1_3	20	1251.2	CL-20-T-2
			CL-20-T-3

3.3 Buckled Bar Tension (BBT) Tests

One of the limit states considered in the seismic design of bridge columns is the fracture of buckled rebar. A recent test has been developed to determine the critical bending strain of buckled reinforcing steel [7], which is associated with the sudden fragile fracture of buckled longitudinal reinforcement of RC columns. The buckled bar tension (BBT) test simulates the bending and tension strain demands on a buckled bar to determine critical bending strain of buckled rebars.

3.3.1 Test Procedure

Barcley et al [7] developed a methodology to calculate local strains on a buckled bar using an LED optical sensor system [50]. Fig. 3.8 shows the basic concept of the BBT test.

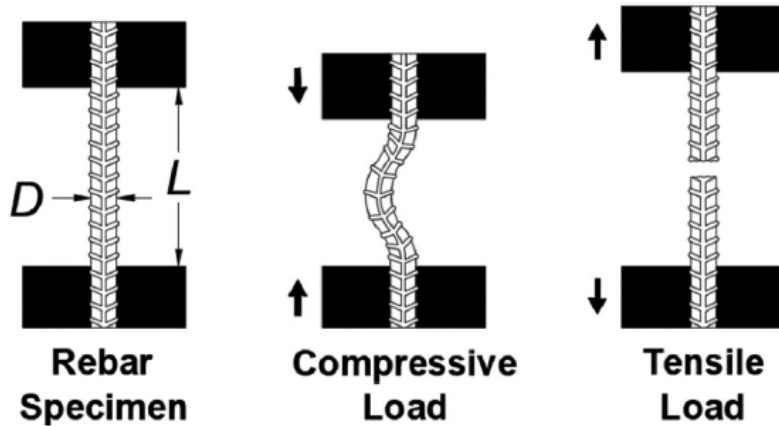


Figure 3.8 BBT test sequence[7]

The procedure to perform the buckled bar tension test consists of:

1. First, the rebar was placed in the universal testing machine (UTM), and the corroded rebar specimen was prepared with LED markers on the surface, such that the displaced shape of the bar could be measured.
2. Second, the rebar specimen was compressed to impose a bending strain of a prescribed level. Barcley et al showed that a fourth order polynomial can be fit to the LED sensors near the buckled region of the bar to obtain the displaced shape (w). The bending strain was calculated using solid mechanics principles. The curvature is the second derivative of

the displaced shape (w) for small displacements, which is calculated as:

$$\phi = \frac{\frac{d^2w(x)}{dx^2}}{\left[1 + \left(\frac{dw(x)}{dx}\right)\right]^{\frac{3}{2}}} \approx \frac{d^2w(x)}{dx^2} \quad (3.2)$$

If we assume that the bending is symmetric for the rebar then the strain in the extreme fibers of the rebar is calculated as:

$$\varepsilon_b = \phi \left(\frac{d_{bl}}{2} \right) \quad (3.3)$$

Combining Eq. 3.2, and Eq. 3.3, the bending strain can be expressed as:

$$\varepsilon_b = \frac{d^2w(x)}{dx^2} \left(\frac{d_{bl}}{2} \right) \quad (3.4)$$

An example of the calculation of the bending strain is shown in Fig. 3.9

3. Third, once buckled to the prescribed curvature, the bar is loaded in tension until fracture is observed
4. Finally, the process was repeated with a different bar for a different bending strain. After all the tests were performed, results from elongation at peak force were generated as in the example shown in Fig. 3.11. The critical bending strain was determined from the results obtained through BBT tests. The critical bending strain is defined as the point at which the uniform elongation reduces, resulting in a brittle fracture as shown in Fig. 3.10(b). Fig. 3.11 shows that for pristine rebars of grade 80 ksi steel the critical bending strain is $\varepsilon_{b,0} = 0.14$.

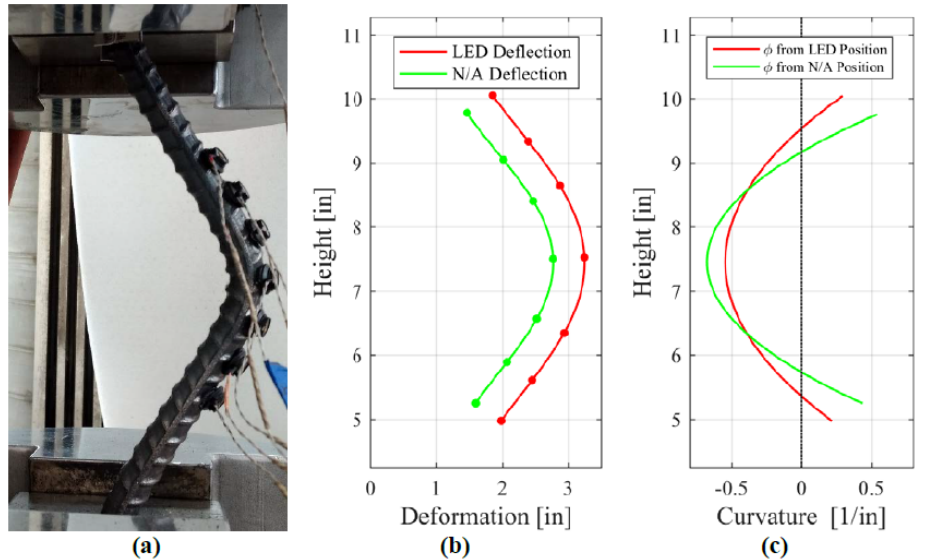


Figure 3.9 a) Picture of buckled bar; (b) Position of optical markers and adjustment to neutral axis;
(c) Calculation of curvature [6]

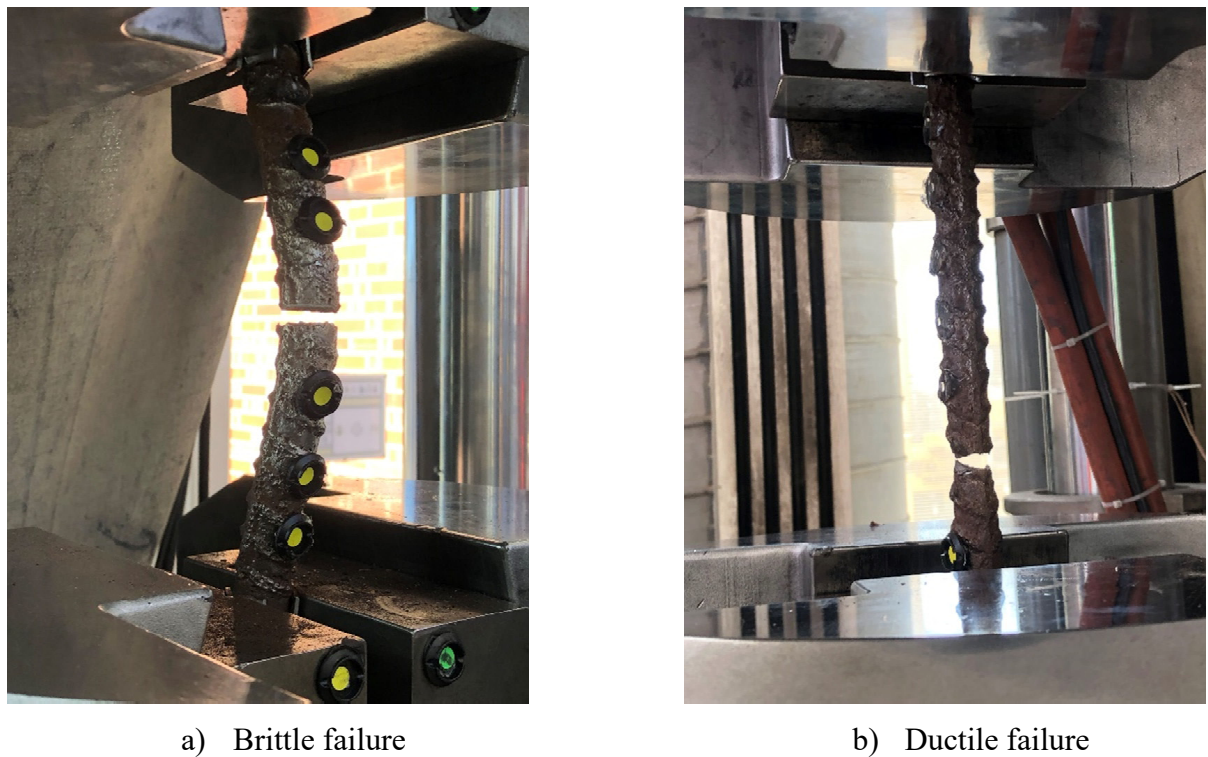


Figure 3.10 (a)Ductile rebar fracture; (b) Brittle rebar fracture

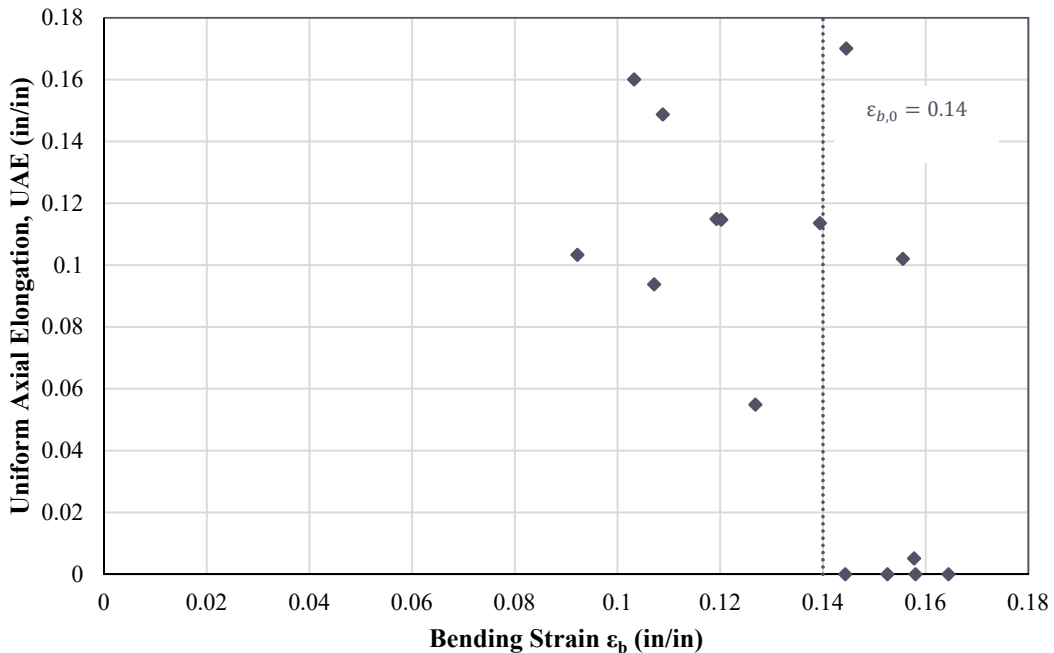


Figure 3.11 BBT results for pristine rebars [6]

3.3.2 Testing Parameters

The main parameter obtained from the BBT test was the critical bending strain. As previously defined, the critical bending strain defines the level of buckling a rebar can sustain before failing in a brittle manner under tension.

Maximum bending strain: This parameter was obtained at the sudden drop in elongation capacity of a bar is subjected to buckling and later pulled. At this level of bending strain, the type of fracture becomes brittle and thus no elongation of the specimen occurs.

3.3.3 Test Matrix

The BBT tests matrix deployed in this research is shown in Table 3.3. A total of 30 tests were performed, six tests for corrosion levels ranging from 0%-20%. The specimens were labeled in accordance with the following format:

CL-(Corrosion level in %)-BBT- Subset specimens (initial specimen_final specimen)

3.4 3D Scanning

The FARO Arm [18] was used to perform 3D scans of the gauge lengths on the corroded specimens. The procedure consisted of using a probe that sends a laser signal to the surface

Table 3.3 BBT test matrix

Parent specimen label	Initial mass (g)	Target CL (%)	Subset specimen label
CL5-BBT-1_3	1249.6	5	CL-5-BBT-1
			CL-5-BBT-2
			CL-5-BBT-3
			CL-5-BBT-4
CL5-BBT-4_6	1255.3	5	CL-5-BBT-5
			CL-5-BBT-6
			CL-10-BBT-1
CL10-BBT-1_3	1248.7	10	CL-10-BBT-2
			CL-10-BBT-3
			CL-10-BBT-4
CL10-BBT-4_6	1258.7	10	CL-10-BBT-5
			CL-10-BBT-6
			CL-15-BBT-1
CL15-BBT-1_3	1217.9	15	CL-15-BBT-2
			CL-15-BBT-3
			CL-15-BBT-4
CL15-BBT-4_6	1265.5	15	CL-15-BBT-5
			CL-15-BBT-6
			CL-20-BBT-1
CL20-BBT-1_3	1245.1	20	CL-20-BBT-2
			CL-20-BBT-3
			CL-20-BBT-4
CL20-BBT-4_6	1272.3	20	CL-20-BBT-5
			CL-20-BBT-6

of the specimens. The reflections from this laser were captured by the probe and the data was acquired in a computer for later post-processing. The probe used in this research had an accuracy of 0.018 mm. The system can be seen in Fig. 3.12. This probe is located at the the Center for Additive Manufacturing and Logistics (CAMAL) at NC State.



Figure 3.12 3D scan probe

The main use of this tool was to obtain an accurate reading of the diameter of the rebar, which provides an accurate reading of the tension and BBT tests results. The reader is referred to Chapter 4 to see the results obtained using this methodology. The data collected in this study can be used in future research to study the effect of imperfections using finite element analysis methods.

3.5 SEM observations

A total of six fracture surfaces were obtained from the BBT tests. Three fracture surfaces were from ductile failure, and the remaining three fracture surfaces were obtained from brittle failures. The collected fracture surfaces were observed under the Scanning Electron Microscope (SEM). In this study a Variable Pressure SEM (VPSEM) was used, since it is more suited to studying metals. The microscope used in this study can be observed in Fig. 3.13 which is located at the Analytical Instrumentation Facility (AIF) at NC State.

The SEM was used with two main objectives. These objectives were: (1) determine if there



Figure 3.13 VPSEM used in observations at AIF

is any change in the microstructural composition of the fracture surface, and (2) use the Energy Dispersive Spectroscopy (EDS) of the VPSEM to determine the presence of chlorides or oxides in the fracture surface.

3.5.1 SEM imaging

As explained previously SEM imaging provided this study with valuable information regarding the type of fracture that was observed at the microstructural level and determine any change in the micro structure of the fractured surface.

3.5.2 EDS Spectrum Analysis

EDS consists of the use of back scatter electrons (BE) to estimate the elements present in a given SEM observation and relies on the interaction of a source of X-ray excitation and the sample. This technology uses the principle that each element has a unique atomic structure allowing a unique set of peaks on its electromagnetic emission spectrum. From this analysis, a spectrum of the elements found for each observed sample was obtained.

3.6 Turned Down Corroded Rebars Tests

The bars that did not reach their intended corrosion level were repurposed and rebars prepared for a CL=20% to be turned down. The objective of turning down the corroded rebars, was to verify that the virgin material of the specimens does not change, but rather the results observed in the tension and BBT tests of corroded rebars correspond to a geometrical effect of the imperfections caused by corrosion on the surface of the specimens. To prove this, a set of three tension tests and six BBT tests were performed.



Figure 3.14 Turned down sample from CL=20% corroded rebar

3.6.1 Test Matrix

The test matrix shown in 3.4 summarizes the specimens used for these tests. Note that specimen CL10-TD-T-1_3* was originally specimen CL15-T-1_3.

Table 3.4 Test matrix for turned down specimens

Parent specimen label	Target CL (%)	Subset specimen label	Type of test
CL10-TD-T-1_3*	10*	CL10-TD-T-1	Tension
		CL10-TD-T-2	Tension
		CL10-TD-T-3	Tension
	20	CL20-TD-BBT-1	BBT
CL20-TD-BBT-1_3	20	CL20-TD-BBT-2	BBT
		CL20-TD-BBT-3	BBT
		CL20-TD-BBT-4	BBT
CL20-TD-BBT-4_6	20	CL20-TD-BBT-5	BBT
		CL20-TD-BBT-6	BBT

3.6.2 Testing Parameters

The testing parameters corresponded to the tension and BBT tests performed on the corroded rebars: (1) Yield Strength, (2) Ultimate Strength, (3) Uniform Elongation, and (4) Critical Bending Strain.

Chapter 4

Experimental Results from Corroded Rebar Specimens

This chapter presents the findings of the experimental program described in Chapter 4. The two types of tests are addressed independently. The chapter opens with a presentation of the corrosion levels obtained for the reinforcing steel specimens using two different approaches: 1) using the mass loss method and 2) using the geometric reduction of the effective diameter of the reinforcing steel via 3D scanning.

The chapter presents the tensile test results obtained from reinforcing steel at corrosion levels ranging from 0% - 20%. The corrosion levels are studied following the relationships between the yield strength, ultimate strength, and uniform axial elongation. The results from the tension tests are coherent with previous research, where it has been noted that as the corrosion level increases, the effective mechanical properties of the material change.

Similarly, for the buckled bar tension (BBT) tests, the results for corrosion levels ranging from 0% - 20% are presented. To the author's knowledge, this test is the first type of its kind performed on corroded reinforcing steel. The results show a decrease in the maximum bending strain as the corrosion level increases. These results will explain the observed reduction in displacement capacity of corroded reinforced concrete members.

In addition to tension tests and BBT tests, it was interesting to determine if there were any changes at the microstructural level and if a concentrated chloride attack induced the failure. Therefore, observations and data obtained from a scanning electron microscope (SEM) will be shown.

Finally, results from the tension and BBT tests on corroded rebar with removed surface imperfections are shown. The results show that the virgin material properties remained unchanged, and the results observed on corroded rebars are due to the geometrical imperfections induced by the corrosion.

Table 4.1 Corroded Level measured from mass loss in gauge length

Specimen ID	Initial mass (g)	Final mass (g)	Mass loss (g)	CL (%)
CL5-T-1_3	1260.8	1197.5	63.3	5.0%
CL5-BBT-1_3	1249.6	1199.8	49.9	4.0%
CL5-BBT-4-6	1255.3	1192.9	62.4	4.9%
CL10-T-1_3	1244.0	1122.6	121.3	9.8%
CL10-BBT-1_3	1248.7	1131.7	117.0	9.4%
CL10-BBT-4-6	1258.7	1143.1	115.7	9.2%
CL15-BBT-1_3	1217.9	1052.3	165.6	13.6%
CL15-BBT-4-6	1265.5	1095.4	170.1	13.4%
CL20-T-1_3	1251.2	1022.9	228.4	18.3%
CL20-BBT-1_3	1245.1	1018.3	226.8	18.2%
CL20-BBT-4_6	1272.3	1013.8	258.5	20.3%

4.1 Measurement of Corrosion Level

4.1.1 Mass loss method

The corrosion level of each specimen was measured after the time to corrode them had passed. The procedure consisted of removing the corrosion products from the surface of the specimens. The bars were then weighted and the mass loss was measured. Finally, the corrosion level is defined as the mass loss divided by the initial mass, as shown in Eq. 4.1.

$$CL = \frac{m_{initial} - m_{final}}{m_{initial}} \quad (4.1)$$

Table 4.1 shows the resulting corrosion level using Eq. 4.1. The resulting corrosion was significantly close to the target corrosion levels, and proved that the test setup successfully achieved the intended corrosion levels. In addition, one parent specimen (containing three specimen subsets) for CL=15% did not achieve the intended corrosion level, mainly due to a faulty welding of the stainless steel wire to the rebar. These bars were repurposed for tension tests of turned down rebars.

4.1.2 3D Scanning Method

The 3d scan Faro Arm was used to obtain 3D models of the corroded rebars to determine the effective diameter in the gauge length of the specimens. The effective diameter was used to determine the stress strain relationships and the bending strain in the rebars. Fig. 4.1 shows a sample of the 3D scans for CL=15% and CL=20%. This figure shows that the 3D scans

captured the imperfections on the surface of the rebars with a high level of precision.

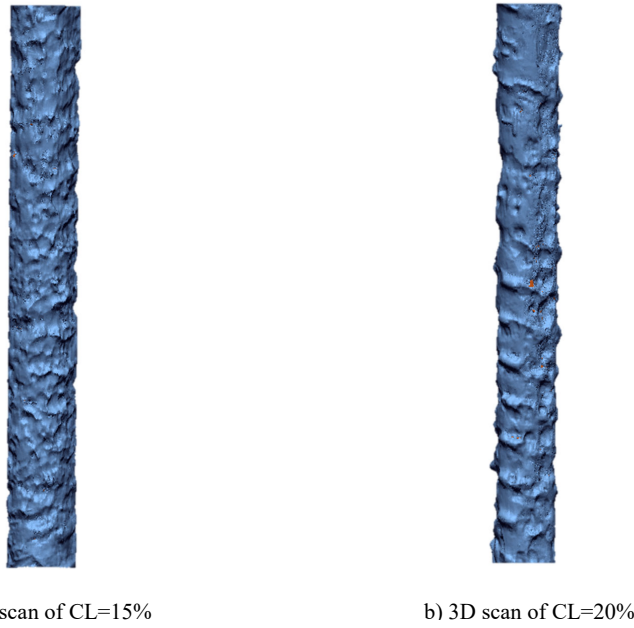


Figure 4.1 Sample of 3D scans obtained for CL=15% and CL=20%

From the 3D model, the volume (V) in the gauge length was obtained, and assuming a cylindrical volume, the effective diameter (d_{eff}) can be obtained as expressed in Eq. 4.2, where L_o is the length of the scanned gauge length. With the effective diameter, the corrosion level can be estimated as shown in Eq. 6.12, where d_o refers to the initial diameter. In the case of the specimens of this study, it corresponds to $d_o = 19mm(0.75in)$

$$d_{eff} = \frac{V}{\frac{1}{4}\pi L_o} \quad (4.2)$$

$$CL = 1 - \left(\frac{d_{eff}}{d_o}\right)^2 \quad (4.3)$$

The data collected from the 3D scans is summarized in Table 4.2. The results shown below demonstrate that the corrosion level (CL) measured using this approach matches well with the intended corrosion level.

Table 4.2 Corrosion levels (CL) measured from 3D scans in gauge length

Specimen ID	Volume (mm ³)	Height (mm)	Diameter (mm)	3D Scans CL (%)	Average CL (%)
CL5-T-1	47702	179	18.4	6.50%	
CL5-T-2	47388	176.5	18.5	5.80%	6.00%
CL5-T-3	44696	166.1	18.5	5.60%	
CL5-BBT-1	48389	178.2	18.6	4.70%	
CL5-BBT-2	48903	178.2	18.7	3.70%	4.80%
CL5-BBT-3	47876	178.6	18.5	5.90%	
CL5-BBT-4	48618	178	18.6	4.20%	
CL5-BBT-5	47984	178.3	18.5	5.60%	4.70%
CL5-BBT-6	48750	178.6	18.6	4.20%	
CL10-T-1	45281	178.8	18.0	11.10%	
CL10-T-2	44658	178.1	17.9	12.00%	11.30%
CL10-T-3	45359	178.1	18.0	10.60%	
CL10-BBT-1	45815	178.5	18.1	9.90%	
CL10-BBT-2	47595	182	18.2	8.20%	9.70%
CL10-BBT-3	45364	178.8	18.0	11.00%	
CL10-BBT-4	46486	178.9	18.2	8.80%	
CL10-BBT-5	45676	178.7	18.0	10.30%	10.00%
CL10-BBT-6	45353	178.2	18.0	10.70%	
CL15-BBT-1	43119	178.8	17.5	15.40%	
CL15-BBT-2	41474	169.7	17.6	14.20%	15.30%
CL15-BBT-3	35373	148.1	17.4	16.20%	
CL15-BBT-4	40485	168.1	17.5	15.50%	
CL15-BBT-5	38297	160.4	17.4	16.20%	15.00%
CL15-BBT-6	41103	166.4	17.7	13.30%	
CL20-T-1	40786	178.2	17.1	19.70%	
CL20-T-2	36577	163.4	16.9	21.40%	20.30%
CL20-T-3	40864	178.6	17.1	19.70%	
CL20-BBT-1	41038	178.9	17.1	19.50%	
CL20-BBT-2	37452	164.3	17.0	20.00%	19.50%
CL20-BBT-3	41186	178.5	17.1	19.00%	
CL20-BBT-4	39645	178.4	16.8	22.00%	
CL20-BBT-5	35364	158.4	16.9	21.70%	21.80%
CL20-BBT-6	39786	178.1	16.9	21.60%	

4.1.3 Comparison of Corrosion Level (CL) Measurements Mass Loss vs 3D Scanning Methods

Finally, the results from the mass loss approach and the 3D scans are compared in Fig. 4.2.4.2. The results from both approaches match very well, and the discrepancy from both could be due to more localized corrosion measured in the single specimens as opposed to those measured in the parent bar specimen, as was the case for the mass loss methodology. These results provided us with the opportunity to use the measured effective diameter from the 3D scans in the tension tests and BBT tests described in the following sections.

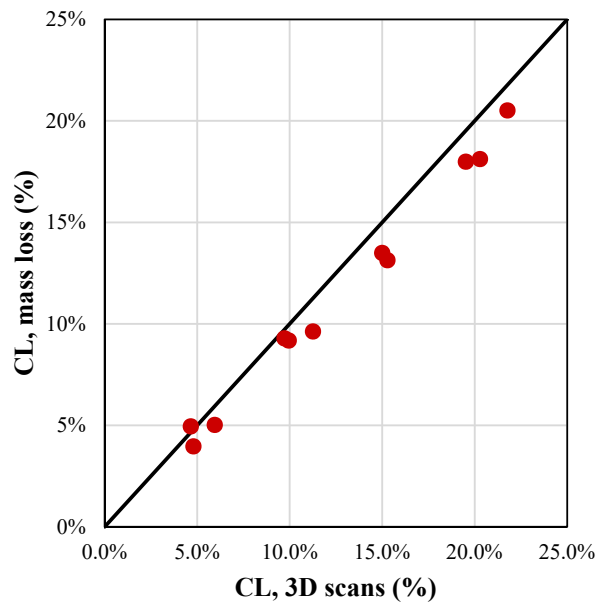


Figure 4.2 Corrosion level (CL) measured using mass loss method vs 3D scans

4.2 Tension Tests

Using the universal testing machine (UTM), the bars were loaded in tension. The data collected corresponded to the force from the UTM, while the Optotrack system was used to calculate the strain.

While there were no differences in the test procedure for corroded and uncorroded bars, it was observed that during the tests that the fracture usually occurred close to the grips, as shown in Fig. 4.3 b). The fracture near the grips was due to the sudden change in the cross-section and rebar imperfections. The strains used in this study correspond to the strain gauges adjacent to the fracture. The fracture of these tests was brittle in nature since the appearance of necking was not significantly observable, as shown in Fig. 4.3 c).

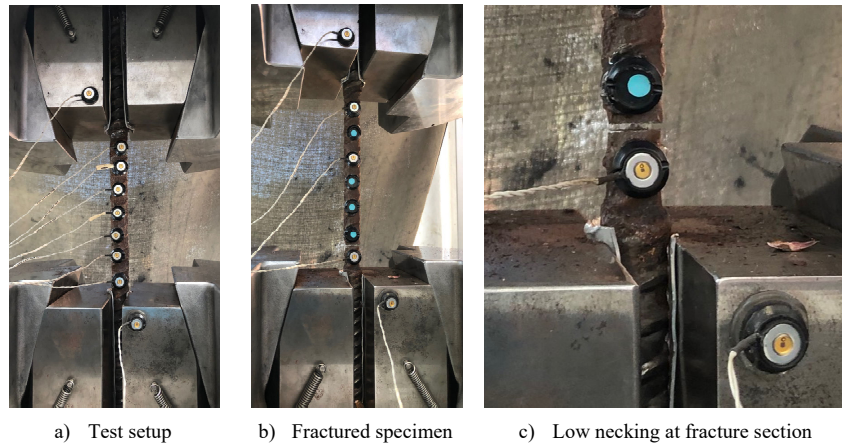


Figure 4.3 Tension test setup and fracture observations

A summary of the stress strain behavior for the corroded rebars is shown in Fig. 4.4. . In addition, the results obtained for pristine bars from research performed by Barcley et al. [6], and Overby et al. [51] are also shown. In general, from Fig. 4.4 it can be observed that as corrosion increases, the effective yield strength, ultimate strength, and uniform elongation tend to decrease. These variables are explained in more detail below.

4.2.1 Effective Yield Strength as a Function of the Corrosion Level

Effective yield strength is a mathematical convenience that considers the effect of imperfections on the observed global reduction of the yield strength. Fig. 4.5 shows the plot of the effective yield strength ($f_{y,e}$) versus the corrosion level (CL). The results show a linear relationship between the effective yield strength and the corrosion level. This is consistent with other studies

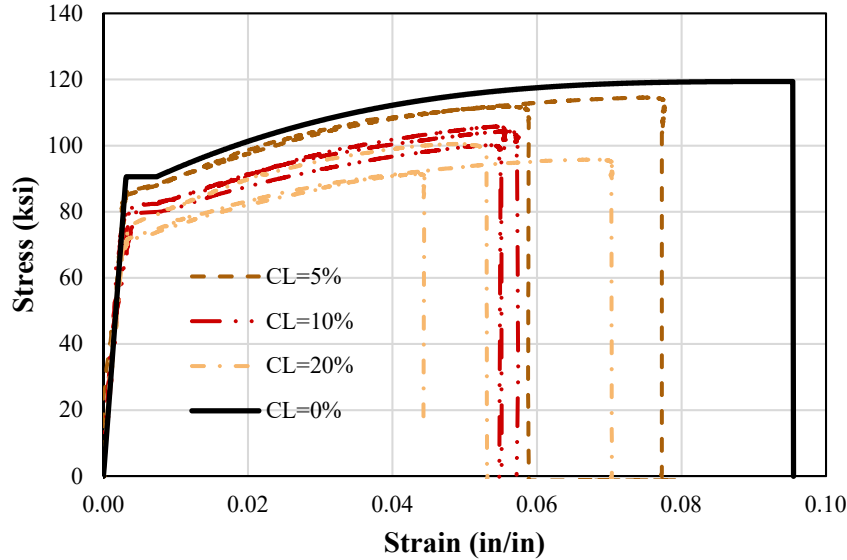


Figure 4.4 Tension test results at different corrosion levels

performed on other types of steel, such as the study done by Du et al [14]. The apparent reduction in effective yield strength is due to points of concentrated reduction in the geometry of the rebars, which act as stress risers near the area of fracture.

The linear trend observed between the effective yield strength and the corrosion level is expressed as:

$$f_{y,CL} = f_{y,o}(1 - 0.0075CL) \quad (4.4)$$

The proposed equation is compared to the model proposed by Du et al [14], replicated here as Eq. 4.5.

$$f_{y,CL} = f_{y,o}(1 - 0.005CL) \quad (4.5)$$

In Fig. 4.6, the Du et al model Eq. 4.5 and our proposed model Eq. 4.4 are compared against the experimental results. Overall it can be observed that the model by Du et al. [14] tends to over-predict the effective yield strength for corroded grade 80 rebars. Therefore, it is possible that there is correlation between the corrosion level and the grade of the rebar; however, the literature on corrosion for different grades of rebar is scarce.

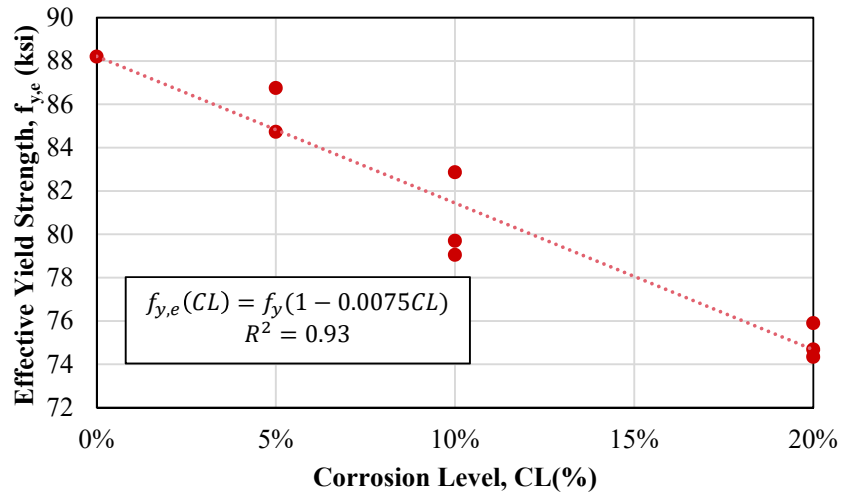


Figure 4.5 Yield strength as a function of corrosion level

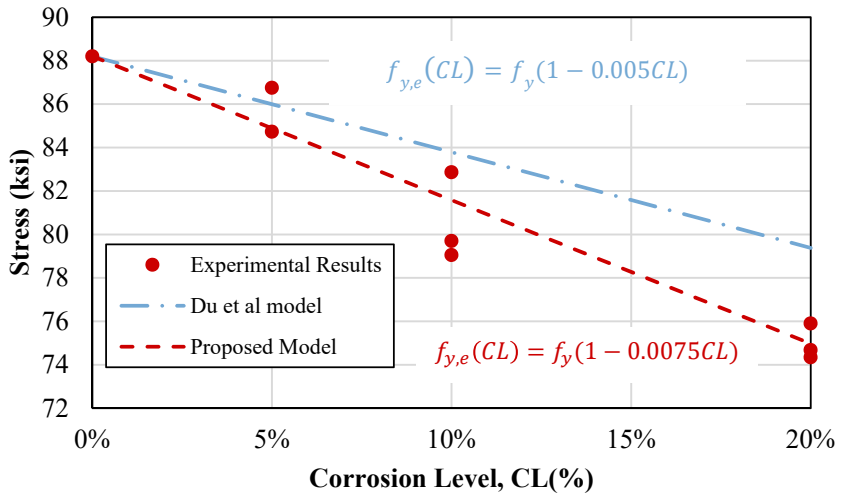


Figure 4.6 Comparison of proposed model and Du et al. model [14] for effective yield strength as a function of corrosion level

4.2.2 Ultimate Strength as a Function of the Corrosion Level

A similar trend was observed on the effective ultimate strength of corroded rebars. Past research has shown that the relationship between effective yield strength and effective ultimate strength tend to remain unchanged. In this study, that proved to be the case as well. Replacing, the initial yield strength (f_y) with the initial ultimate strength (f_u) in Eq. 4.4, the effective ultimate strength can be expressed as shown in Eq. 4.6. The proposed equation is plotted against the experimental results in Fig. 4.7. The proposed model predicts the relationship between effective ultimate strength and corrosion level well.

$$f_{u,CL} = f_{u,o}(1 - 0.0075CL) \quad (4.6)$$

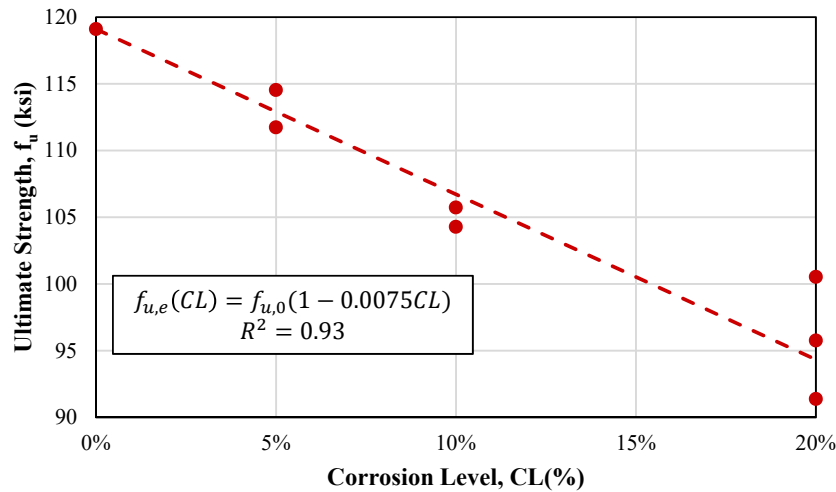


Figure 4.7 Ultimate strength as a function of corrosion level

4.2.3 Effect of Corrosion on Uniform Elongation

Another interesting result was observed on the uniform axial elongation (ε_u) property of the corroded rebars. As the rebar corrodes and develops more imperfections on the geometry of the rebar, the uniform axial elongation decreases. The reduction in the uniform axial elongation is linear from the uncorroded state (CL=0%) to a corrosion level of 10%, Fig. 4.8 shows this trend more clearly.

We propose the following model to predict the uniform axial elongation of corroded grade 80 rebars:

For corrosion level between 0% - 10%

$$\varepsilon_{CL} = \varepsilon_o - 0.05CL \quad (4.7)$$

For corrosion level larger than 10%

$$\varepsilon_{CL} = 0.045 \quad (4.8)$$

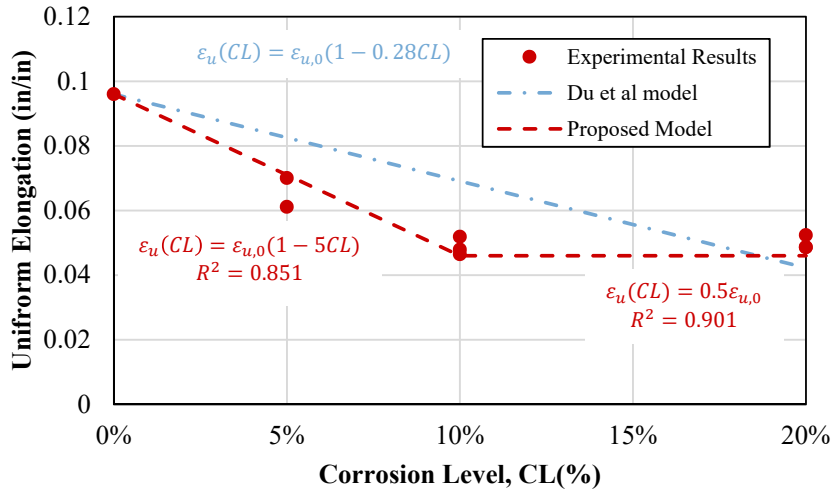


Figure 4.8 Comparison of proposed model and Du et al. model [14] for uniform axial elongation (ε_u) as a function of the corrosion level (CL)

4.3 Buckled Bar Tension (BBT) Tests

4.3.1 Summary of BBT Procedure

The buckled bar tension test is shown in Fig. 4.9 and consists of: 1) Loading the bar with the LED markers in the UTM machine, 2) Compressing the bars to a prescribed level of bending strain, 3) Loading the rebar in tension, and 4) Recording the type of fracture: Ductile or Brittle, see Fig. 4.10.

The data obtained from the BBT test was then processed and two parameters were obtained: 1) the critical bending strain, based on the curvature, and 2) the maximum uniform axial deformation (obtained from the measured stress strain curve). These two values are obtained as shown in Fig. 4.11. In the case of brittle failure, if the bar does not elongate compared to its



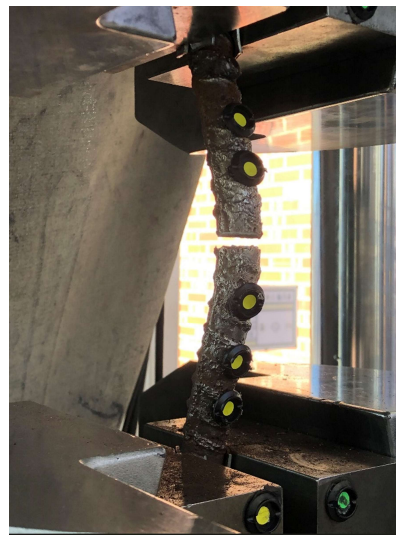
a) Test setup



b) Bar loaded in UTM



c) Buckled bar in compression loading



d) Fractured bar

Figure 4.9 General procedure of buckled bar tension (BBT) test

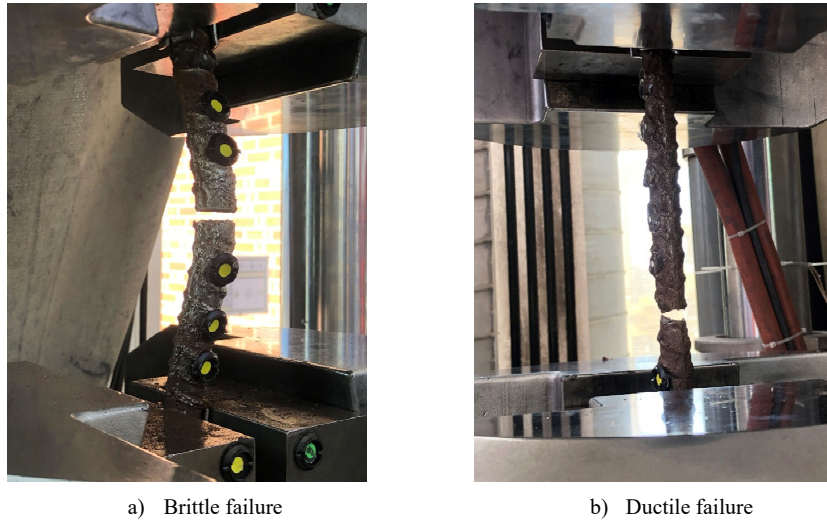


Figure 4.10 Type of failures in BBT tests

original length, the uniform axial elongation is assigned a value of zero.

4.3.2 Effect of Corrosion on Critical Bending Strain

The buckled bar tension test was applied to rebars with varying levels of corrosion ranging from 0% - 20%. For each corrosion level a total of 6 BBT tests were performed. From the BBT tests data, the bending strain versus the uniform axial elongation is plotted. As shown in Fig. 4.12 the critical bending strain is defined as the bending strain at which, after pulling the buckled bar in tension, the uniform axial elongation is zero, which is the case for brittle failures for brittle. The process described previously is repeated for each corrosion level. The bending strain versus uniform axial elongation for each corrosion level, along with the critical bending strain at a given corrosion level ($\varepsilon_{b,CL}$) are shown in Fig. 4.12. The benchmark value of pristine bars (CL=0%) was obtained from the study by Barcley et al [6]. In Fig. 4.13 it is noticeable that as corrosion level increases the maximum bending strain reduces. There is also a significant reduction in the uniform axial elongation for the ductile failures at all corrosion levels.

Plotting the critical bending strain versus the corrosion level as shown in Fig. 4.13, it can be seen that there is a linear relationship between both variables, similar to the results observed in the tension tests. The relationship between corrosion level and critical bending strain (ε_b) using linear regression can be expressed as shown below in Eq. 4.9.

$$\varepsilon_b(CL) = \varepsilon_o - 0.0045CL \quad (4.9)$$

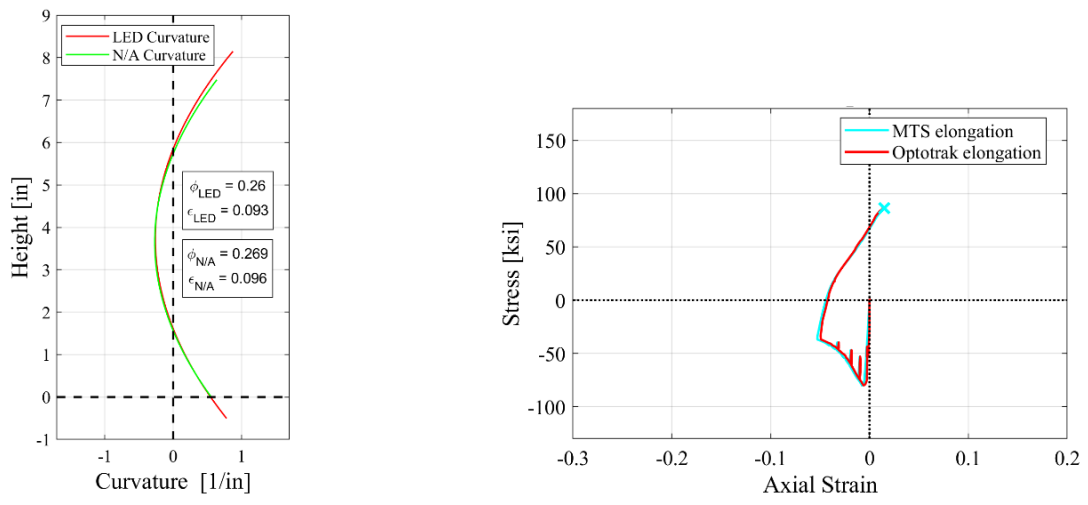


Figure 4.11 Obtaining critical bending strain

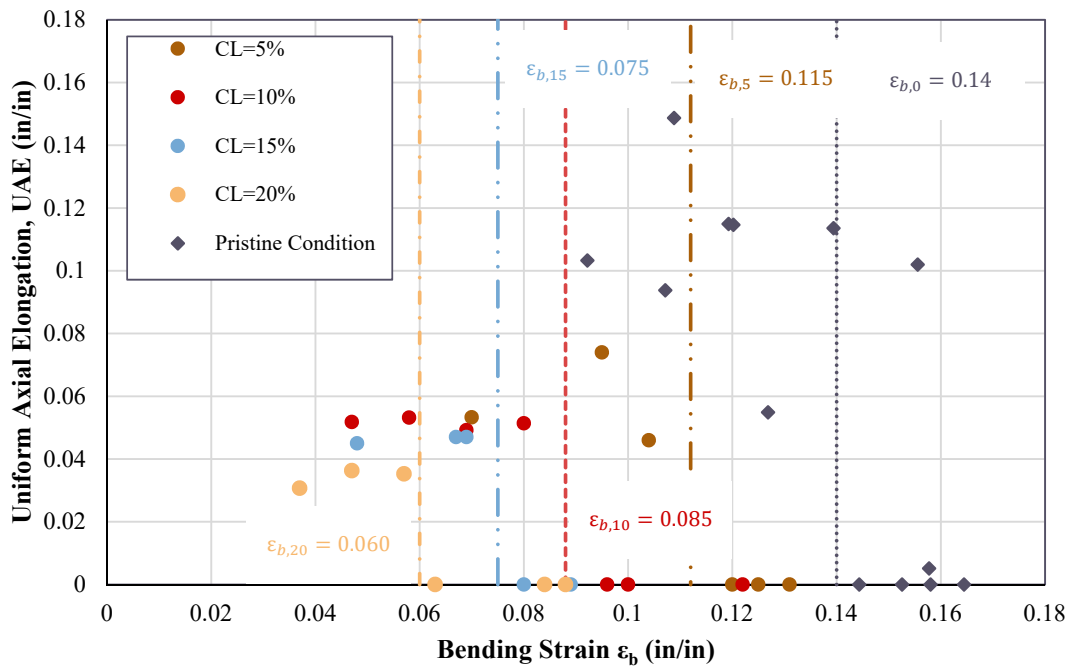


Figure 4.12 Bending strain at different corrosion levels

It is interesting to notice the sharp drop in critical bending strain capacity as corrosion increases. For CL=5%, There is a drop of about 20%; for CL=10%, the change is 60% of the pristine condition; and for CL=20%, that difference is more than 140% decrease in the critical bending strain. This is a significant outcome as it implies that corroded rebar will fracture at lower levels of bending strain, likely resulting in a reduction in member deformation capacity. Based on the reduction in the critical bending strain as the corrosion level increases and previous tests performed on corroded RC beams reported by Du et al. [14], and on RC columns as shown by Ma et al. [35] and Meda et al. [41]. Their studies showed that at corrosion levels closer to 10%, the ductility is reduced, and the failures were brittle. While further tests on RC members are required, based on previous studies and the present research, a limiting value of corrosion level for serviceability is tentatively recommended at CL=10%.

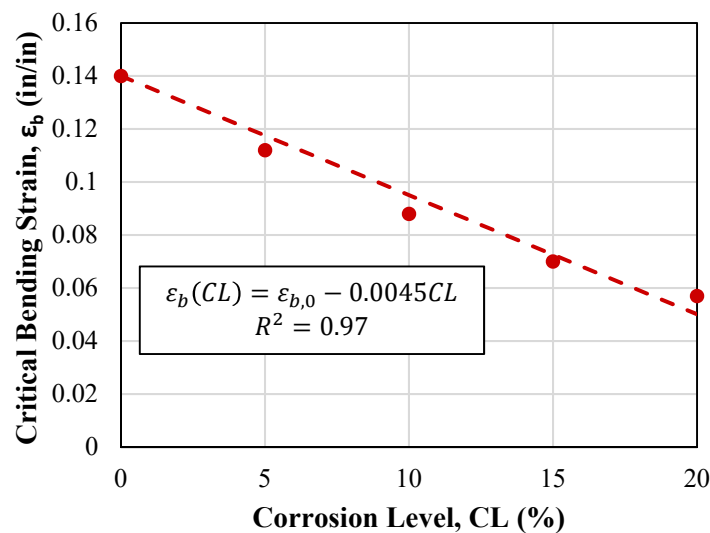


Figure 4.13 Maximum bending strain as a function of corrosion level

4.3.3 Effect of Corrosion at the Micro-structural Level

To study if there was any change in the microstructural behavior of the rebars as they corroded and explore if the chlorides induced fracture in the rebars at the point of fracture, the rebars' fracture surfaces were observed under a Variable Pressure Scanning Electron Microscope (VPSEM). Fracture surfaces from ductile and brittle failures were obtained at ductility levels of 5%-20%.

Fractography of BBT test specimens fracture surfaces

As previously observed in Fig. 4.10, at the macro level brittle fractures typically consist of flat fracture surface, and in ductile fractures, there is necking and rougher edges along the fracture surface. The observations at the macro level translate into similar observations at the microstructural level. To analyze the images obtained from the Scanning Electron Microscope (SEM), it is important to understand what brittle and ductile fractures in metals look like under the SEM. Fig. 4.14 summarizes the typical features for brittle fractures and ductile fractures. Brittle fractures present features that tend to promote flat surfaces. The two main types of brittle fractures are granular and cleavage. Ductile fractures, on the other hand, have dimple features, which is due to the extension of the fracture surface at the point where atomic bonds are broken.

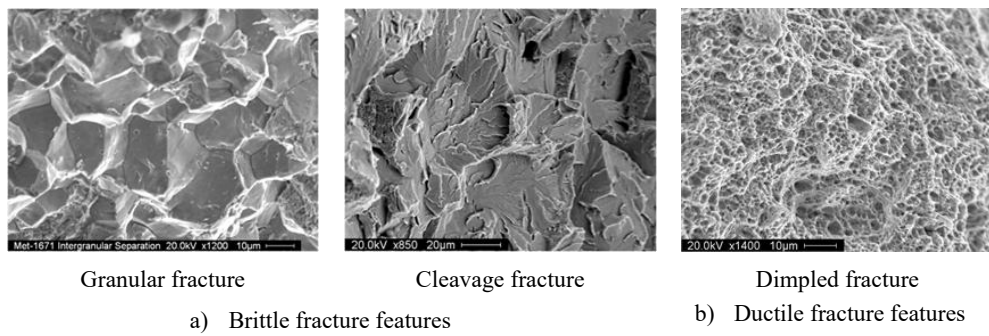


Figure 4.14 Basic features analysis of fracture surfaces in metals

Fig. 4.15 summarizes the observations performed on the fracture surfaces. While VPSEM images were obtained for each corrosion level, no substantial differences for brittle and ductile samples were observed as the corrosion level increased. Therefore, the observations performed on the CL=10% samples are shown here to represent all the observations. Three observations were performed at three points along the line that connect the point of initiation of the fracture and the point where the fracture ended. Fig. 4.15 shows three main sectors: 1) the point of initiation of fracture, 2) the midpoint, and 3) the extreme fiber opposite of the initiation of fracture.

Comparing the images obtained for the brittle and ductile response in Fig. 4.15, we can make the following observations. 1) At the point of initiation of fracture for the brittle and ductile surfaces, there is no difference in the behavior of the fracture surfaces observed, indicating that the point of initiation of fracture is always brittle in nature. This can be seen in the presence of flat surfaces. 2) At the midpoint we start to observe some differences in the brittle sample. Flat surfaces are still observed, but for the ductile sample, a mixture of flat surfaces and dimples typical of ductile surfaces are observed. This mixture of responses is similar to SEM observations

of fracture surfaces of fatigue fractures. 3) At the extreme fiber point, the difference between ductile and brittle is more prominent, since the ductile response has a predominant presence of dimples and the brittle response still shows flat surfaces. These results tell us the different mechanisms that occur between the brittle and ductile response, and correlate well with the observed behavior of the BBT tests.

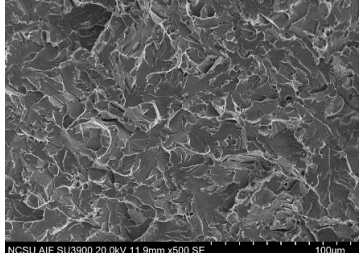
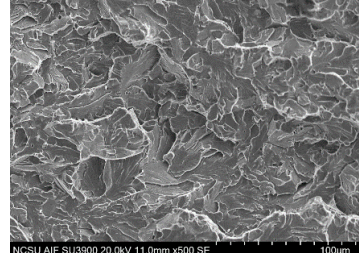
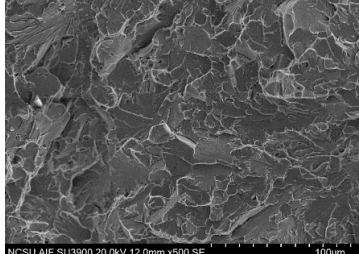
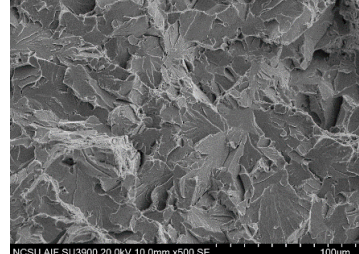
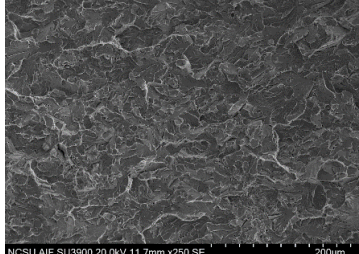
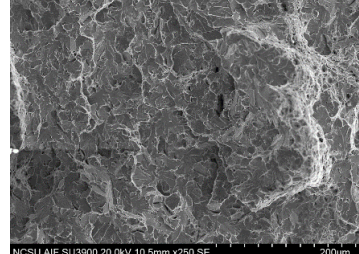
	Observation Location	Brittle failure	Ductile Failure
Fracture Initiation		 NCSU AIF SU3900 20.0kV 11.9mm x500 SE 100µm	 NCSU AIF SU3900 20.0kV 11.0mm x500 SE 100µm
Center		 NCSU AIF SU3900 20.0kV 12.0mm x500 SE 100µm	 NCSU AIF SU3900 20.0kV 10.0mm x500 SE 100µm
Opposite extreme		 NCSU AIF SU3900 20.0kV 11.7mm x250 SE 200µm	 NCSU AIF SU3900 20.0kV 10.5mm x250 SE 200µm

Figure 4.15 SEM observations for brittle and ductile failure at different positions of the fracture surface

An important feature from the images obtained in the VPSEM observations was river-like features observed through all the points of observations, as shown in Fig. 4.16. These types of features are typical of cyclic fatigue tests, which is coherent with the BBT tests since the bar is loaded in compression and then loaded in tension.

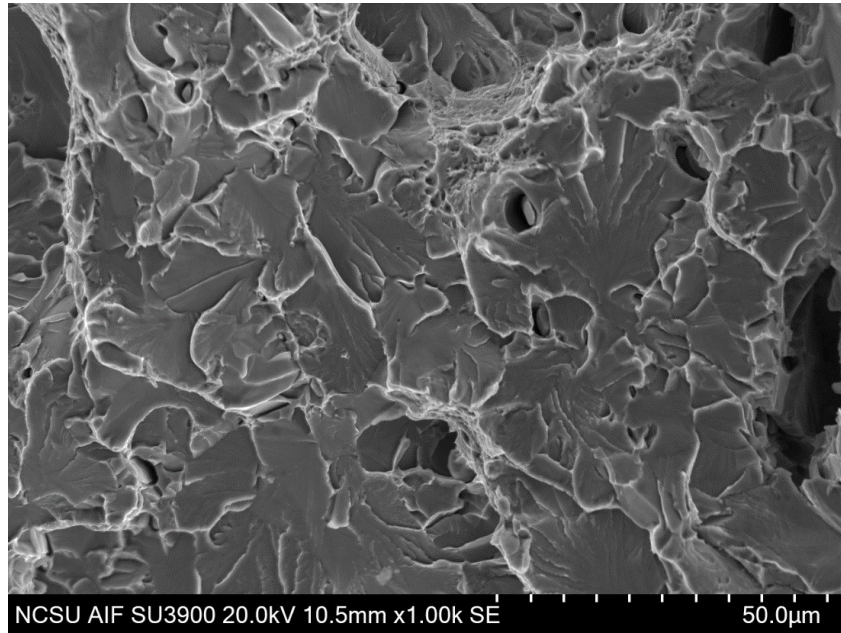


Figure 4.16 SEM cyclic loading features on fracture surface at 500x magnification

Spectrum analysis

In order to rule out the preclusion to failure due to inclusion of chlorides in the fracture surface, Back Scatter Electron (BSE) SEM images were evaluated through the use of spectrum analysis of the X-ray energy of the fracture surface. Fig. 4.17 shows the spectrum analysis of a brittle and ductile sample. The results obtained show elements that are expected on alloyed steel such as iron (Fe), carbon (C), chromium (Cr), manganese (Mn), and vanadium (V), among others. But no presence of chlorides (such as NaCl) or oxides (such as FeO) was detected. Thus, we are able to rule out the onset of fracture due to the presence of these compounds.

4.4 Tests on Turned Down Corroded Rebars

The tension and BBT tests show that the virgin material in the corroded reinforcing steel bars remains unchanged, as shown in Fig. 4.18, and Fig. 4.19. In Fig. 4.18, the yield and ultimate strength remain unchanged compared to reinforcing steel bars in pristine conditions. Similarly, in Fig. 4.19, the BBT test results are compared to pristine condition reinforcing steel bars with the ribs removed from the study by Barcley et al [6]. Again, it can be observed that the results match well. Therefore, it can be concluded that corrosion induces geometrical imperfections along the reinforcing steel bar surfaces, which then contribute to a perceived reduction in the performance of the corroded reinforcing steel bars, but the intrinsic material properties do not

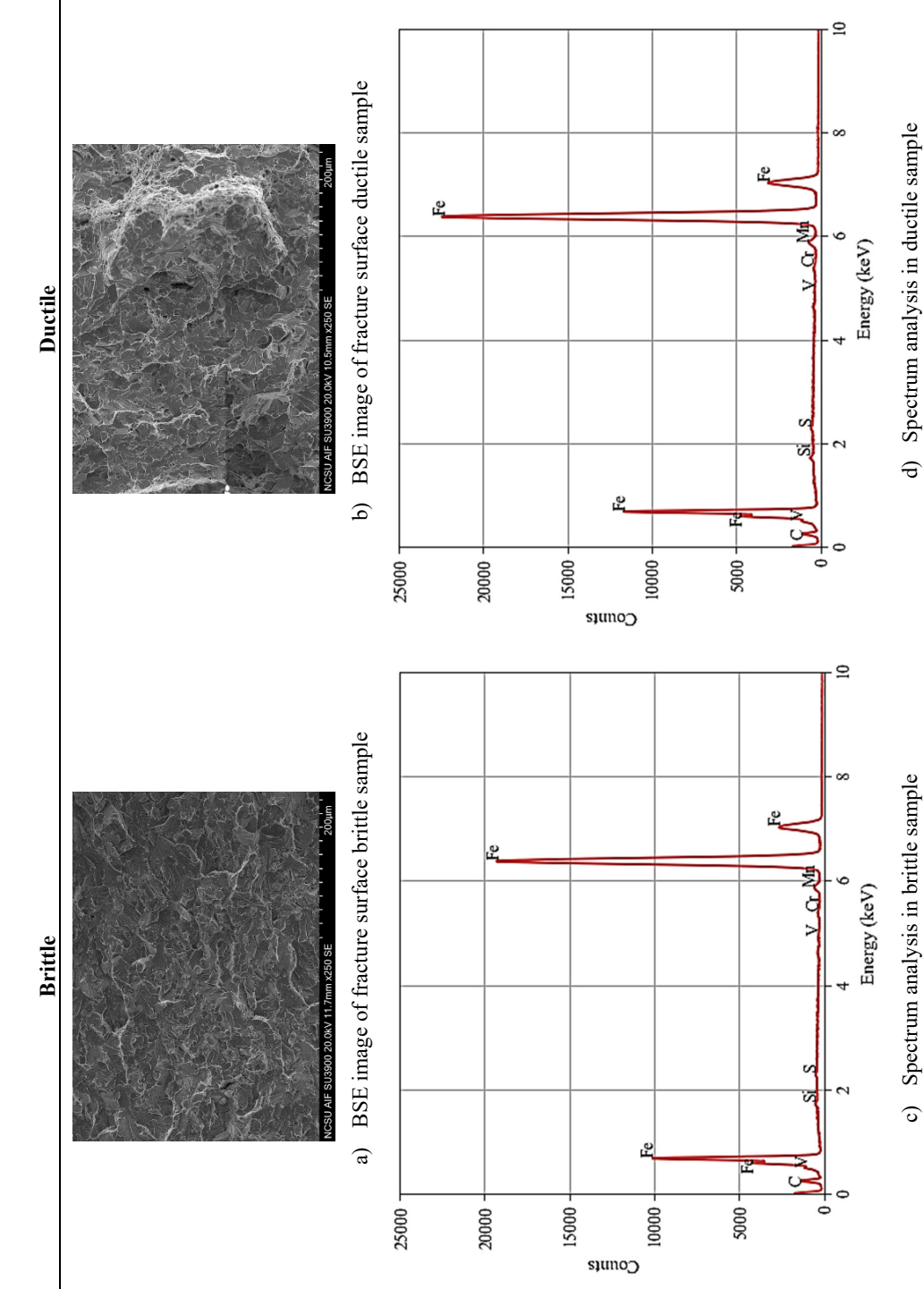


Figure 4.17 Spectrum analysis of back scatter electrons (BSE) imaging of fracture surface for brittle and ductile failures

change.

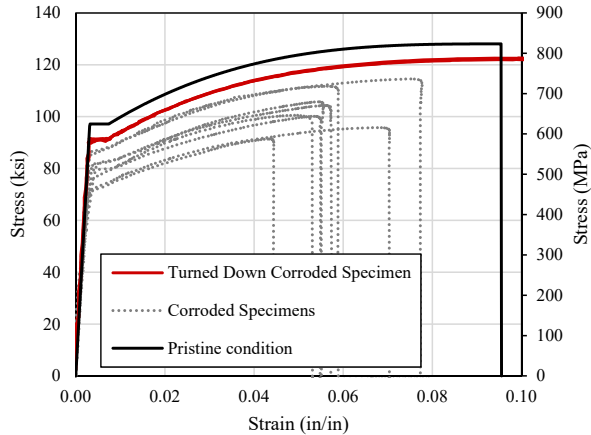


Figure 4.18 Tension tests on turned down specimens

4.5 Discussion of Results

The experimental program in this study found the following results:

The use of the effective diameter is a reliable tool to estimate the corrosion level based on geometrical measurements. The use of an effective diameter is especially useful in the case of field measurements taken from corroded rebars.

In order to conduct an accurate structural assessment, the in-situ properties of corroded reinforcing steel is essential. These properties include yield strength, tensile strength, uniform elongation, and the critical bending strain replicated here as Eq. 4.10 developed by Barcley et al [7]. This model was implemented in the analytical model presented in Chapter 5.

$$\varepsilon_t = \frac{\ln(\frac{\varepsilon_b}{0.001})}{\frac{300p}{f'cA_g} + \frac{0.7}{\rho_t}} \quad (4.10)$$

The use of SEM observations for specific goals proved very useful since this study determined that the microstructural integrity of the material is not changed or affected by any inclusion of chlorides in the fracture surface but instead shows a geometrical effect of the imperfections of the corroded surface of the rebar. These imperfections act as stress risers and fail the reinforcing steel at lower levels of critical bending strain. These results became more evident as we removed the imperfections. We can observe that both the tension tests and BBT tests show that the virgin metal in the reinforcing steel remains unchanged and unaffected by the corrosion.

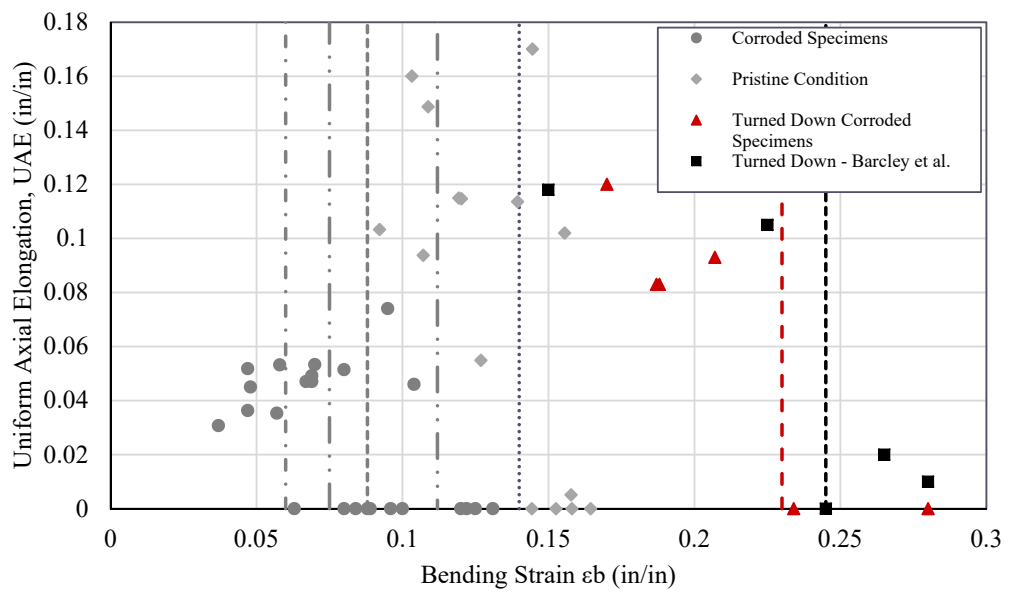


Figure 4.19 BBT tests on turned down specimens

Chapter 5

Analytical Program

This research developed an analysis procedure that incorporated the effect of cumulative damage in RC structures. While previous studies have obtained results using the Ang and Park Damage Index and obtained fragility curves using the assumptions of that model, this research evaluated the performance of structures using strain limit states since they provide a better estimate of the level of damage sustained by structures during an earthquake. Therefore, an analytical model of an SDOF cantilever RC column was subjected to a series of nonlinear time history analyses (NLTHA) that considered aging conditions and sequences of mainshock and aftershock. The analytical model incorporated the effective mechanical properties found in the experimental program.

The results from the analytical program showed that recorded ground motion sequences did not increase the strain demands. The maximum strain demands were achieved in all cases after a significant ground motion occurred. On the other hand, corrosion levels increased the demands and decreased the capacity of structures. Furthermore, the results show that as corrosion increases, a structure is more likely to achieve a given limit state for a prescribed earthquake intensity level. In addition, from the NLTHA results, it was determined that for a level of corrosion is CL=10%, the increase in the likelihood of reaching a limit state increased, which was congruent with the experimental program results. Therefore, a proposed maximum level of corrosion of 10% is recommended.

5.1 Modeling of Corrosion for Structural Analysis

The main objective of the analytical program is to determine the effects of corrosion on the demands of reinforced concrete columns. The results obtained in the experimental program have shown that corrosion affects the geometry of the surface of reinforcing steel bars by generating imperfections. The geometrical imperfections induced by the corrosion caused a reduction in

the effective mechanical properties of the reinforcing steel material. The effective mechanical properties are a mathematical convenience to evaluate corroded RC structures. In general, as corrosion increases, the effective material properties of the steel decrease, as well as the average bar diameter.

In order to incorporate the effect of corrosion in the structural analysis, it is necessary to reduce the bar diameter and the effective mechanical properties of the reinforcing steel bar. For this study, uniform corrosion is the only type of corrosion considered. Therefore, assuming uniform corrosion, the diameter is reduced per the following expressions:

$$d_{b,CL} = d_{b,o}\sqrt{1 - CL * 0.01} \quad (5.1)$$

Where CL corresponds to the corrosion level, and $d_{b,CL}$, $d_{b,o}$ are the reduced diameter and the initial diameter correspondingly.

Similarly, the mechanical properties of the reinforcing steel are modified with the expressions for effective yield and ultimate strengths found in the experimental program. The expressions proposed in Chapter 4 are replicated here for convenience:

$$f_{y,CL} = f_{y,o}(1 - 0.0075CL) \quad (5.2)$$

$$f_{u,CL} = f_{u,o}(1 - 0.0075CL) \quad (5.3)$$

In addition, the ultimate limit state uses the maximum bending strain to calculate the previous tension strain for buckled bar fracture. Since the analytical program evaluates different corrosion levels, Eq. 4.9 which defines the degradation of the maximum bending strain with corrosion level is used. Eq. 4.9 is replicated here for convenience as Eq. 5.4

$$\varepsilon_b(CL) = \varepsilon_o - 0.0045CL \quad (5.4)$$

5.2 Multiple Seismic Events

The evaluation of multiple seismic events is a topic that has been scarcely studied. However, their effects have been felt in numerous earthquake sequences, such as the Christchurch 2010, Umbria-Marche Earthquake 1997, and the Puerto Rico Earthquakes 2020. The hypothesis was that after a mainshock event, the accumulation of damage would restart in a minor seismic event and achieve a higher limit state than the limit state achieved in the mainshock.

This study determined that not all damage in structures is dependent on multiple events. The condition of the structure when the event occurs must also be quantified. Therefore, in this

study, the sequences of mainshock and aftershock (MS-AS) were evaluated at different levels of corrosion.

5.2.1 Earthquake Selection

The ground motions were taken from the NGA2 West Database of earthquake records provided by the Pacific Earthquake and Engineering Research Institute (PEER) [3]. This database consists of 2578 different earthquake events that characterize shallow crustal earthquakes. To study the effect of mainshock and aftershock sequences, only records that had aftershocks recorded were used. In addition, the parameters shown below were also used to filter the database to ensure that the records would produce inelastic displacement in the structures being analyzed.

- Moment magnitude $M_w \geq 5$
- $PGA > 0.04$
- $PGV > 1 \text{ cm/s}$
- $V_{s30} > 100 \text{ m/s} \& V_{s30} < 1000 \text{ m/s}$
- Lowest usable frequency is less than 1Hz
- $R_{rup} < 60 \text{ km}$

Figure Fig. 5.1 summarizes the results from filtering the data available in the PEER NGA West2 database which resulted in 456 aftershocks and 375 mainshocks. Fig. 5.1 shows the earthquakes as moment magnitude M_w vs rupture distance (R_{rup}). In addition, the spectral displacement is an important intensity measure used in this study. Therefore, the displacement spectrum for the ground motions used in this research are shown in Fig. 5.2. Figures Fig. 5.1 and Fig. 5.2, show that there is a good level of variability between the records and provide a wide range of ground motion properties.

5.2.2 Modeling of Mainshock-Aftershock Series for Corrosion

In order to analyze the structure of a sequence of mainshock and aftershock, it was necessary to clip together two ground motions. The process consisted of 1) selecting mainshocks and aftershocks from the same recording station and assigned to the same earthquake sequence, 2) the records were combined into a single file to run the sequence in order. Thus, a 4-second gap of zero acceleration was added between the mainshock and the aftershock. The 4-second gap between the mainshock and aftershock ground motions represents the situation in which the structure comes to rest after the first event. Although the time to reach the at-rest position

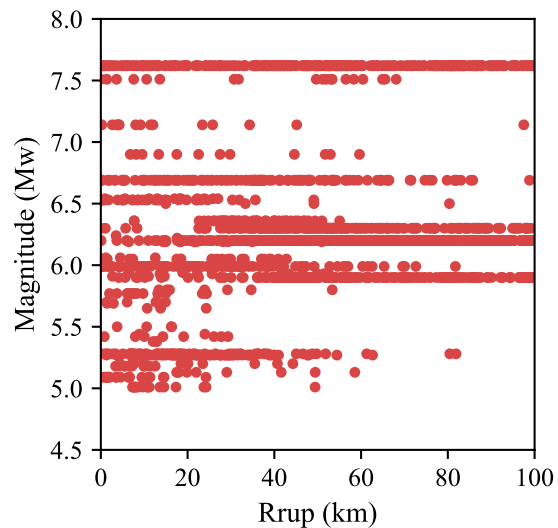


Figure 5.1 Mainshock selection from PEER NGA West2 database

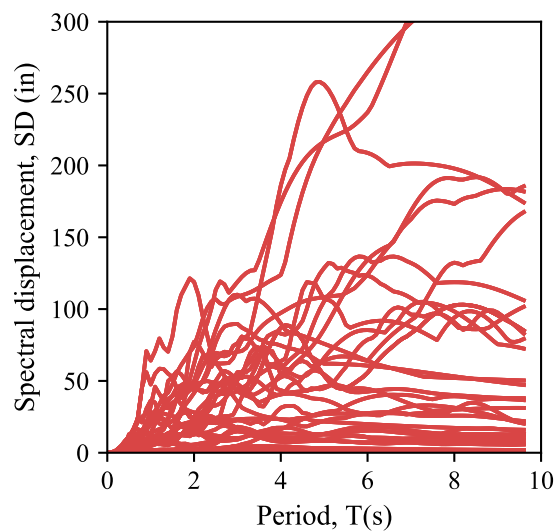


Figure 5.2 Mainshock selection from PEER NGA West2 database

can vary depending on the structural and ground motion properties, the recommendation from Raghunandan et al. [56] found that 4-seconds gave enough time for a structure to reach the at-rest position for most single degree of freedom systems while keeping computational costs low. A more significant time gap is possible, but it increases the computational cost significantly. An example of the resulting mainshock and aftershock sequence is shown in Fig. 5.3.

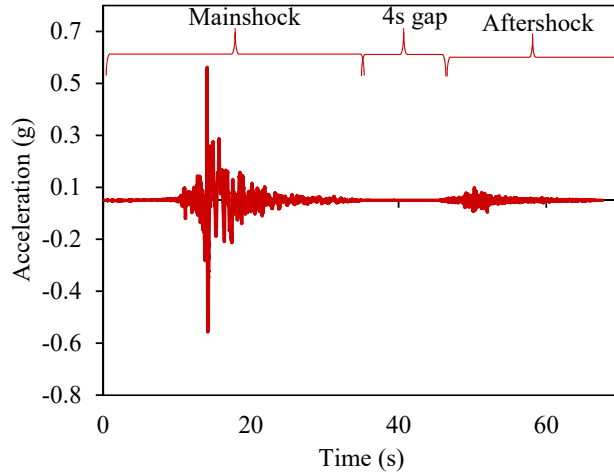


Figure 5.3 Mainshock selection from PEER NGA West2 database

5.3 Analytical Model

5.3.1 SDOF System: Cantilever Column

This study focused on the behavior of a single degree of freedom (SDOF) system representing a cantilever reinforced concrete column. The column is modeled as shown in Fig. 5.4. This structure is modeled in OpenSeesPy [40][79] using the *forceBeamColumn* element [61]. The *forceBeamColumn* element is used with two-point Gauss-Radau integration applied in the hinge regions, and two-point Gauss integration applied on the element interior for a total of six integration points [61]. The force-based formulation requires only a single element to represent the full nonlinear deformation of the member accurately, and the integration scheme selected prevents the loss of objectivity during the softening response while also providing integration points at the member ends [10],[61]. The element requires the length of plasticity to be defined at each end of the member, for which the tension-based rectangular plastic hinge length is

calculated using the following expressions [26]:

$$L_{pc} = k * L_{eff} + 0.4D \quad (5.5)$$

$$k = 0.2 * (Fu/Fy - 1) \leq 0.08 \quad (5.6)$$

$$L_{pt} = L_{pc} + \gamma * D \quad (5.7)$$

For single bending the parameter γ is:

$$\gamma = 0.33 \quad (5.8)$$

The two-point Gauss-Radau integration was applied such that each end node integration is weighted equal to the specified plastic hinge length, as illustrated in Fig. 5.5. In this figure, D is the diameter of the column, and c is the concrete cover. Therefore, strains recorded at the end sections represented accurate values even when deformation localizes to the ends from strain-softening behavior. For the case of the cantilever column, only one plastic hinge length is defined, and the opposite end is given an arbitrary unit length.

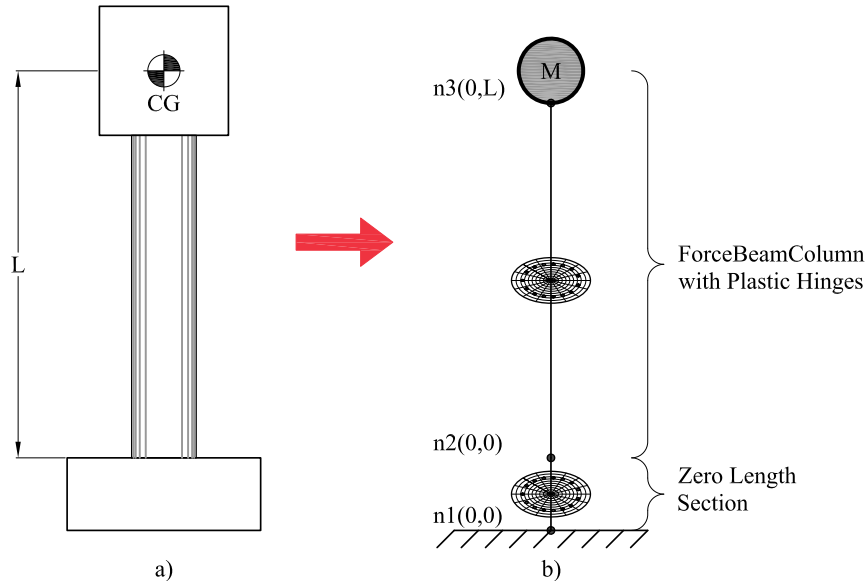


Figure 5.4 Structural Model: a) SDOF Column b) Fiber Model Representation

The cross section of the column is shown in Fig. 5.6. The column cross section is discretized with concrete and steel material fibers. Concrete fibers are modeled using the *Concrete01* mate-

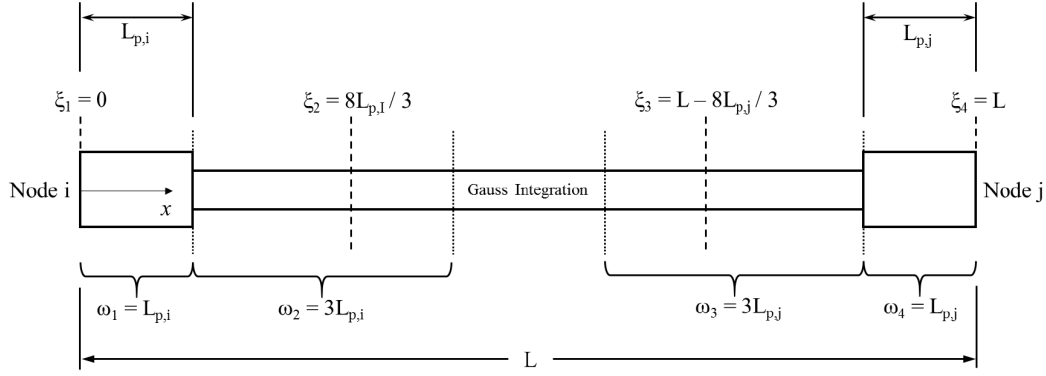


Figure 5.5 End point plastic hinge method [61]

rial, modified for confined material strength based on the Mander confined concrete model [39]. The *Steel02* material, based on the Giuffre-Menegotto-Pinto model [20] is used for the longitudinal reinforcement with recommended parameters ($b = 0.01$, $R0 = 20$, $cR1 = 0.925$, $cR2 = 0.15$).

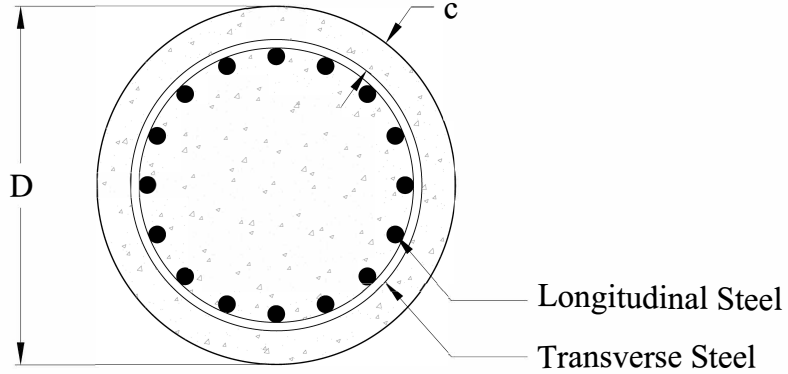


Figure 5.6 Section of the RC Column

5.3.2 Strain Penetration

The strain penetration considers the additional deformation due to anchorage of the reinforcement into the foundation, since tension strain in the reinforcement will drop to zero at a depth equal to the true development length of the rebar [55]. Experimental studies have generally reported that this end rotation contributes up to 35% to the lateral deformation of flexural members[78]. Therefore, it is important to incorporate it into the analytical model. A way to capture this effect is by using a zero-length section element implemented in the nonlinear fiber-

based analysis of concrete structures, which is available in the material library of OpenSeesPy as *BondSP1* [78]. This is the material model used for the steel fibers of the zero-length section element.

The required parameters for this model are:

- F_y Yield strength of the reinforcement steel
- S_y Rebar slip at member interface under yield stress (see Eq. 5.9)
- F_u Ultimate strength of the reinforcement steel
- S_u Rebar slip at the loaded end at the bar fracture strength a value of $35S_y$ is recommended [78]
- b Initial hardening ratio in the monotonic slip vs. bar stress response $b = 0.45$ is recommended [78]
- R Pinching factor for the cyclic slip vs. bar response $R = 1.01$ is recommended [78]
- d_b Rebar diameter
- $f'c$ Concrete compressive strength of the adjoining connection member
- α Parameter used in the local bond-slip relation and can be taken as $\alpha = 0.4$ in accordance with CEB-FIP Model Code 90 [12]

Bar slip is calculated as:

$$S_y(\text{in}) = 0.1 \left(\frac{d_b F_y}{4000 \sqrt{f'_c}} (2\alpha + 1) \right)^{\frac{1}{\alpha}} + 0.013(\text{in}) \quad (5.9)$$

5.3.3 Design Limit States

Design limit states are defined based on strains in the material since they can more accurately represent the different performance levels. Structure limit states are tension strains in the rebars or compression strains in the concrete core. It has been shown that tension strain limits are reliable indicators of structural damage [25]. The values used in this study for the performance-based analysis of reinforced concrete bridge columns are shown in Table 5.1. The serviceability limit states correspond to the compression strain at which concrete cover begins to crush and the peak tension strain, resulting in residual crack widths of approximately 1 mm. These limits are generally accepted as nominal limit states for RC members. The compression limit state for

damage control is defined by the expression shown in Eq. 5.10, and it refers to the compression strain in the confined concrete, at which fracture of the transverse reinforcement confining the core occurs [55]. This equation is obtained using the strain-energy balance between that absorbed by the confined core concrete and the capacity of the confining steel. The damage control limit state is defined by the strain at the onset of buckling, which can be expressed according to Eq. 5.11. This model demonstrated accurate predictions of the onset of bar buckling on physical tests in SDOF concrete column [25]. Finally, the ultimate limit state was taken from Barcley et al. [7]. The ultimate limit state is the previous tension strain before bar fracture due to bar buckling. The limit state can be expressed as shown in Eq. 5.12. For the case of corrosion, the effective material properties of the reinforcing steel bars were used, and in the case of the ultimate limit state, the equation that relates corrosion and the maximum bending strain was used. It must be noted that Eq. 5.10, Eq. 5.11 have been recommended for the AASHTO Guidelines for Performance Based Seismic Bridge Design [**eq:es'DamageControl**].

$$\varepsilon_{c,spiralyield} = 0.009 - 0.3 \frac{A_{st}}{A_g} + 3.9 \frac{f_{yhe}}{E_s} \quad (5.10)$$

$$\varepsilon_{s,BB} = 0.03 + 700\rho_s \frac{f_{yhe}}{E_s} - 0.1 \frac{P}{f'_c A_g} \quad (5.11)$$

$$\varepsilon_t = \frac{\ln(\frac{\varepsilon_b}{0.001})}{\frac{300P}{f'_c A_g} + \frac{0.7}{\rho_t}} \quad (5.12)$$

Table 5.1 Design limit states

Limit State	Concrete Limit State (in/in)	Reinforcing Steel Limit State (in/in)
Serviciability	0.04	0.015
Collapse Prevention	Eq. 5.10	Eq. 5.11
Fracture	N/A	Eq. 5.12

5.4 Comparison with Existing Physical Tests

The model used in this research was calibrated for the case of pristine conditions and the case of corroded columns. First, the calibration to a pristine condition column shows how reliable the results from the structural model are. Then the pristine condition model is modified with the corrosion model, as explained in section 5.1. Finally, the analytical model is compared to

the results from the physical test on corroded RC columns. The analytical model confirmed that the results obtained from the analytical program are reliable.

5.4.1 Pristine Condition Column

Goodnight et al performed a total of 30 circular RC columns quasi-static tests to evaluate strain limit states [25]. From this set of tests, a sample of one was taken to calibrate the analytical model. The test performed by Goodnight et al on an SDOF cantilever column shows similar geometry to that presented in Fig. 5.5. The parameters used in this large scale test were: diameter $D = 24.0\text{inch}$, height of the column $L = 8.0\text{ft}$, yield strength of steel $f_y = 83\text{ksi}$, ultimate strength of steel $f_u = 109\text{ksi}$, longitudinal steel volumetric ratio $\rho_s = 1.5\%$, transverse steel volumetric ratio $\rho_v = 1.0\%$, and strength of concrete at 8 days $f'_c = 6\text{ksi}$.

The analytical model used these parameters to compare the results from the model to the experimental results. The results from the analysis show good agreement with the experimental results as evidenced in Fig. 5.7. Thus, the results obtained from the model predict the overall system behavior and can be used to analyze other configurations of the structural model.

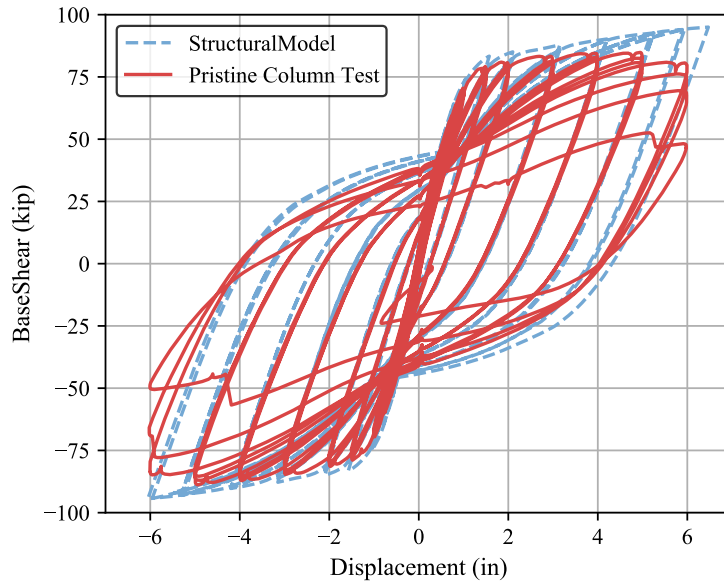


Figure 5.7 Force-Displacement results from experimental results [26] and analytical model

In addition, to verify the applicability of the strain limit states defined in the previous section, the limit states that correspond to bar buckling ($\varepsilon_{s,bb}$) and fracture of buckled bar (ε_t) were evaluated for this test. From Fig. 5.8 if the strain hysteresis is intercepted by each of the strain limits states, it can be observed that for the bar buckling limit state, the displacement

corresponds to a 5.5 inch, it is at this displacement in Fig. 5.7 that the first drop in the strength of the system is observed. Similarly, for buckled bar fracture, the displacement corresponds to 5.8, which is where there is a substantial drop in the strength of the column due to fracture of the buckled bar in Fig. 5.7. Thus, the analysis can capture the limit states in the structure.

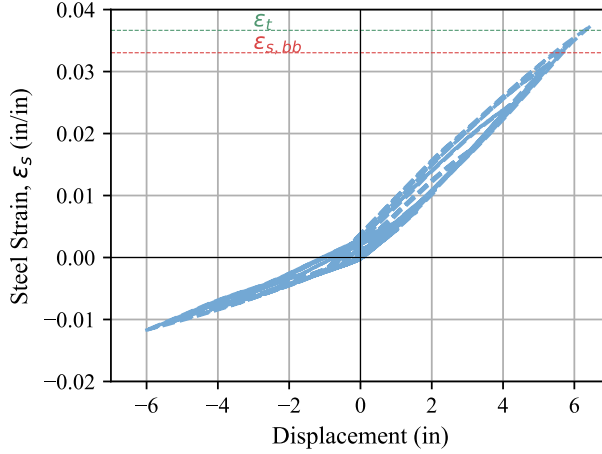


Figure 5.8 Strain hysteresis from experimental RC column in pristine condition

5.4.2 Accelerated Corrosion Column

For the case of RC columns with accelerated corrosion, Ma et al performed a series of quasi-static tests on RC columns with different corrosion levels and axial load ratios [35]. From their study, the test with a corrosion level $CL = 9.5\%$ was taken for calibration since the other tests presented in their study had excessively high axial load ratios which are not common in RC bridges. The results from the Ma et al test [35] were used to compare against the analytical model. The column had the following parameters: diameter $D = 260.0\text{mm}$, height of the column $L = 820.0\text{mm}$, yield strength of steel $f_y = 375.0 \text{ MPa}$, ultimate strength of steel $f_u = 572.3 \text{ MPa}$, longitudinal steel area ratio $\rho_l = 2.73\%$, transverse steel volumetric ratio $\rho_v = 1.0\%$, strength of concrete at 8 days $f'_c = 39.8 \text{ MPa}$, and axial load ratio of $ALR = 15\%$. Equation 2.6 is used to modify the material properties of the reinforcing steel and considers the effects of corrosion.

Figure 5.9 shows that the results obtained from the analytical model capture the response of the structure with reasonable accuracy up to a displacement of $\pm 33\text{mm}$. The observed discrepancies are due to the inability of fiber models to represent buckling in the longitudinal reinforcing steel and the lack of strain data and material quantification from the authors' study [35]. In addition, Ma et al. [35] did not report if bar buckling and bar fracture occurred during

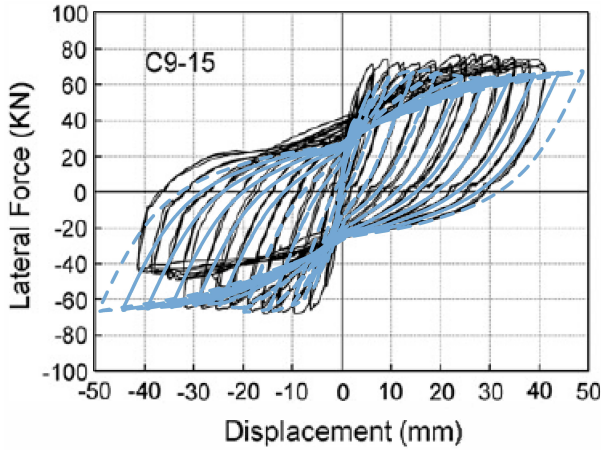


Figure 5.9 Force-Displacement results from experimental RC column with corrosion in longitudinal bar ($CL=9.5\%$) [35] and analytical model results (shown in light blue)

the test. However, the hysteresis curve shown in their study suggests that some damage limit state was reached.

In order to prove that Eq. 5.11 can predict buckling relatively close for corroded RC Columns, the strain at the extreme longitudinal bar from the analytical model is compared with the value obtained using the equation limit stateEq. 5.11. Using Eq. 5.11 the bar buckling limit state is calculated as ($\varepsilon_{s,BB} = 0.016$). Intersecting $\varepsilon_{s,BB} = 0.019$ with the strain hysteresis from the analytical model results shown in Fig. 5.10, the displacement that corresponds to this limit state was 36mm which is higher than the -33mm obtained from the test results. The value obtained using Eq. 5.11 is within 10% of the value obtained from the test results. Therefore, the analytical model results are appropriate for the scope of this research. The reasons for the differences might be related to the effect corrosion has on RC columns which were out of the scope of Goodnight et al. in the development of Eq. 5.11.

Finally, for the buckled bar fracture limit state, equation Eq. 5.4 and the effective mechanical properties expression Eq. 5.2 and Eq. 5.3 were obtained for the test data provided by [35]. The limit state calculated using Eq. 5.12 was $\varepsilon_s = 0.023$. The strain predicts the fracture of the bars reported by Ma et al. [35] at a displacement of -50mm, as shown in Fig. 5.10. While the result obtained from the analytical model developed in this research seems to predict with relative accuracy the performance of corroded RC columns reported by Ma et al. [35], ongoing research at NC State will further improve the estimation of the limit states for corroded RC columns.

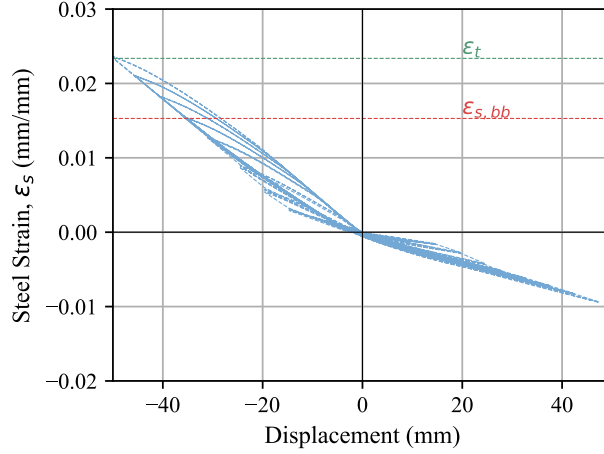


Figure 5.10 Strain hysteresis from experimental RC column with corrosion in longitudinal bar (CL=9.5%) results from analytical model

5.5 Intensity Measure: $Sd(T_{eff}, \xi)$

When relating ground motions to structural response parameters, selecting appropriate quantities that accurately capture their relationship is crucial. Krish [32] showed in a recent study that there is a good correlation between strain obtained from fiber modeling and first mode effective spectral displacement ($IM = Sd(T_1)$). On the other hand, peak ground acceleration (PGA) did not correlate well. These conclusions are congruent with the results found by Mackie et al. [37].

In this study, the intensity measure was improved further by correlating the strains to the effective period of the structure (T_{eff}) and the equivalent damping (ξ). These parameters are of substantial use in the Direct Displacement Based Design Methodology. The calculation of the effective period of the structure and the equivalent damping are explained below.

5.5.1 Effective Period Calculation

The process to calculate the effective period consists of obtaining first the effective stiffness of the structure. From the Non-Linear Time History Analysis (NLTHA) of a structure, the maximum displacement and force at the maximum displacement are obtained, as shown in Fig. 5.11. With these values, the effective stiffness can be calculated as:

$$K_{eff} = \frac{F(d_{max})}{d_{max}} \quad (5.13)$$

After obtaining the effective stiffness, the effective period can be calculated with the relationship for the period of a structure. The effective period is calculated as:

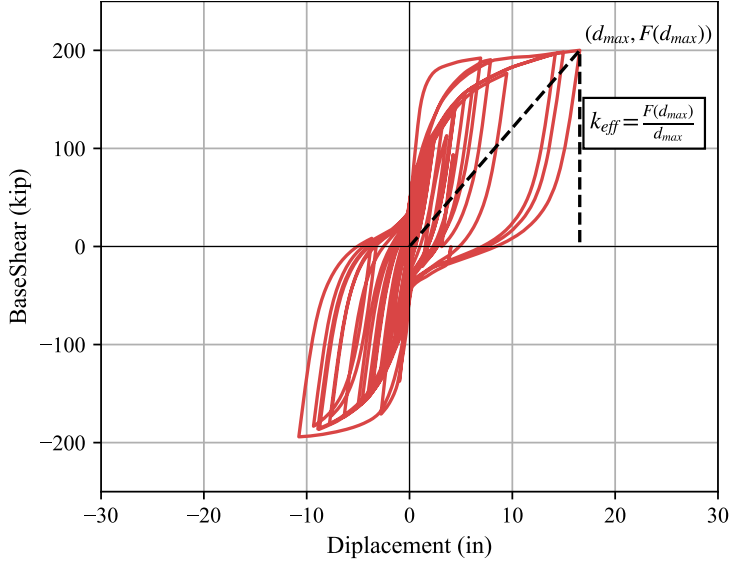


Figure 5.11 Calculation of effective stiffness (k_{eff})

$$T_{eff} = 2\pi \sqrt{\frac{M}{K_{eff}}} \quad (5.14)$$

In the analytical program the mass is calculated on the basis of the axial load applied to the structures.

$$M = \frac{P}{g} \quad (5.15)$$

5.5.2 Calculate $Sd(T_{eff}, \xi)$

After obtaining the effective period of the structure for each ground motion, it is possible to obtain the spectral displacement at 5% damping for each ground motion for a given effective period. Finally, the equivalent damping that the system reached for a given ground motion must be found to obtain the spectral displacement at the effective period and equivalent damping. Using the expressions for equivalent damping from Priestley et al. for circular columns in bridges, the equivalent damping can be expressed as:

$$\xi_{eq} = 0.05 + 0.444 \frac{\mu - 1}{\mu\pi} \quad (5.16)$$

The damping factor that corresponds to the equivalent damping is calculated as:

$$DF = \sqrt{\frac{0.07}{0.02 + \xi_{eq}}} \quad (5.17)$$

Equations 5.16 and 5.17 are part of the DDBD procedure outlined by Priestley et al [55]. Finally, the spectral displacement at effective period and equivalent damping can be expressed as:

$$Sd(T_{eff}, \xi) = DF \times Sd(T_{eff}, 5\%) \quad (5.18)$$

The methodology to obtain $Sd(T_{eff}, \xi)$ can be seen graphically in Fig. 5.12.

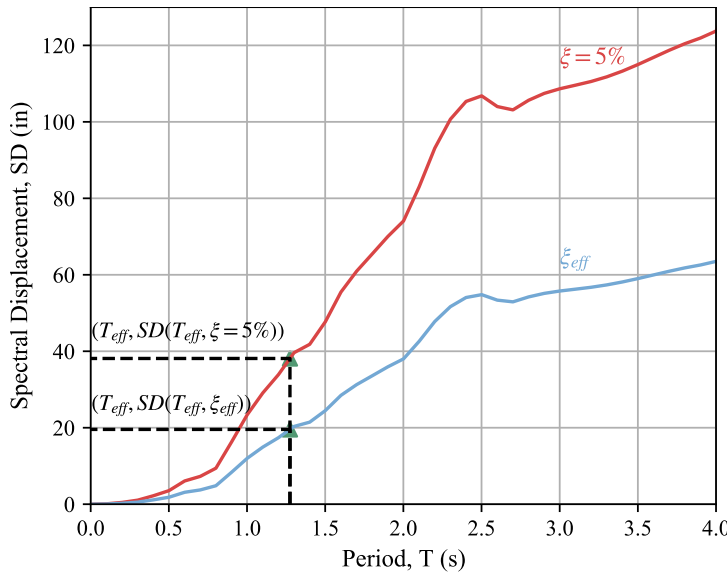


Figure 5.12 Calculation of spectral displacement at effective period at 5% damping $Sd(T_{eff}, 5\%)$ and at equivalent damping $Sd(T_{eff}, \xi)$

5.6 Analysis of Results Using MSA

The Multiple Stripe Analysis (MSA) procedure was used to fit fragility curves to the raw data, as described by Baker [5]. The MSA procedure consists of: First, at each intensity level, x_j , the probability, P , of observing z_j collapses in n_j observations is given by the binomial distribution, as shown in Eq. 5.19, where p_j is the probability of a single ground motion with $IM = x_j$ to cause the collapse of the structure, this is expressed as:

$$P = \binom{n}{z_j} p_j^{z_j} (1 - p_j)^{n_j - z_j} \quad (5.19)$$

Then, A collapse in the MSA methodology indicates that the specified limit state has been exceeded. Afterward, to consider the overall likelihood of observing multiple instances of this distribution across multiple IM levels, the product of this distribution is taken for each IM level considered and can be expressed mathematically as:

$$\text{Likelihood} = \prod_{j=1}^m \binom{n}{z_j} p_j^{z_j} (1 - p_j)^{n_j - z_j} \quad (5.20)$$

Finally, a lognormal cumulative distribution function (CDF) is used to define the fragility function and is substituted for p_j . The fragility function parameters are defined as the median of the fragility function, θ , and the standard deviation of $\ln(\text{IM})$, β (also referred to as the dispersion of IM). Hence, the solution is simplified by taking the natural logarithm of each side, and the product formulation in Eq. 5.20 is reduced to a summation that is computationally more efficient. The resulting function is expressed as:

$$\begin{aligned} \{\hat{\theta}, \hat{\beta}\} = \arg \max_{\theta, \beta} & \sum_{j=1}^m \left\{ \ln \left(\binom{n}{z_j} \right) + z_j \ln \Theta \left(\frac{\ln(x_j/\theta)}{\beta} \right) \right. \\ & \left. + (n_j - z_j) \ln \left[1 - \Theta \left(\frac{\ln(x_j/\theta)}{\beta} \right) \right] \right\} \end{aligned} \quad (5.21)$$

In Eq. 5.21, n_j , z_j , and x_j are all defined via the analysis results, and θ and β are the only unknowns. These two unknown parameters are then optimized using numerical solution techniques to find the values that produce the highest probability of observing the analysis results. The Excel spreadsheets and MatLab codes, developed by Baker [5], were used to produce the analysis of the results.

The MSA procedure was selected since it is well suited for unscaled ground motions, which are the types of ground motions used in this study. An example of curves fit the analysis data for the limit state of damage control for steel and corrosion level of 10% is shown in Fig. 5.13

5.7 Analytical framework

The analytical framework was established to obtain the change in the structure performance due to aging conditions and to evaluate the effect of seismic events on the achievement of strain limit states for single degree of freedom columns. This framework consisted of a program that performed and analyzed a series of nonlinear time history analyses (NLTHA). From these analyses, it was then possible to the effects of condition on the achievement of different performance

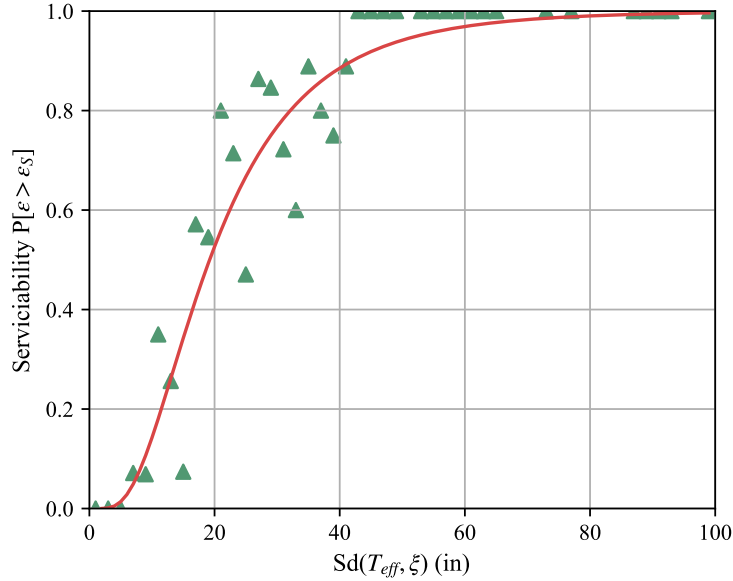


Figure 5.13 MSA analysis

limit states for a given seismic intensity. The proposed analytical framework process consisted of:

1. Read the cross sectional properties of the SDOF column from the database of columns(12 different cross sectional properties). Read the Aspect Ratio ($L/D = [4, 6, 8]$), read the axial load ratio ($ALR = [5\% - 20\%]$), read the level of corrosion ($CL = [0\% - 20\%]$).This resulted in 168 different columns.
2. Evaluate, the effective mechanical properties of the reinforcing steel for each of the corrosion levels evaluated using.
3. Perform the Non Linear Time History Analysis (NLTHA) of discrete ground motions and sequence of ground motions
4. Evaluate the results from the NLTHA to post-process the data and store it in a database for easy access in the MSA analysis.

The analysis matrix for the corrosion aging phenomenon that was analyzed in this study is shown in Table 5.2. A total of 54 Mainshocks and 405 Mainshock-Aftershock sequences were used in the analysis. The area or extent covered in the analysis corresponds to the range of variables that are common for RC columns in bridges.This analysis matrix resulted in a total of 36,000 analyses for the discrete ground motion analysis and 96,000 analyses for the sequences of ground motion case. To perform this large volume of analyses the Henry2 High Performance

Computer (HPC) at NC State was used to run the analyses in parallel. Table 5.3 shows the detailing and column diameters used in the analytical program.

Table 5.2 Analysis matrix

Parameter	Parameter	Range
Diameter of column	D	28-90 in
Column aspect ratio	L/D	4-8
Longitudinal ratio	ρ_s	0.01-0.04
Axial load ratio	ALR	5%-20%
Corrosion level	CL	0%-20%

Table 5.3 Detailing of columns for NLTHA

Diameter, $D(in)$	Bar diameter, $d_b(in)$	Number of bars, n_b	Trans. diameter, $d_t(in)$	Spacing, $s(in)$	ρ_l	ρ_v
48	0.875	30	0.625	2.5	0.01	0.01
48	1.000	45	0.625	2.5	0.02	0.01
48	1.125	54	0.625	2.5	0.03	0.01
48	1.250	56	0.625	2.5	0.04	0.01
72	1.000	52	0.75	2.5	0.01	0.01
72	1.125	82	0.75	2.5	0.02	0.01
72	1.250	96	0.75	2.5	0.03	0.01
72	1.750	72	0.75	2.5	0.04	0.01
90	1.000	80	0.75	2	0.01	0.01
90	1.125	128	0.75	2	0.02	0.01
90	1.250	150	0.75	2	0.03	0.01
90	1.750	114	0.75	2	0.04	0.01

5.7.1 Analysis Algorithm

In order to run the analysis efficiently, a program was developed to perform three main routines:
1) Main program: setting conditions, the geometry of the model, effective material properties,
2) Run the Non-Linear Time History Analysis, 3)Post-processing of data

The main program is shown in Fig. 5.14. This program has three main inputs the ground motion records, the geometry of the column, and the aging conditions. The aging conditions

relate include the corrosion level, the initial material properties, the axial load ratio, and the aspect ratio. After the inputs are selected, a nested loop goes through the different parameters. The basic flow consists of submitting the data to the NLTHA subroutine and the post-processor subroutine. Once the program goes through the subroutines, the data output from OpenSees is deleted to use the HPC resources efficiently. This process is repeated until all the variables have been evaluated and the program finishes.

The NLTHA subroutine consisted of a sequential process as shown in Fig. 5.15. First, the geometry of the model is established as per the model shown in Fig. 5.4. Then the material properties and the cross-sectional fibers are defined per the details shown in 5.3. Next, the recorders that store the analysis results throughout the NLTHA are set. Then the axial load is run and kept constant throughout the analysis. Finally, the NLTHA runs until it finishes.

The post-processor subroutine also consisted of a sequential process as shown in Fig. 5.16 and Fig. 5.17 . The main goal of this subroutine is to store the data related to the model, including the geometry and material properties used in the analysis. The post-processor calculates the limit states as explained in section 5.3.3. Then the spectral displacement at the effective period is calculated for the ground motion following the procedure explained in section 5.5. Finally, a collapse analysis for each limit state is performed in order to perform the multi-stripe analysis explained in the following section. All the relevant data is then stored in a database for further analysis.

5.8 Results from Analytical Program

This section presents the results obtained from a non-linear time history analysis (NLTHA) performed using OpenSeesPy [79]. The structures were subjected to a total of 54 earthquake mainshock records and where applicable 405 Mainshock-Aftershock sequences. The mainshock records displacement spectrum are shown in Fig. 5.2, and a list of the records is shown in Appendix C. The primary responses obtained from these analyses correspond to the maximum strain obtained for the different levels of corrosion. The structures were analyzed for the range of corrosion levels [0%-20%] in the longitudinal rebars.

5.8.1 Structural Response at Different Corrosion Levels

Figures 5.18 and Fig. 5.19 are presented as an example of the results obtained using NLTHA. The column shown in this example had the following details:

- Diameter, $D = 48\text{in}$
- Aspect ratio, $L/D = 4$

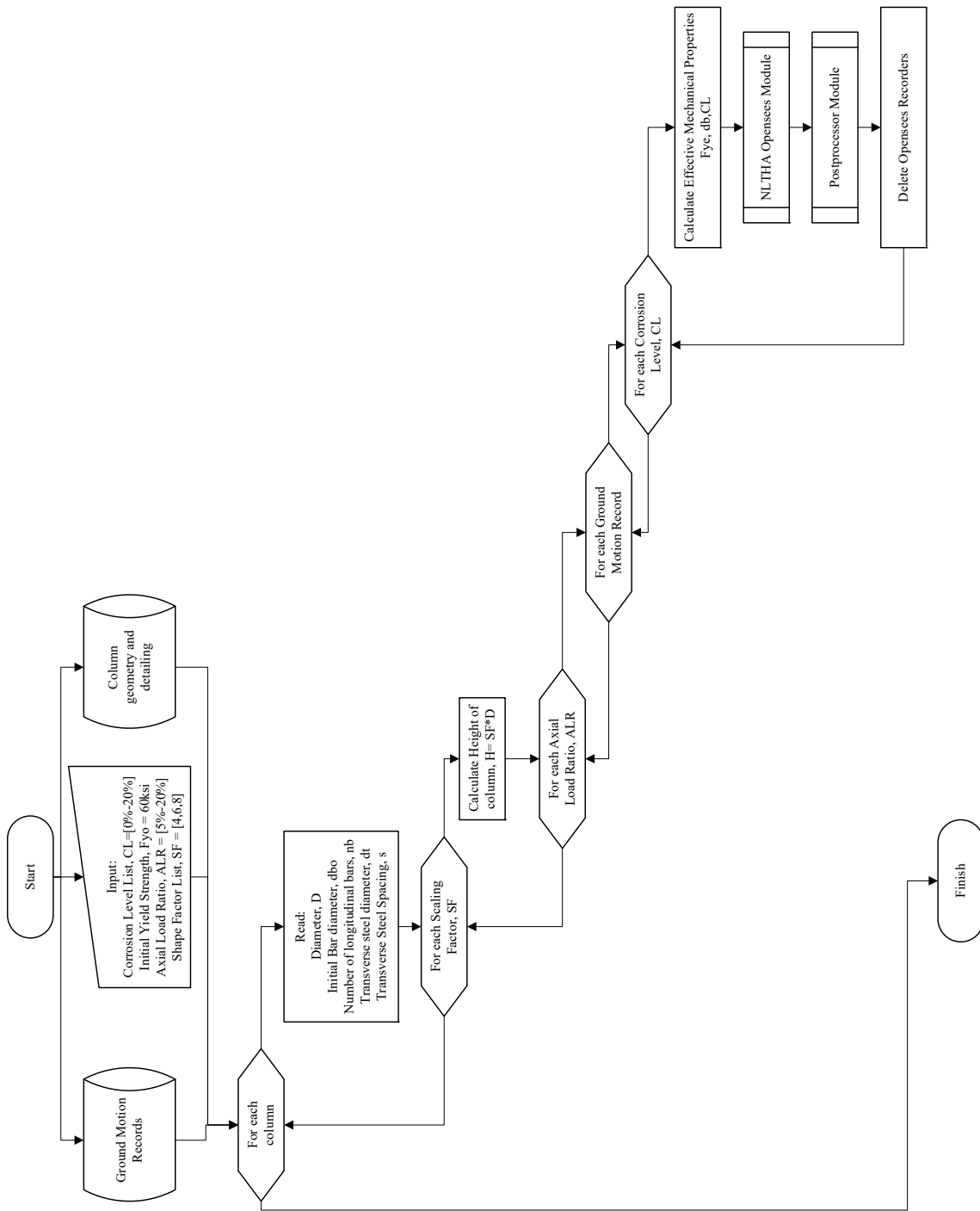


Figure 5.14 Main Flow-Chart

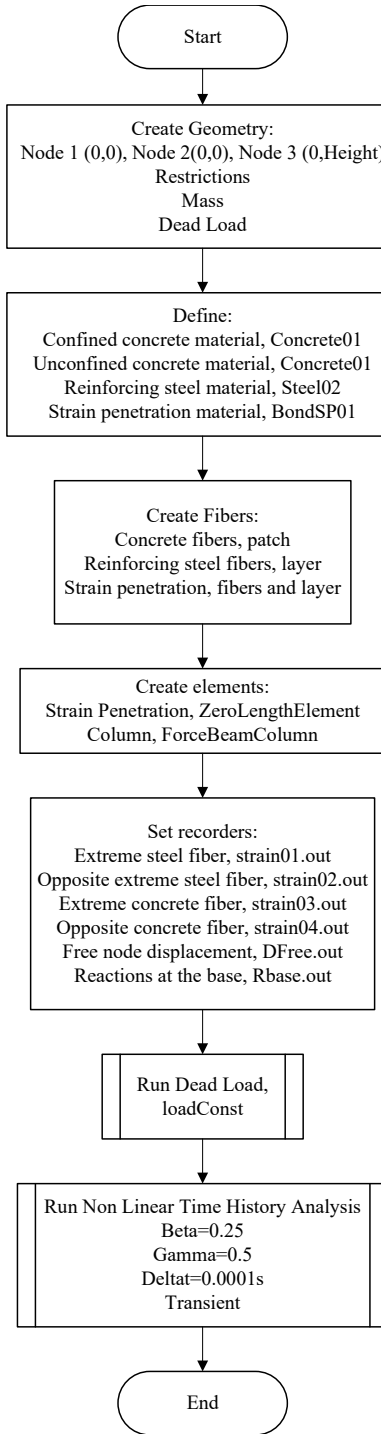


Figure 5.15 NLTHA Flow-Chart

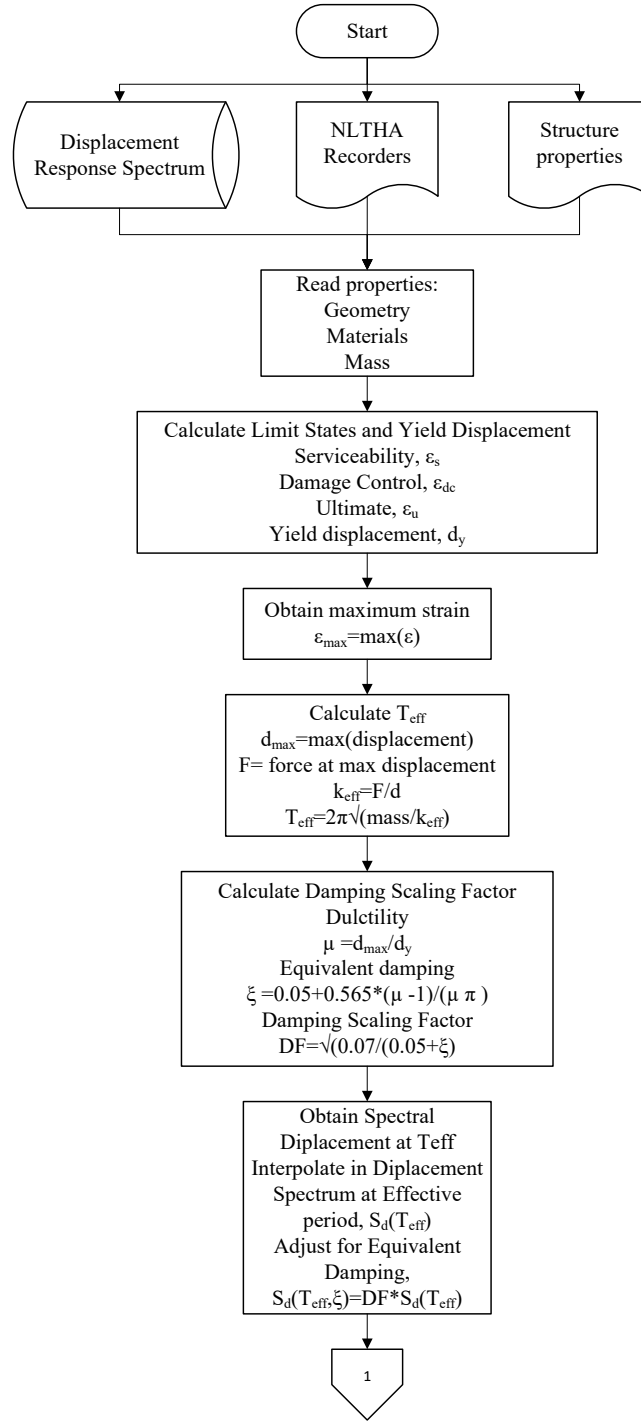


Figure 5.16 Post-processor Flow-Chart

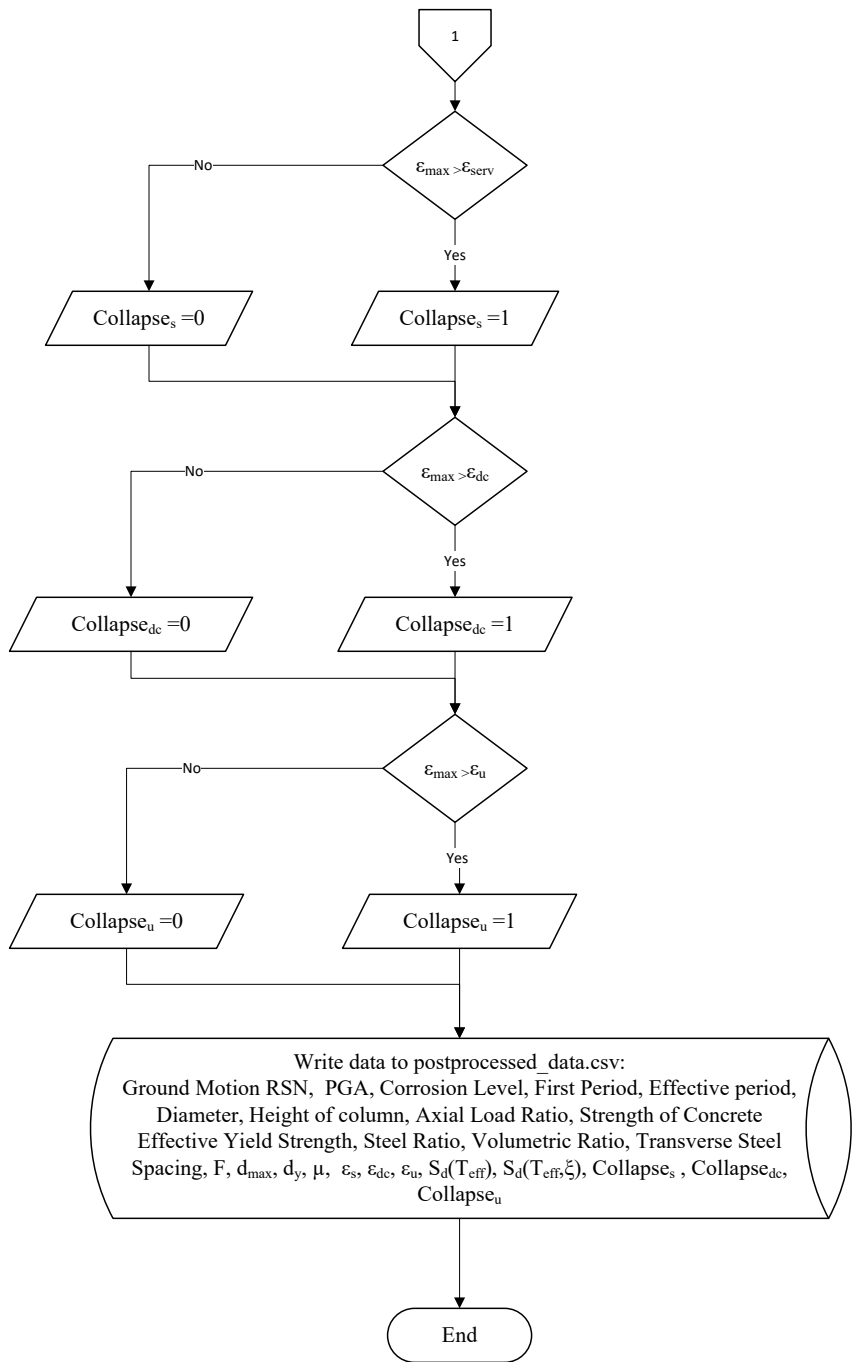


Figure 5.17 Post-processor Flow-Chart continued

- Longitudinal Bar Diameter, $d_b = 0.875\text{in}$; Number of Longitudinal Bars, $n_b = 30$
- Transverse Bar Diameter, $d_t = 0.625\text{in}$; Spacing of transverse steel, $s = 2.5\text{in}$
- Axial Load Ratio, $ALR = 10\%$
- Corrosion Level, $CL = [0\%, 5\%, 10\%, 15\%, 20\%]$
- Pristine Condition yield strength of reinforcing steel, $F_y = 60\text{ksi}$
- Concrete strength at 28 days, $f'c = 5\text{ksi}$

Here results are extracted from the structure's response to the Chi-Chi earthquake (RSN1505 in the PEER database). Fig. 5.18 shows the global system response. It can be observed that as the corrosion level increases, the displacement demands also increase. On the other hand, it is known that corrosion tends to degrade the capacity of an RC system, as will be shown in section 5.8.3. As corrosion increases, the likelihood of reaching a limit state also increases. Similarly, in Fig. 5.19 and Fig. 5.20 shows first that the strength of the corroded reinforcement decreases and therefore induces higher strain demands on the system, and the strain demands from the same ground motion increases as the corrosion level increases. These results further illustrate the effect corrosion could have on an RC structure.

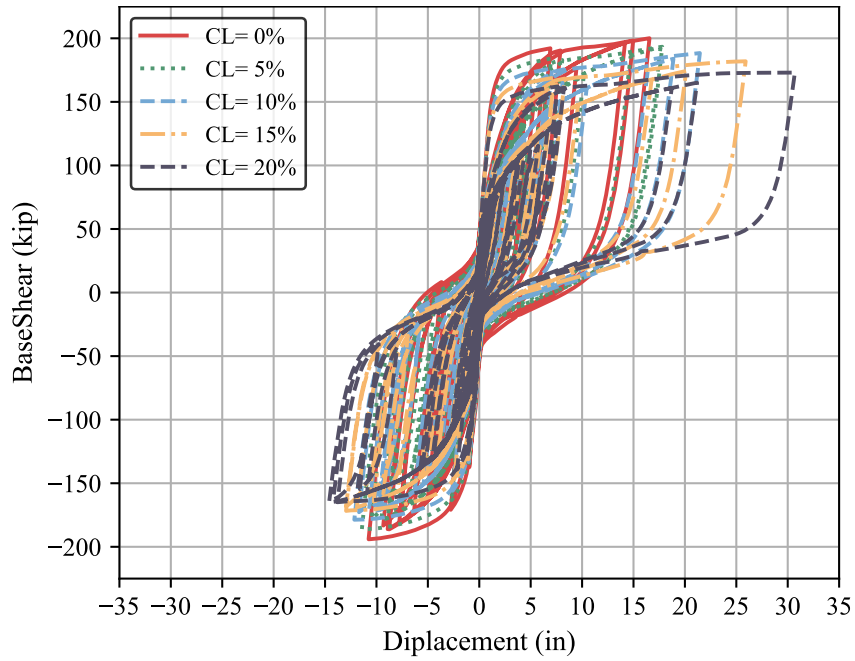


Figure 5.18 Force-Displacement results

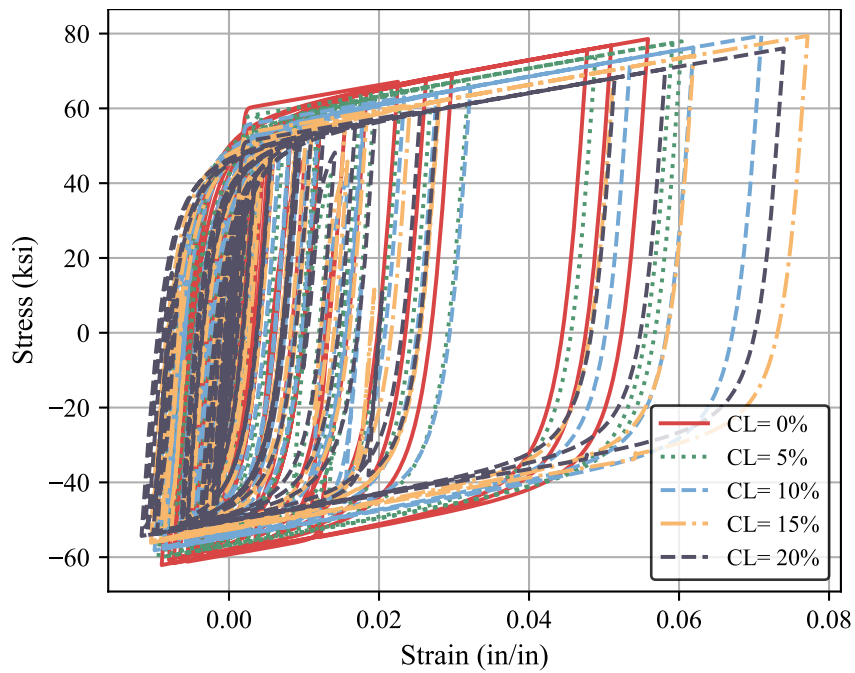


Figure 5.19 Stress strain response for extreme rebar location

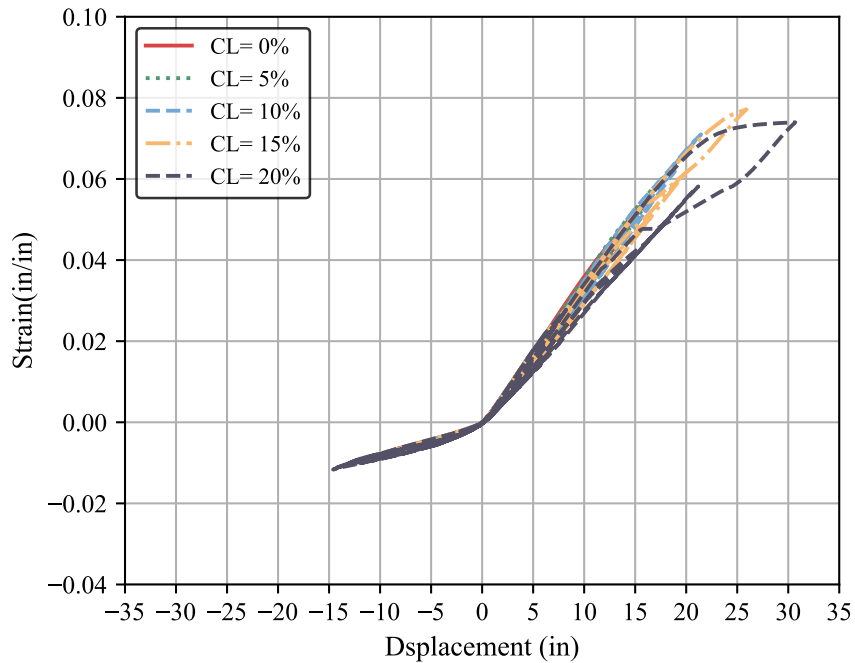


Figure 5.20 Strain hysteresis

5.8.2 Effect of Ground Motion Sequences

The as-recorded ground motion sequences found in the NGA2West database [3] did not induce an increase in the strain demands for corroded RC structures. It was observed that the strains obtained with only the mainshock and the mainshock-aftershock sequence had the same strain demands as shown in Fig. 5.21. Therefore, the mainshock dominated the strain demand for all the ground motions, and the subsequent aftershocks did not appear to increase the highest demand further. The results from this analysis are congruent with studies on pristine condition structures subjected to ground motion sequences[60][77]. Other studies that have used the incremental dynamic analysis or scaling factors on the mainshock-aftershock sequences have increased the demands due to these sequences, and it is possible that altering the records modifies their dynamic properties and induces the observed increase in the demands[56][67]. At the same time, all these studies have been performed on shallow crustal earthquakes. Changing the ground motion regime to subduction earthquake sequences could have a different outcome. Only the mainshocks were used to save computational costs for the rest of this study.

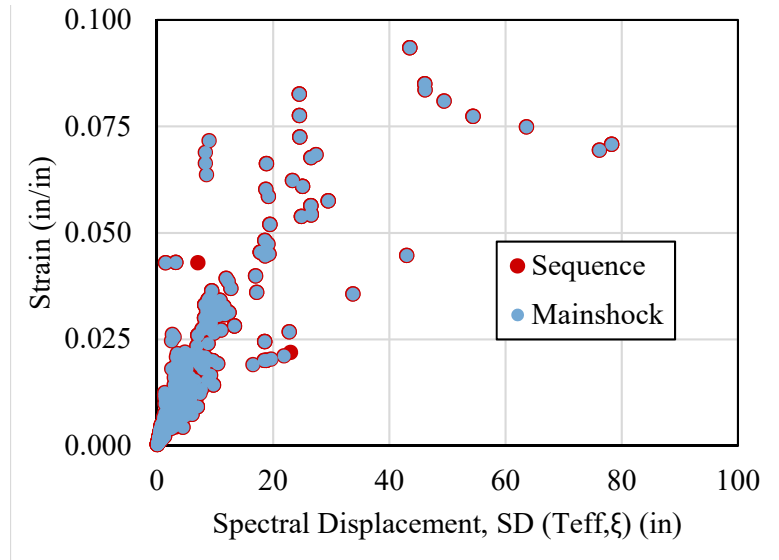


Figure 5.21 Non Linear Time History Analysis (NLTHA) results showing no increase in the strain demands due to as recorded sequence of mainshock and aftershock

5.8.3 Effect of Corrosion Level on Strain Demands

For all 144 columns and all 56 mainshocks, the strain demands (ε) were plotted against the spectral displacement at the effective period and the equivalent structure damping ($Sd(T_{eff}, \xi)$).

These two parameters seem to have a linear correlation for all the corrosion levels evaluated. These results are shown in Fig. 5.22. Through the post-processor subroutine, the results obtained from the NLTHA were separated for each corrosion level (CL) and the MSA methodology was used to analyze the effect of corrosion level in the strain demands.

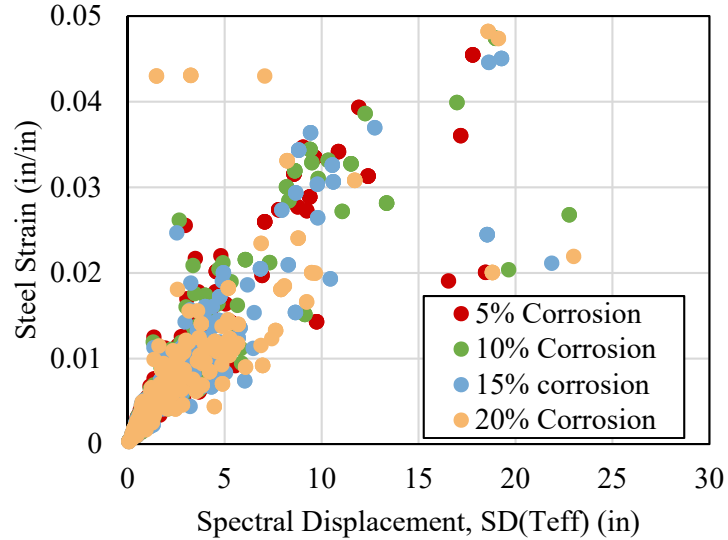


Figure 5.22 Non Linear Time History Analysis (NLTHA) results for Strain demands vs Spectral Displacement at Effective Period (T_{eff}), and Equivalent Damping (ξ)

The multi-stripe analysis(MSA) was used to obtain a series of cumulative distribution functions to evaluate the effect of corrosion and other variables. The most impactful variables are the corrosion level and the axial load ratio. The effect of these variables are shown in Fig. 5.23. These figures show that as corrosion level increases, the mean spectral displacement required to reach a given limit state is decreased. Similarly, the effect of the axial load ratio becomes substantial as it increases.

In order to observe the effect of corrosion level and axial load ratio, the mean spectral displacement, defined as the point where the probability of reaching a limit state is 50% ($P(\varepsilon > \varepsilon_{ls} = 0.5)$), is plotted against these two variables. The results are shown in Fig. 5.24. Similar results were plotted for the 84th percentile. The 84th percentile corresponds to the mean value plus one standard deviation ($\mu + 1 \times \sigma$), and represents the spectral displacements for which there is a probability of 84% to reach a given limit state. The results for the the 84th percentile are shown in Fig. 5.25.

From the results shown in Fig. 5.24, and Fig. 5.25, two main tendencies can be observed. First, as corrosion level increases, the mean spectral displacement required to reach a limit

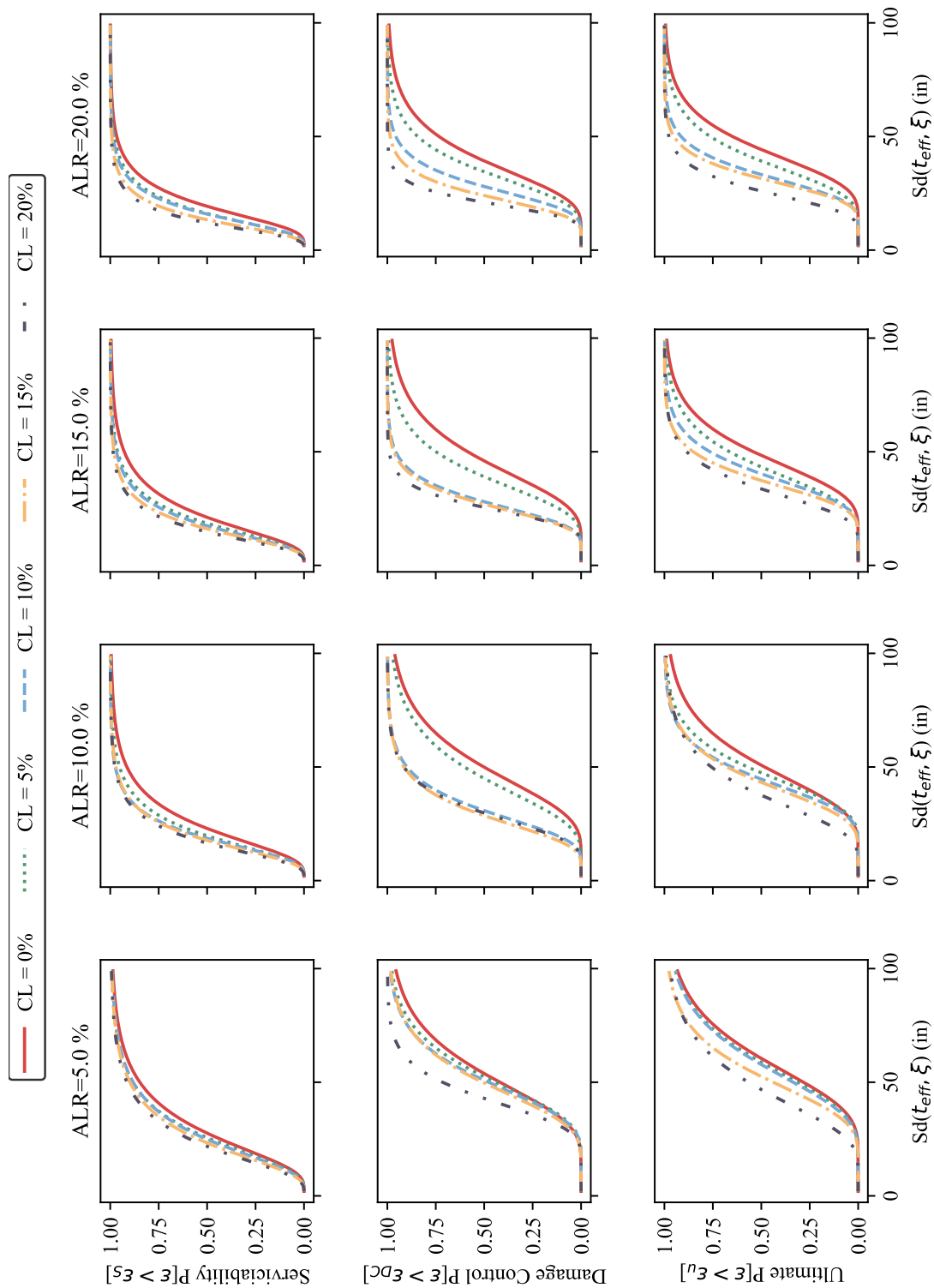


Figure 5.23 Cumulative Distribution Function (CDF) for steel strain limit states and different Axial Load Ratios (ALR)

state decreases, thus precluding an earlier limit state in a corroded structure. It also appears that there is a significant drop at a corrosion level of 10% ($CL = 10\%$), especially for the damage control limit state and the ultimate limit state. This result indicates that a corrosion level this high has potentially undesirable consequences. Research performed on RC members has shown that corrosion levels of 10% are brittle. Thus, these results are congruent with those observations.

The second observation is that columns with an Axial Load Ratio (ALR) greater than 10% show a more significant drop in the spectral displacement required to reach a limit state as the corrosion increases. This ALR value is commonly found in bridges, thus the importance of limiting the corrosion level that bridge columns develop in their service years.

The results obtained from these analyses are important since they provide limiting values for the level of corrosion that could be acceptable in new structures and assessment of existing structures. Therefore, a limiting value for the level of corrosion in new designs should be between 0%-5%. For existing structures, a maximum acceptable level of corrosion could be set at $CL = 10\%$. This recommendation is made because existing structures would not have been designed to account for aging or corrosion inhibitors. These existing structures would have to consider the effective properties and reduce the cross-section of the reinforcing steel bars.

5.8.4 Discussion of results

The Nonlinear Time History Analysis results show that, in general, there is an increase in the strain demands due to corrosion. The increase in the strain demands depends on the limit state being evaluated and the axial load ratio.

For all limit states, a corrosion level of 10 percent is a reasonable estimate of the maximum acceptable corrosion level, as values greater than this result in a significant change in limit state displacements. This result agrees with observed behavior in large-scale tests conducted on RC members [35][34]. An ideal maximum level of corrosion is a 5% corrosion level.

Therefore, the analytical program agrees with observed experimental material tests conducted as part of this research and observations on corroded RC member tests. Thus, for the design of new structures, it is recommended that an acceptable level of corrosion range is 5%-10%. Moreover, for assessment, it is recommended that if a corrosion level greater than 10% is found, an NLTHA must be performed to assess the existing structure. This analysis will have to consider the effective mechanical properties of the reinforcing steel and the reduction in the cross-sectional properties. These recommendations are applied in the following chapter.

Another interesting finding was that the effect of recorded sequences (mainshock-aftershock) appears to be negligible. This result is in agreement with previous studies performed on MDOF systems that included degradation of the system in steel frames [60]. However, other studies

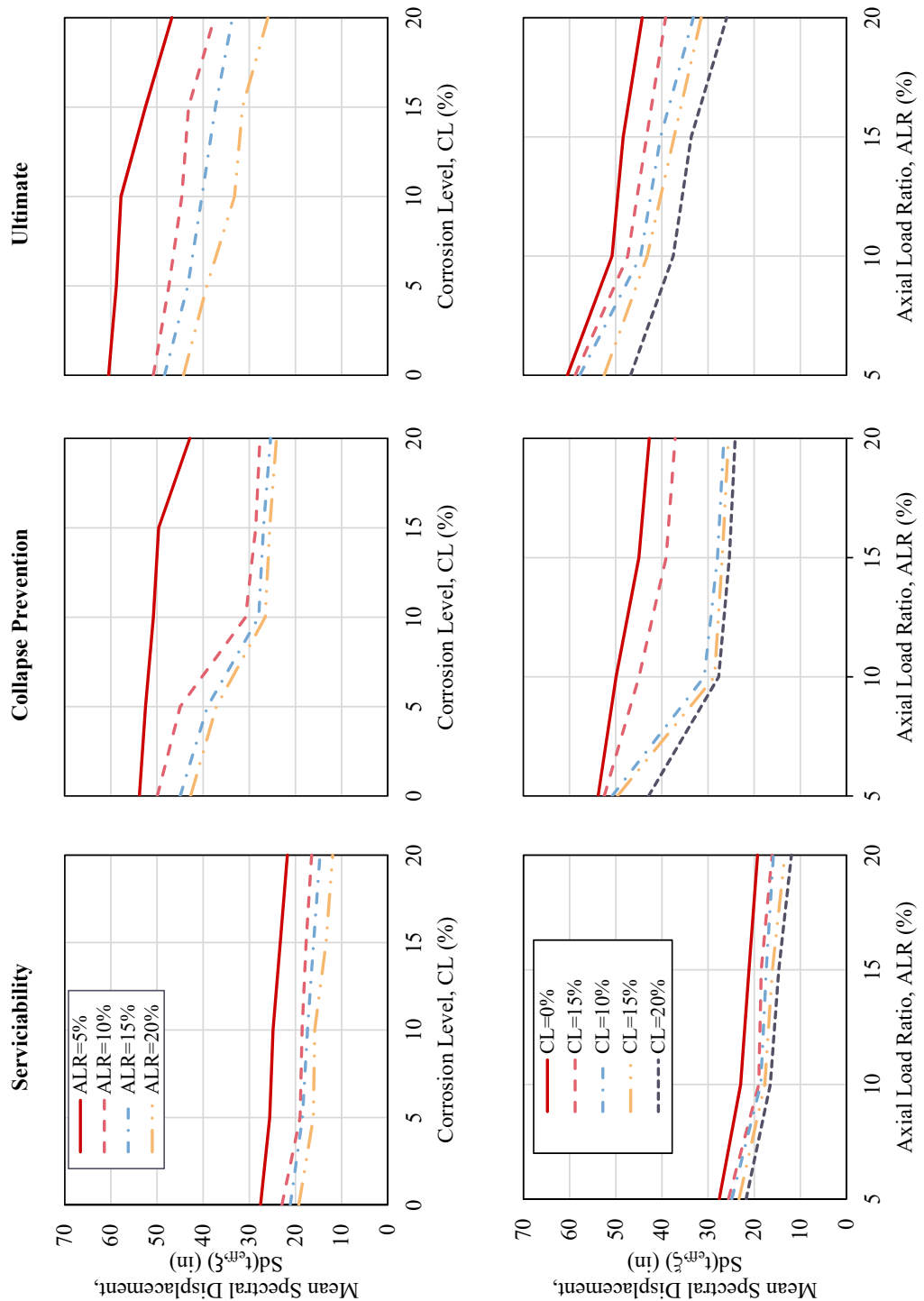


Figure 5.24 Analysis of mean values ($P = 0.5$) for the performance limit states

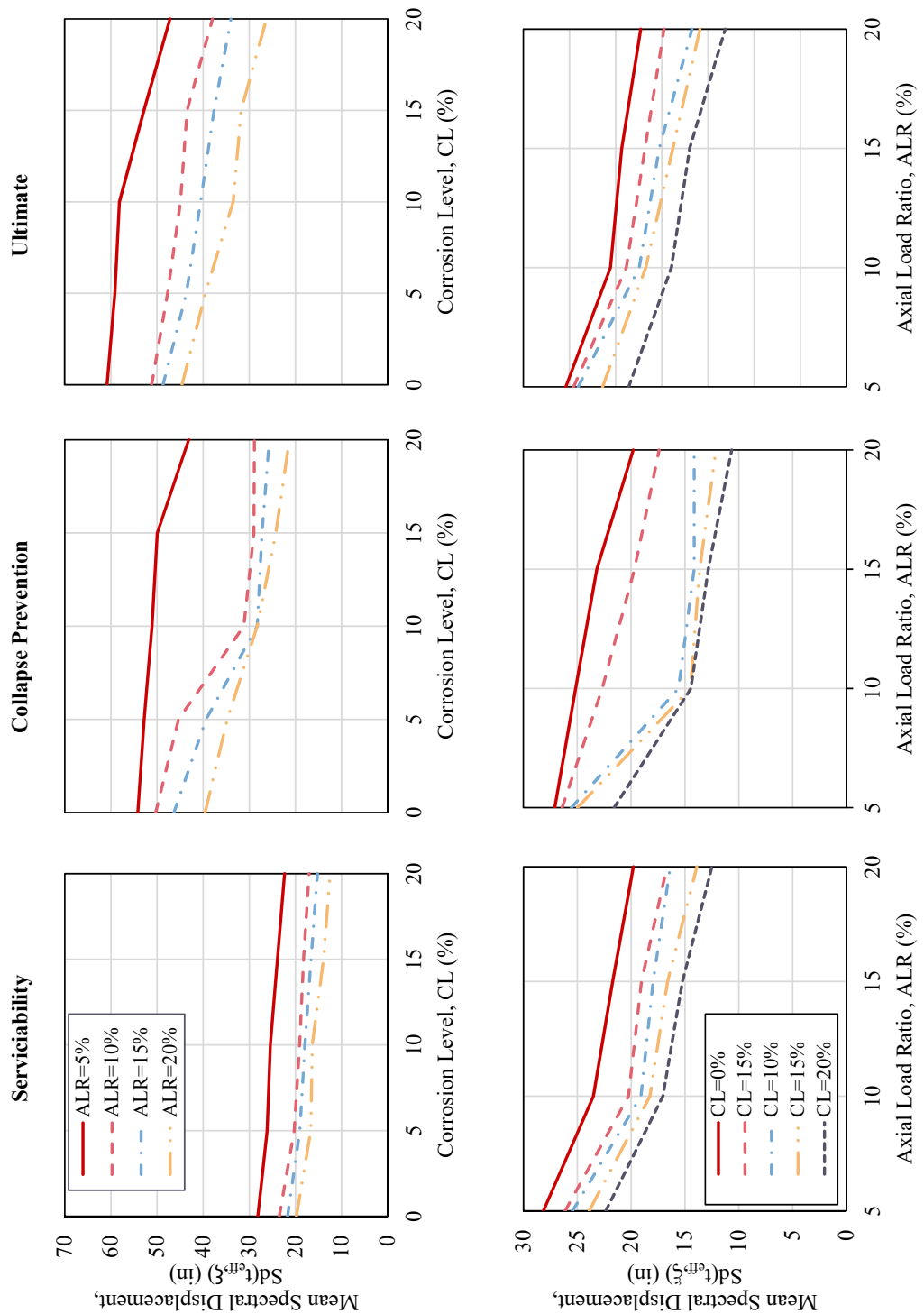


Figure 5.25 Analysis of the 84th percentile ($P = 0.84$) for the performance limit states

that rely on altered records obtain the opposite result because they use amplifiers to change the peak ground acceleration (PGA), thus changing the frequency content of the records.

A limitation of this research was that limit state equations based on pristine condition elements with modern detailing were used for the analytical program. While the limit state equations provide the overall effect of corrosion in RC structures, future studies will provide more information on limit states for corroded RC columns.

Chapter 6

Condition Dependent Performance Based Design and Assessment

In this chapter, the experimental and analytical program results are used for two application examples. Two examples of the design and assessment of bridges that consider their corrosion are shown.

In addition, the existing methodologies to design structures for life service and assessment for existing structures are evaluated. As will be seen, these methodologies provide tools to consider aging in structures. However, none of these methodologies directly evaluate corrosion in the structural analysis and design of the structure. Therefore, this study proposes a design and assessment methodology for a single degree of freedom for RC columns subjected to corrosion.

6.1 Design of new structures for condition dependent PBD

One of the biggest challenges in Civil Engineering is to provide infrastructure that is resilient, affordable, and safe. Currently, the design approach assumes that the material properties will remain unchanged throughout the life of the structure. However, built structures age and deteriorate and could potentially lead to the unintended consequence of aging induced failure. Therefore, it is of interest to ensure that new structures are designed to an acceptable level of performance and maintain that level of performance as the structure ages. Fig. 6.1 shows the concept of condition-dependent performance-based design versus the traditional design approach.

Currently, existing methodologies provide probabilistic frameworks to design structures for aging. While these methodologies have been used in recent years for significant bridge projects such as the Samuel de Champlain Bridge and the New Bonner Bridge, there is a gap in determining the level of performance as the structure deteriorates.

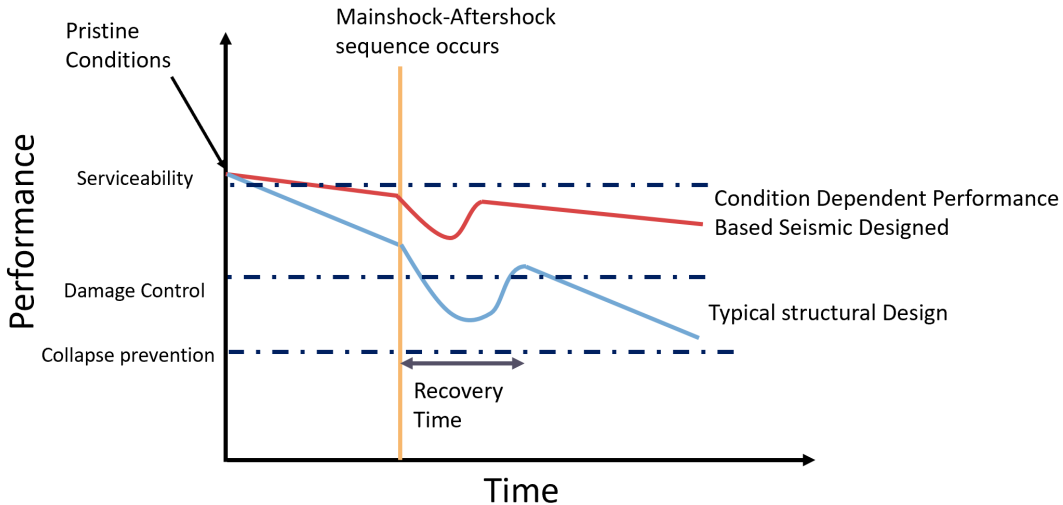


Figure 6.1 Philosophy of Condition Dependent Performance Based Design

6.1.1 Acceptable level of corrosion for new designs

The experimental program resulted in equations that relate the degradation of the yield strength and maximum bending strain to corrosion level. It was also noticeable in the experimental results that for corrosion levels of 10% and greater, the bar's strength and capacity to sustain significant buckling levels were significantly reduced. Similarly, corrosion levels beyond 10% significantly increased the likelihood of reaching the damage control and ultimate limit states according to the computational studies described in Chapter 5. Therefore, it becomes evident that for design, a level of corrosion less than 10% is acceptable for the design of new structures, although a level of corrosion of 5% or less is desirable.

6.1.2 Life Service Design Existing methodologies

6.1.2.1 Life 365

The Life 365 Consortium III developed the software Life365 to estimate the service life and life-cycle costs of alternative concrete mixture designs and corrosion protection systems[8]. The software uses probabilistic analyses of the service life of reinforced concrete structures. The software can calculate the probability distributions within a known time when reinforcement corrosion initiation is expected to occur for a structure. In addition, representative values of the variability of the parameters used in the analysis are provided, such as average temperature throughout the year, corrosion concentration limits, type of environment (Tidal zone, Spray zone, 800m from the ocean, 1.2 km from the ocean), and the type of structure (Parking garage, Urban highway, Rural highway). One of the assumptions is that the deterioration time after

corrosion initiation is constant at six years. This program makes it practical to use such distributions in making engineering judgments regarding selecting reinforcement corrosion protection strategies and considering the life costs of different designs. In this study Life 365 is used to accurately determine the time of initiation of corrosion. An example on how the different environments affect the corrosion process is shown in Fig. 6.2. It can be seen in Fig. 6.2 that as the structure is closer to a marine environment the time of initiation of corrosion and the level of corrosion achieved is higher.

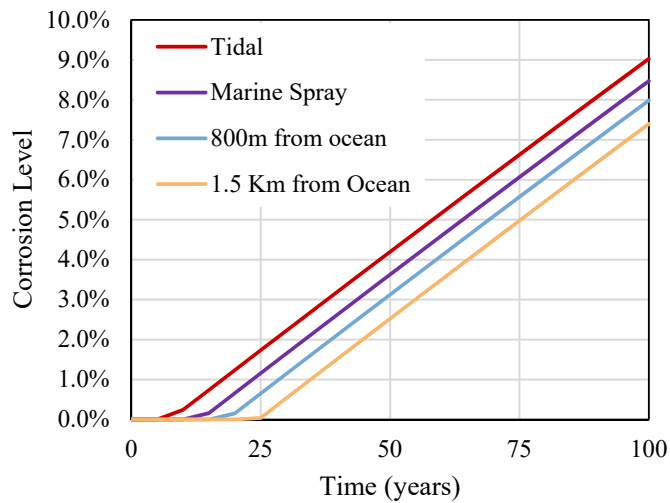


Figure 6.2 Life 365 corrosion level for 100 years of life service in different environments

6.1.2.2 FIB 34 Model Code

FIB 34 model code addresses Service Life Design (SLD) for plain concrete, reinforced concrete, and pre-stressed concrete structures, focusing on design provisions for managing the adverse effects of degradation. Its objective is to guide bridge stakeholders, practicing engineers, and contractors to ensure that the condition of the bridge components and materials are kept above a minimum acceptable level throughout the structure's lifespan. With new bridges having requirements to last for at least 100 years, the design of structures that consider the life service variable has become ever more critical. Therefore, it is crucial to consider one of the primary aging conditions that affect bridges, such as corrosion.

Four different options for SLD are available in FIB 34:

1. Full probabilistic approach,

2. Semi probabilistic approach (partial factor design),
3. Deemed to satisfy rules
4. Avoidance of deterioration.

An application of the FIB 34 model code has been implemented in a design guide developed by the Federal Highway Administration (FHWA) and the American Association of State Highway and Transportation Officials (AASHTO) to implement a Service Life Design for Bridges (also referred to as R19A) through the second Strategic Highway Research Program (SHRP2)[62]. Multiple tools, products, and training materials aimed at practitioners and state bridge engineers were developed for the implementation effort. In SHRP2-R19A, FIB 34 with a fully probabilistic approach is used to design bridges. The design must ensure that the corrosion is reduced to a 10% probability of occurrence. In addition, the methodology is implemented to different parts of the structure with exposure zones assigned to them, as shown in Fig. 6.3. Based on the reliability obtained, changes in the mix design, the reinforcing steel, the cover, and other variables can be made to increase the reliability of the structure.

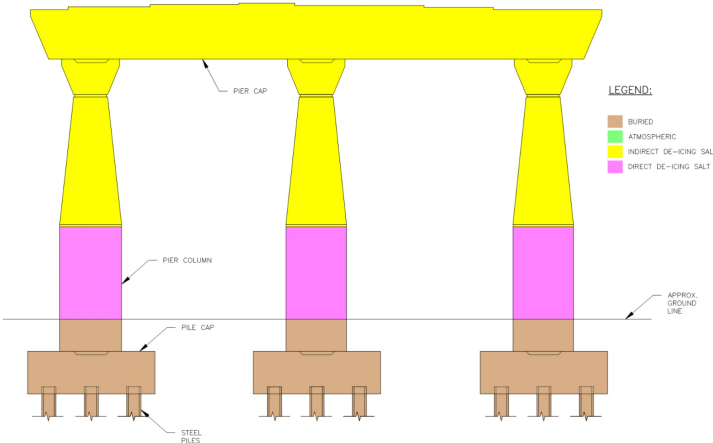


Figure 6.3 Example of identification of exposure zones according to SHRP-R19A [62].

This methodology provides a probabilistic methodology to reduce the likelihood of corrosion throughout the structure's life. However, the methodology does not provide a way to directly consider the effect of corrosion on the structure's performance as it ages. Therefore, to ensure that the bridge's condition remains above a minimum acceptable level, it is necessary to evaluate the structure's performance at a given acceptable level of corrosion. The reliability check process is shown in Fig. 6.4.

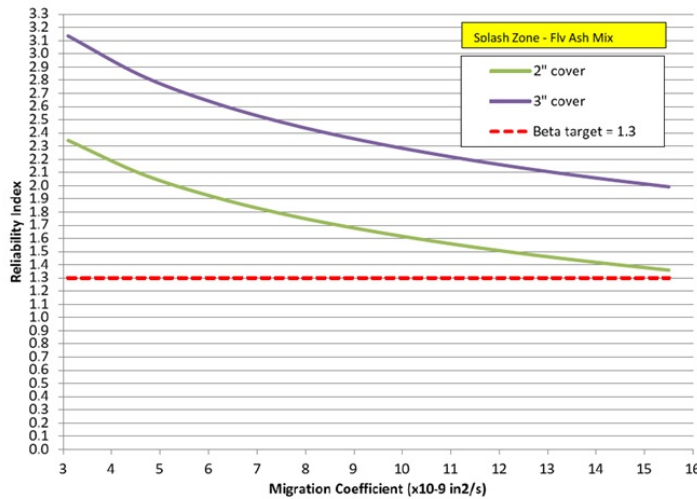


Figure 6.4 Reliability for structure with fly ash for 100 years of service life using the FIB-34 full probabilistic method [62].

6.1.3 Direct Displacement Based Design (DDBD) Methodology

The Direct Displacement Based Design (DDBD) was first proposed by Priestley et al. [55]. It is currently one of the design methods accepted in the Proposed AASHTO design Guidelines for Performance-Based Seismic Bridge Design, developed by the National Cooperative Highway Research Program (NCHRP) [47]. DDBD characterizes a structure as an equivalent single degree of freedom system (SDOF) that represents the properties of the structure being designed at peak displacement response. This methodology makes it possible to design a structure to achieve a design limit state under the seismic intensity at the structure's location. This design is later combined with capacity design principles to ensure that the structure behaves as intended by the structural designer.

The basic steps to apply the DDBD methodology are:

1. Determine the structure effective mass (m_e)
2. Determine the target displacement. The target displacement can be established by the maximum admissible ductility (μ_{adm}), the maximum drift (θ), or the design limit state (LS).
3. Calculate the initial design ductility (μ_{adm})
4. Calculate the equivalent damping based on the structural element and hysteresis types.
5. Calculate the effective period of the structure (T_{eff}) based on the displacement spectrum at the site of the structure.

6. Calculate the effective stiffness of the structure as follows:

$$K_{eff} = \frac{4\pi^2 m_e}{T_{eff}^2} \quad (6.1)$$

7. Obtain base shear of the structure

The methodology is summarized in Fig. 6.5, where the basic steps shown above are explained. Fig. 6.5.

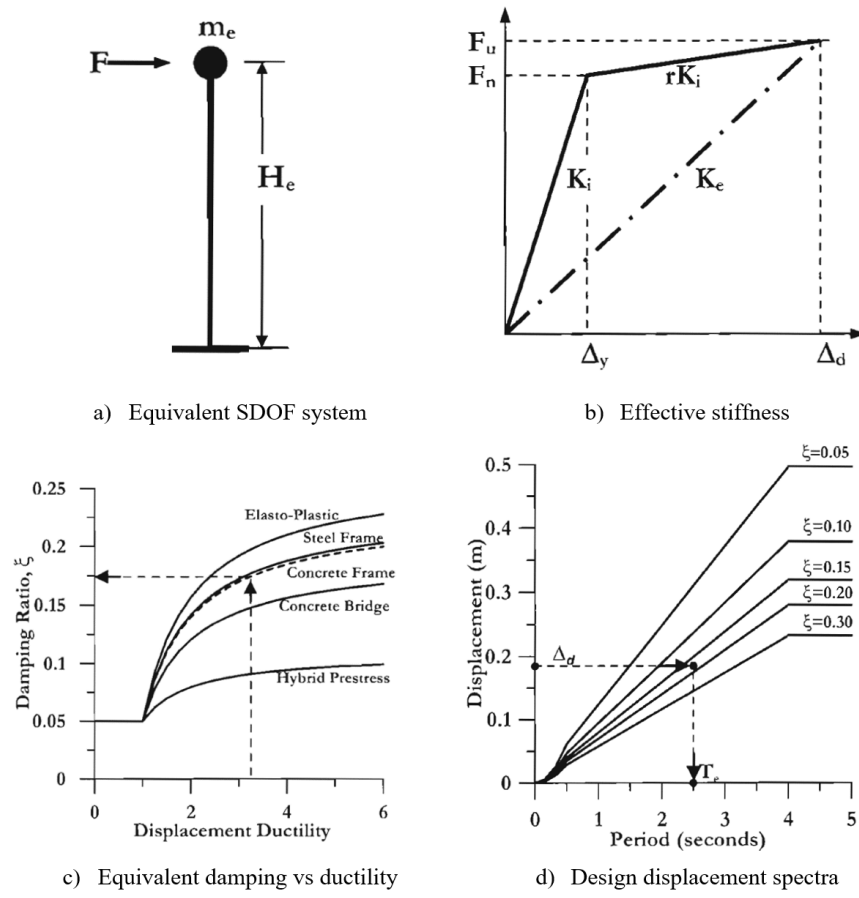


Figure 6.5 Direct Displacement Based Design (DDBD) methodology [55].

6.1.4 Proposed Condition Dependent DDBD Methodology

The existing methodologies are robust in predicting the time for initiation of corrosion and obtaining the reliability that the structure will have low probabilities of developing corrosion of the reinforcing steel. However, these tools do not provide a way to estimate the degradation of the structural performance in the case corrosion occurs. In order to design a structure for corrosion, it is necessary to estimate the highest level of corrosion that will be experienced by the structure. To estimate the highest level of corrosion the main variables are the time of initiation of corrosion and the rate of corrosion. Therefore, a procedure to obtain the level of corrosion and estimate the deterioration of the structure is needed.

The proposed methodology consists of:

1. Estimate the time of initiation of corrosion. In this study Life 365 is used. An initial concrete mix is made to initiate the design process. Also the water to cement ratio, and cover are specified. The program will calculate the time of initiation of corrosion (T_{corr}), based on the design inputs and the type of environment.
2. The level of corrosion at the end of the life of the structure is determined. First the rate of corrosion needs to be established, as a rule of thumb the rate of corrosion for reinforcing steel is 0.5 mills per year. The reader should be aware that the rate of corrosion can depend on several factors such as the water to cement ratio (w/cm), the cover, the size of the reinforcement. As presented in Chapter 2 the studies by Stewart et al. [65], Liu et al. [73], Chirstensen et al. [68] and others, could be used to estimate the rate of corrosion if a more refined calculation is needed. For practical purposes a 0.5 mpy (0.0005 in/year) is assumed in this application methodology, the rate of corrosion (λ) can be expressed as:

$$\lambda(t) = 0.0005 \text{ in/year}(t - T_{corr}) \quad (6.2)$$

Then the reduction of the reinforcing steel can be calculated as:

$$d_b(t) = d_{bi} - 0.0005(t - T_{corr})(\text{in}) \quad (6.3)$$

Finally, the level of corrosion (CL), at the end of the life of the structure (t), is calculated as:

$$CL = 1 - \left(\frac{d_b(t)}{d_{bi}} \right)^2 = 1 - \left(\frac{d_{bi} - 0.0005(t - T_{corr})}{d_{bi}} \right)^2 \quad (6.4)$$

Where d_{bi} is the initial diameter of the reinforcing steel bar.

3. If CL is less than the admissible level of corrosion CL_{adm} , then the concrete mix design, cover or bar diameter can be changed until the corrosion level is acceptable $CL > CL_{adm}$.

4. The effective mechanical properties of the reinforcing steel can be calculated using the expressions developed from the experimental program. The relationships for yield strength and maximum bending strain are replicated here:

$$f_{y,CL} = f_{y,o}(1 - 0.0075CL) \quad (6.5)$$

$$\varepsilon_b(CL) = \varepsilon_o - 0.0045CL \quad (6.6)$$

5. The strain limit states for the structure are evaluated with the expressions from 5.1.
6. Perform the seismic design of the structure using the DDBD methodology.
7. Final check on the strength of the system $\phi R_n > R_u$

The design process is outlined in the flowchart shown in Fig. 6.6.

6.1.5 Condition Dependent DDBD application example: SDOF Bridge Pier RC Column

The example shown below is adapted from Priestley et al [55]. The bridge column shown in Fig. 6.7, and the detailing for the proposed column cross section is shown in Fig. 6.8. The structure is to be designed for 100 years of life service for the displacement response spectrum shown in Fig. 6.11. The structure is located within 800 m of the ocean in the city of Anchorage, Alaska.

Step 1: The structure is designed for the environment of 800m from the ocean. The material data used in the structural design are shown in Table 6.1. Using life 365 the time of initiation of corrosion is determined to be 18.7 years at the location of the structure. Fig. 6.9 shows the corrosion degradation that the structure will sustain at 100 years of life service.

The resulting level of corrosion is calculated as

$$CL = 1 - \left(\frac{d_{bi} - \lambda_t(t - T_{corr})}{d_{bi}} \right)^2$$

$$CL = 1 - \left(\frac{1.57in - 0.0005in/year(100years - 18.7years)}{1.57} \right)^2 = 5.03\% \approx 5\%$$

Step 2: Determine the equivalent mechanical properties of the structure:

$$f_{y,e} = f_{y,o}(1 - 0.0075 \times CL) = 420(1 - 0.0075 \times 5.0) = 389 MPa$$

$$\varepsilon_b = 0.14 - 0.0045 \times CL = 0.14 - 0.0045 \times 5.0 = 0.1175 mm/mm$$

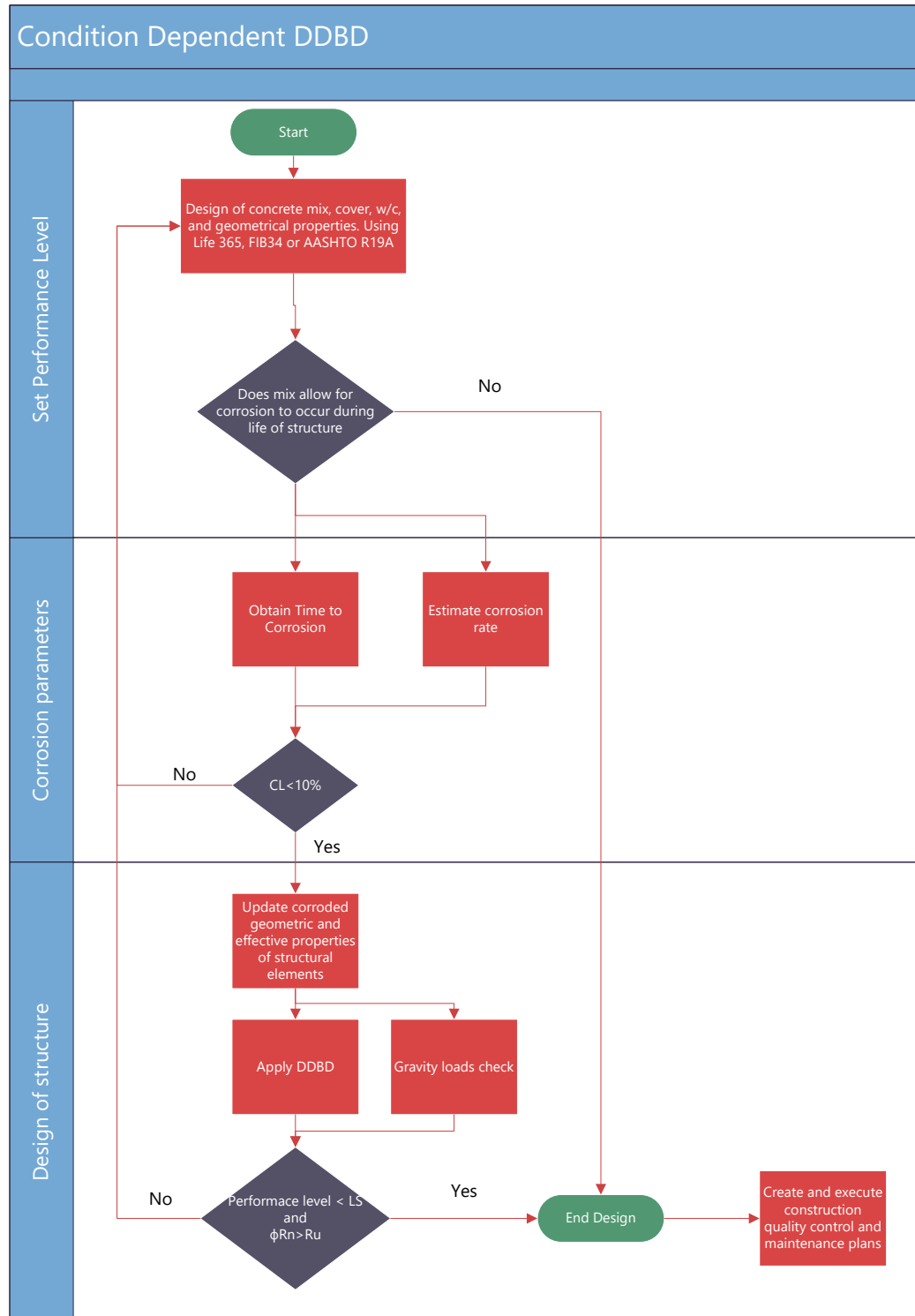


Figure 6.6 Proposed Condition Dependent DDBD Methodology flowchart

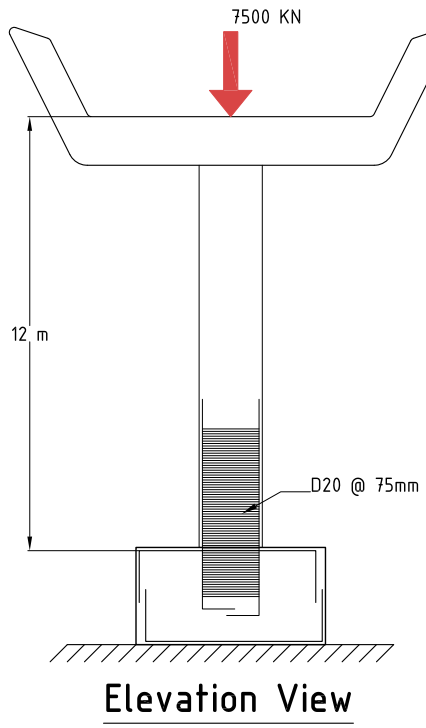


Figure 6.7 Column Elevation

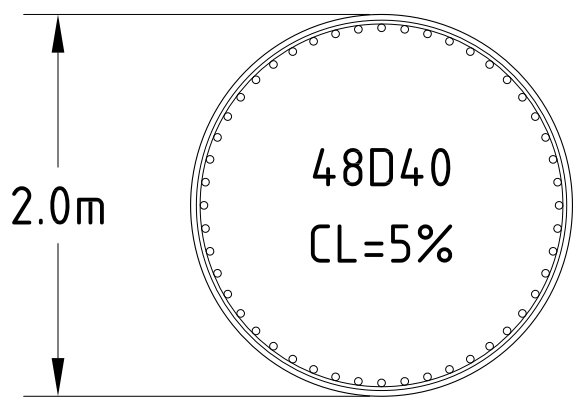


Figure 6.8 Column cross-section

Table 6.1 Detailing of structure for design

Item	Value
Cover to longitudinal bars	50.0 mm
Number of longitudinal bars	48
Diameter of longitudinal bars	39.0 mm
Diameter of transverse steel	20.0 mm
Spacing of transverse steel	75.0 mm
Type of transverse reinforcement	spirals
Axial load	8310.00 KN
Concrete compressive strength	30.00 MPa
Long steel yielding stress	404.25 MPa
Long steel max. stress	545.74 MPa
Transverse steel yielding stress	420.00 MPa
Member Length	12000.0 mm
Longitudinal Steel Ratio	0.018
Transverse Steel Ratio	0.009
Axial Load Ratio	0.088

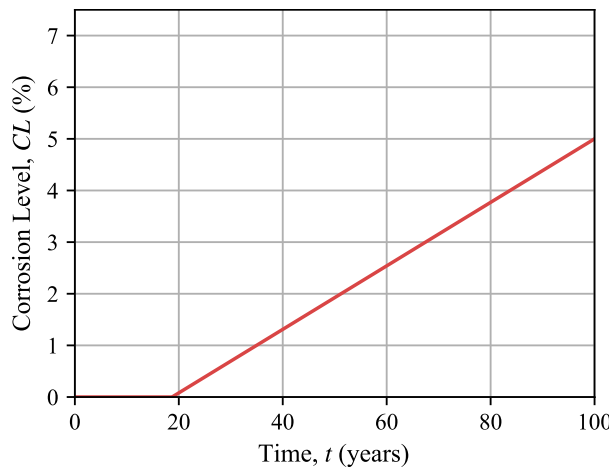


Figure 6.9 Calculating corrosion level at 100 years of service life

Step 3: Calculate the damage control and ultimate limit states using equations 5.11, and 5.12.

$$\varepsilon_{s,BB} = 0.03 + 700\rho_s \frac{f_{yhe}}{E_s} - 0.1 \frac{P}{f'_c A_g}$$

$$\varepsilon_{s,BB} = 0.03 + 700(0.00872) \frac{420 MPa}{200,000 MPa} - 0.1 \frac{8310 KN}{33 MPa(3.1416 m^2)}$$

$$\varepsilon_t = \frac{\ln(\frac{\varepsilon_b}{0.001})}{\frac{300P}{f'cA_g} + \frac{0.7}{\rho_t}} = \frac{\ln(\frac{0.1175}{0.001})}{\frac{300(8310 KN)}{33 MPa \cdot 3.1416 m^2} + \frac{0.7}{0.00872}} = 0.045$$

Step 4: Determine the force-displacement response of the structure using CUMBIA. The displacements for the column at the design limit states are shown below in Fig. 6.10.

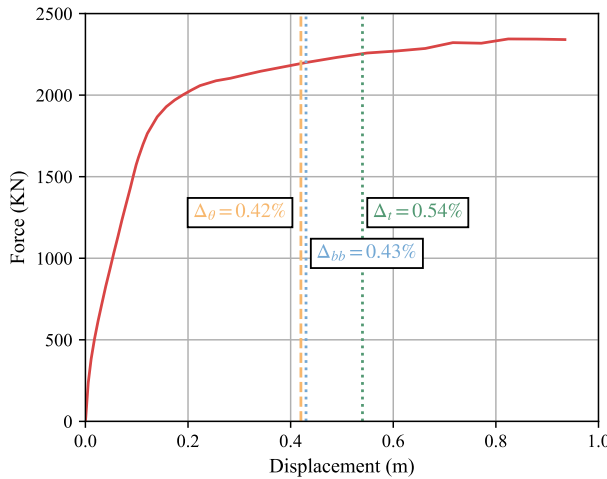


Figure 6.10 Force displacement response for structure considering CL=5%

Step 5: Determine the target displacement. The displacements being considered are the damage control limit state, the ultimate limit state and the maximum allowable drift set to $\theta = 0.035$.

$$Ultimate \rightarrow \Delta_t = 0.54m \rightarrow \mu = 4.42$$

$$DamageControl \rightarrow \Delta_{bb} = 0.43m \rightarrow \mu = 3.5$$

$$Drift \rightarrow \Delta_\theta = 0.42m \rightarrow \mu = 3.42$$

$$\therefore \Delta_D = 0.42m$$

Step 6: Determine the equivalent damping.

$$\xi_A = 0.05 + 0.444 \frac{\mu - 1}{\mu\pi} = 0.05 + 0.444 \frac{3.42 - 1}{3.42\pi} = 0.15$$

Step 7: Determine the corner period at the effective damping.

$$\Delta_{c,15} = 1m \times \sqrt{\frac{0.07}{0.02 + 0.15}} = 0.642m$$

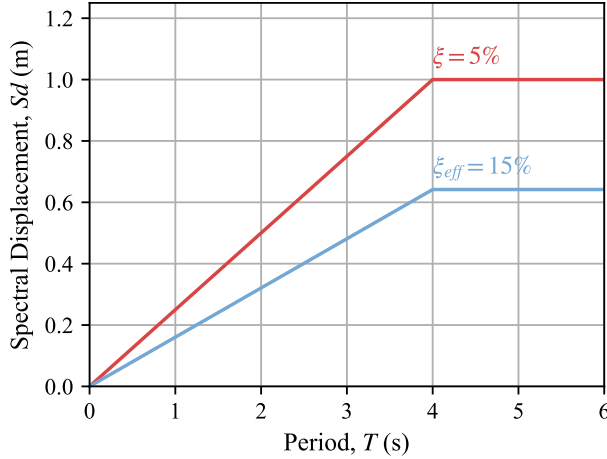


Figure 6.11 Spectral displacement for $\xi = 5\%$, and at the equivalent damping $\xi_{eq} = 15\%$

Step 8: Since $\Delta_D < \Delta_{c,15}$, and the corner period $T_c = 4s$ the effective period can be calculated as shown below.

$$T_{eff} = 4s \left(\frac{0.42m}{0.642m} \right) = 2.62s$$

Step 9: Calculate the effective stiffness.

$$K_e = \frac{4\pi^2 m_e}{T_{eff}^2} = \frac{4\pi^2 792.5 KN \cdot s^2 / m}{(2.62s)^2} = 4557.5 KN/m$$

Step 10: Calculate the base shear.

$$V_b = K_e \cdot \Delta_D = 4557.5 KN/m \times 0.42m = 4557.54 KN$$

Step 11: Check strength of the structure.

$$M_u = V_b \times H = 4557.54 KN \times 12m = 22,970 KN-m$$

From CUMBIA $M_n = 26407 KN-m$, using a reduction factor of $\phi = 0.9$

$$\phi M_n > M_u \rightarrow 23,766.3 KN-m > 22,970 KN-m$$

Therefore the structure has sufficient strength to sustain the demands even with a corrosion level of 5% at 100 years of service life.

6.2 Assessment of existing structures considering aging conditions

For the assessment of structures, it is necessary to have the most accurate information from the structure being assessed. Equally important is that the material behavior is modeled accurately to represent the behavior with corrosion. While current methodologies provide a framework to assess structures in a standardized manner, there is also a gap in how to guide practicing engineers on how to consider aging conditions such as corrosion. Therefore, this section shows the application of a proposed assessment methodology using Direct Displacement Based Assessment for a single degree of freedom RC columns.

6.2.1 Recommendations from the experimental and analytical programs

The experimental program results showed that corroded reinforcing steel degrades as corrosion increases. Therefore, the methodology proposed here is similar to the design case for structures with corrosion levels less than 10%. These recommendations are because the loss of strength and performance of corroded reinforcing steel substantially decreased after the value of $CL = 10\%$. Therefore, as was shown in the analytical program using a more detailed collection of samples from the existing structure and using a more refined analysis such as Non-Linear Time History analysis (NLTHA) is advised for structures that are found in the field to have corrosion levels higher than 10%

6.2.2 Existing methodologies

6.2.2.1 ASCE 41

ASCE 41 is the Seismic Evaluation and Retrofit of Existing Buildings code by the American Society of Civil Engineers (ASCE) [2]. This code has evolved from FEMA 310 Handbook for the Seismic Evaluation of Building. This code consists of three-tiered procedures for seismic evaluation of existing buildings appropriate for use in areas of any Level of Seismicity. Each tier increases the level of complexity and detail for the structural analysis of the existing structure. The first tier consists of checklists that depend on the type of building and material and the available information to identify deficiencies. If the first tier demonstrates deficiencies, then the second tier is activated. The second tier corresponds to more detailed analysis and verification of the elements that had deficiencies. In the second tier, force-based checks are modified with factors to account for the nonlinearity of the structural elements. During the second tier, if the deficiencies are corroborated, retrofits must be performed, or a more detailed analysis is required to verify the performance of the structures, which triggers the third tier. The third

tier corresponds to a more detailed collection of data from the existing structure, and advanced methods of analysis such as Non-Linear Time History Analysis (NLTHA) are required.

While the code provides a framework to evaluate and retrofit existing structures, it is a force-based methodology for tiers 1 and 2, and the code does not guide how to account for aging in the properties of the materials used in the analysis.

6.2.2.2 SLaMA

Simple Lateral Mechanism Analysis (SLaMA) is a part of the Seismic Assessment of Existing Buildings Guidelines from the New Zealand Society for Earthquake Engineering (NZCEE) [48]. The Displacement-based assessment (DBA) procedure is used in SLaMA. The procedure focuses on establishing the probable displacement capacity of the primary lateral system. DBA utilizes displacement spectra which can more readily and directly represent the response of a building to earthquake shaking. Displacement-based methods use the same methods as a force-based assessment to determine the force-displacement response of the structure. However, the expected displacement demand is based on the structural characteristics (effective stiffness and equivalent viscous damping) at the assessed displacements rather than on initial elastic characteristics. Displacement spectra set for different levels of elastic damping or ductility are used rather than the acceleration spectra reduced for ductility used for force-based design. The displacement-based approach enables degrading strength and the influence of poor hysteretic response characteristics to be incorporated in the analysis. Similarly, the concepts can be extended to seismic retrofit design. The basic steps for the SLaMA methodology are enumerated below:

1. Assess the structural configuration and load paths to identify critical structural elements, potential structural weaknesses (SWs), and severe structural weaknesses (SSWs).
2. Calculate the relevant probable strength and deformation capacities for the individual members.
3. Determine probable inelastic behavior of elements by comparing probable member capacities and evaluating the hierarchy of strength.
4. Assess the inelastic sub-system mechanisms by extending local to global behavior.
5. Form a view of the potential governing mechanism for the global building by combining the various individual mechanisms and calculating the probable base shear and global displacement capacity measured at the top of the primary lateral structure. The global displacement capacity will typically be limited to the system with the lowest displacement capacity.

6. Determine equivalent SDOF system, seismic demand, and %NBS.

The %NBS is used as an indicator of risk and defines a structural weakness within the context of SLaMA. For example, SW is an aspect of the building structure and the foundation soils that score less than 100%NBS. Note that an aspect of the building structure scoring less than 100%NBS but greater than or equal to 67%NBS is still considered a structural weakness even though it is considered an acceptable risk. An example of the evaluation of the %NBS is shown in Fig. 6.12, and the flow chart for the SLaMA procedure is shown in Fig. ??.

This method uses a displacement-based assessment methodology, and therefore a better estimate of the structure's performance is possible. However, similar to ASCE 41, the methodology does not explicitly address how to consider corrosion or aging in assessing the structure.

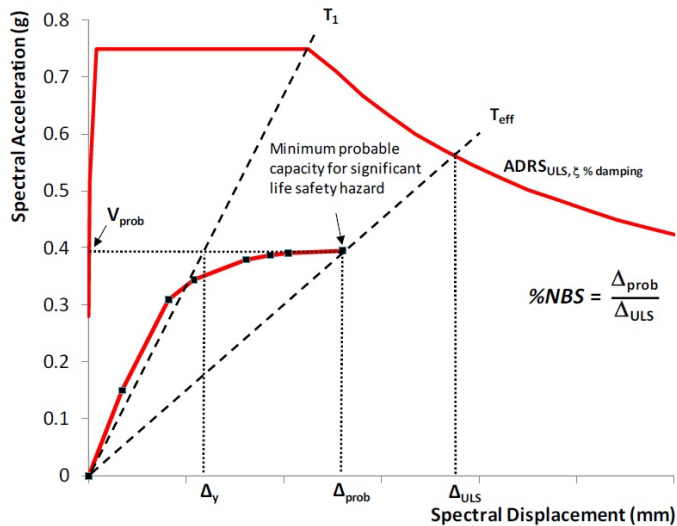


Figure 6.12 SLaMA %NBS calculation for assessment [48].

6.2.3 Direct Displacement Based Assessment (DDBA) Methodology

The Direct Displacement Based Assessment (DDBA) uses DDBD principles to assess the compliance of a structure on the premise of the displacement demands and capacities. The advantage of a displacement-based assessment is that the risk of a structure reaching a performance limit state can be readily obtained, incorporating the structure's effective dynamic and structural properties.

The assessment procedure methodology consists of:

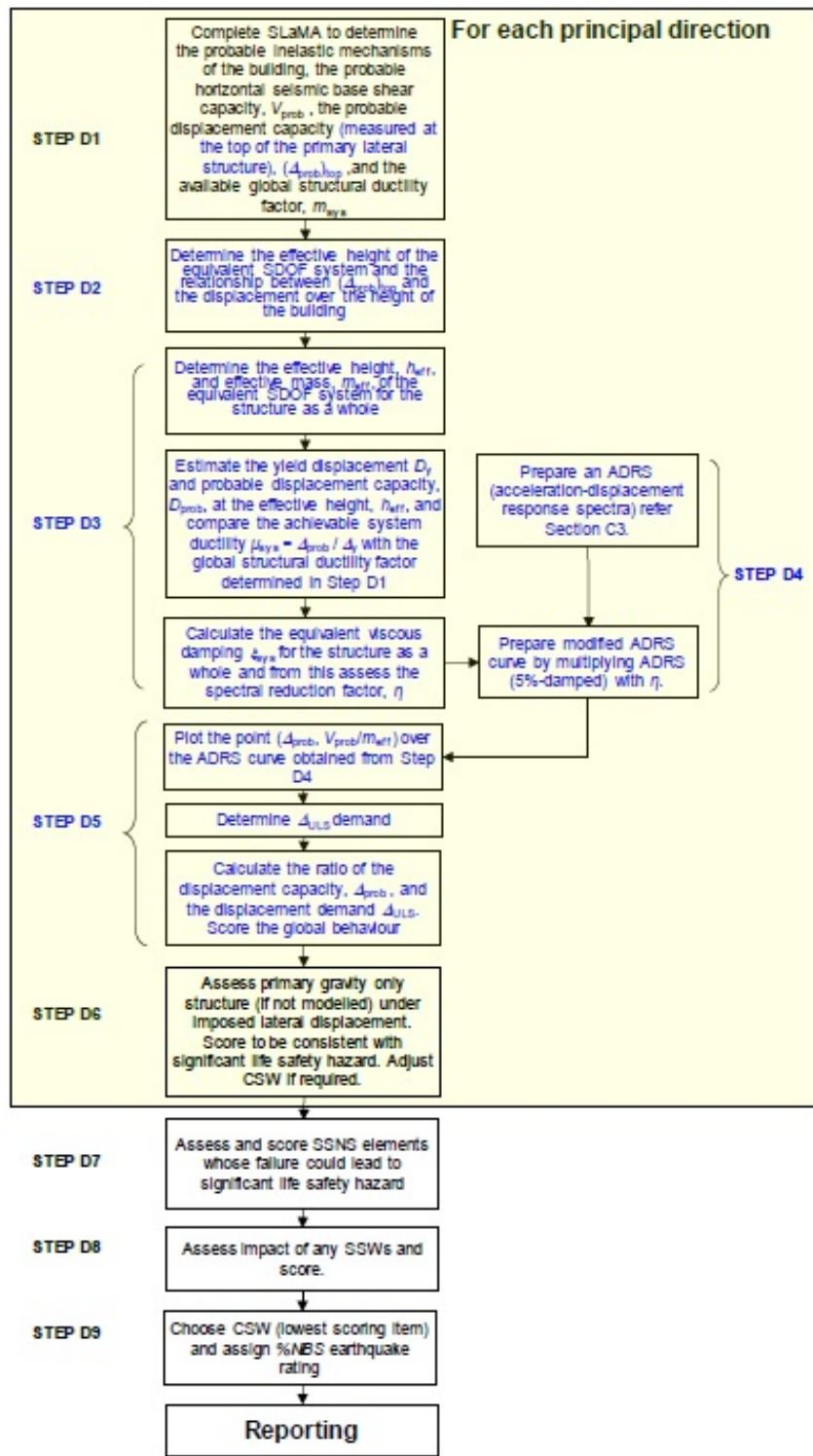


Figure 6.13 SLaMA flowchart for the assessment of existing buildings [48].

Item	value
Cover to longitudinal bars	50.0 mm
Number of longitudinal bars	48
Diameter of longitudinal bars	38.0 mm
Diameter of transverse steel	20.0 mm
Spacing of transverse steel	75.0 mm
Type of transverse reinforcement	spirals
Axial load	8310.00 kN
Concrete compressive strength	30.00 MPa
Long steel yielding stress	389.00 MPa
Long steel max. stress	525.00 MPa
Transverse steel yielding stress	420.00 MPa
Member Length	12000.0 mm
Single Bending	
Uniaxial Bending	
Longitudinal Steel Ratio	0.017
Transverse Steel Ratio	0.009
Axial Load Ratio	0.088

1. Determine the effective mass (m_e)
2. Obtain the force-displacement response of the structure using moment-curvature analysis.
In this study, CUMBIA is used for this step [45].
3. From the previously calculated force-displacement response, determine the effective assessment stiffness ($K_A = F_A/\Delta_{Cap}$) using the displacement (Δ_{Cap}) and force (F_A) corresponding to the limit state being evaluated.
4. Determine the effective period as:

$$T_A = 2\pi \sqrt{\frac{m_e}{K_A}} \quad (6.7)$$

5. Determine the displacement ductility (μ)
6. Determine the effective damping (ξ_A)

$$\xi_A = 0.05 + 0.444 \frac{\mu - 1}{\mu\pi} \quad (6.8)$$

7. Calculate the spectral reduction factor R_ξ corresponding to ξ_A , using the expression taken

from Priestley et al [55], and shown below:

$$R_\xi = \left(\frac{0.07}{0.02 + \xi_A} \right)^\alpha \quad (6.9)$$

8. Calculate the equivalent elastic spectral displacement capacity as follows:

$$\Delta_{Cap,el} = \frac{\Delta_{Cap}}{R_\xi} \quad (6.10)$$

9. Calculate the equivalent elastic demand ($\Delta_{dem,el}$) by reading the displacement demand from the spectrum displacement at the effective period of the structure.
10. Finally, check the capacity demand displacement ratio, expressed as:

$$C/D = \frac{\Delta_{cap,el}}{\Delta_{dem,el}} \quad (6.11)$$

if the ratio is less than one the structure has an satisfactory response, otherwise measures are required to improve the structural performance of the structure.

The DDBA methodology can be summarized in

6.2.4 Proposed Condition Dependent Performance Based Seismic Assessment

In order to provide tools for practicing engineers to assess aging structures, and specifically include corrosion in their assessment of existing structures, a methodology that uses the Direct Displacement Based Assessment (DDBA) is proposed. Similar to the case of new structures design the degradation of the material properties are included. Some assumptions are necessary to estimate the time of initiation of corrosion of the structures.

The procedure of the Condition Dependent DDBA consists of:

1. Obtain information from the existing structure, such as, as built drawings, material certifications, mix design, observations during construction, original structural design calculations.
2. Historical data, that may include inspection reports, observed deterioration reports.
3. Site measurements: Corrosion rate (using GalvaPulse), reduced diameter due to corrosion, samples from concrete cover to obtain chloride concentration.

4. Calculate the level (CL) of corrosion based on the measured bar diameter (d_m), and the initial bar diameter (d_o), using the expression:

$$CL = 1 - \left(\frac{d_m}{d_o} \right)^2 \quad (6.12)$$

5. If it is not possible estimate the corrosion level from measured diameter or the rate of corrosion, empirical equations relating the water to cement ratio (w/c), bar diameter (d_b) and cover (c) are available in the literature [71][68] or by using life 365 [8].
6. Estimate probable mechanical properties of materials
7. Apply the Displacement Based Assessment (DBA) procedure
8. Check the strength of the system with the effective properties of the materials.

6.2.5 Condition Dependent DDBA application Example: SDOF Bridge Pier RC Column

The example shown below is adapted from Priestley et al [55]. The bridge column shown in Fig. 6.14. presents damage due to corrosion. The structure was built in the year 2000 the geometry and detailing of the column are shown in Fig. 6.15. The column is assessed to the ultimate limit state defined in (5.12) using the DDBA procedure. From a site visit it was determined that the longitudinal reinforcement had reduced to $d_{b,m} = 38mm$. The single column pier has a height $H = 12m$, and a diameter $D = 2m$. The column is assumed to have a rigid foundation and supported on stiff rock. The material properties from the as built drawings are summarized in Table 6.2.

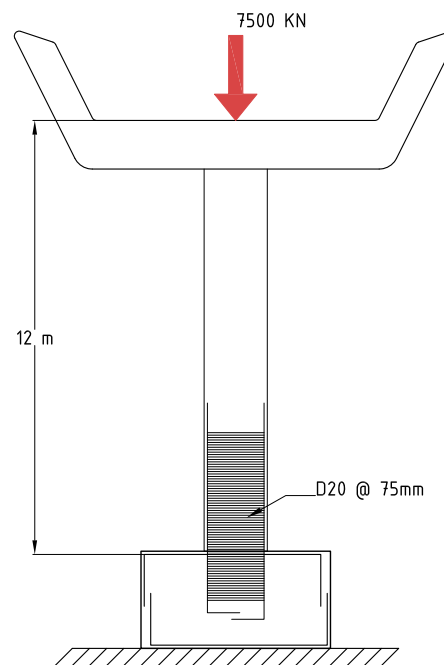
Step 1: The corrosion level of the longitudinal reinforcement is estimated:

$$CL = 1 - \frac{d_{b,m}}{d_o} = 1 - \frac{38}{40} = 9.75\%$$

Step 2: The effective mechanical properties of the longitudinal steel are defined

$$f_{y,e} = f_{y,o}(1 - 0.0075 \times CL) = 420(1 - 0.0075 \times 9.75) = 389MPa$$

$$\varepsilon_b = 0.14 - 0.0045 \times CL = 0.14 - 0.0045 \times 9.75 = 0.096mm/mm$$



Elevation View

Figure 6.14 Column Elevation

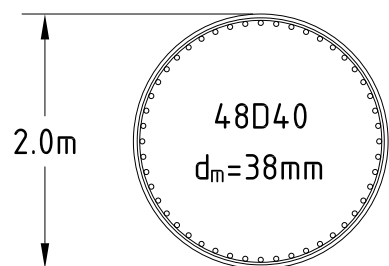


Figure 6.15 Column cross-section

Table 6.2 Detailing of structure for design

Item	Value
Cover to longitudinal bars	50.0 mm
Number of longitudinal bars	48
Diameter of longitudinal bars	39.0 mm
Diameter of transverse steel	20.0 mm
Spacing of transverse steel	75.0 mm
Type of transverse reinforcement	spirals
Axial load	8310.00 kN
Concrete compressive strength	30.00 MPa
Long steel yielding stress	404.25 MPa
Long steel max. stress	545.74 MPa
Transverse steel yielding stress	420.00 MPa
Member Length	12.0 m
Longitudinal Steel Ratio	0.018
Transverse Steel Ratio	0.009
Axial Load Ratio	0.088

Step 3: Define ultimate limit state

$$\varepsilon_t = \frac{\ln(\frac{\varepsilon_b}{0.001})}{\frac{300P}{f'cA_g} + \frac{0.7}{\rho_t}} = \frac{\ln(\frac{0.096}{0.001})}{\frac{300(8310KN)}{330MPa \times 3.1416m^2} + \frac{0.7}{0.00872}} = 0.04275$$

Step 4: Obtain the force displacement response for the column using CUMBIA [45]. The response is shown in Fig. 6.17.

Step 5: The effective mass of the structure is calculated

$$m_e = \frac{7500KN + 810/3}{9.805} = 785KN \cdot s^2/m$$

Step 6: Calculate the effective assessment stiffness.

$$K_A = \frac{F_A}{\Delta_A} = \frac{2099.4KN}{0.498m} = 4,215KN/m$$

Step 7: Determine the effective period.

$$T_A = 2\pi \sqrt{\frac{m_e}{K_A}} = 2\pi \sqrt{\frac{785}{4215}} = 2.724s$$

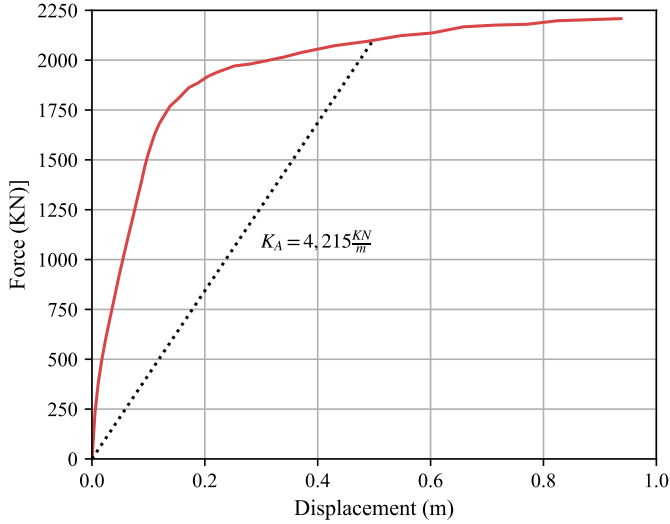


Figure 6.16 Force-Displacement response for assessment of column

Step 8: Determine the ductility capacity.

$$\mu = \frac{\Delta A}{\Delta_y} = \frac{0.498}{0.12} = 4.23$$

Step 9: Determine the effective damping.

$$\xi_A = 0.05 + 0.444 \frac{\mu - 1}{\mu\pi} = 0.05 + 0.444 \frac{4.23 - 1}{4.23\pi} = 0.158$$

Step 10: Calculate the spectral reduction factor.

$$R_\xi = \left(\frac{0.07}{0.02 + \xi_A} \right)^{0.25} = \left(\frac{0.07}{0.02 + 0.158} \right)^{0.25} = 0.792$$

Step 11: Determine the equivalent elastic spectral displacement.

$$\Delta_{Cap,el} = \frac{\Delta_{Cap}}{R_\xi} = \frac{0.498m}{0.792} = 0.629$$

Step 12: Determine the demand spectral displacement, using the displacement spectrum.

$$\Delta_{dem,el} = \frac{\Delta_c \times T_A}{T_c} = \frac{1m \times 2.724s}{1s} = 0.681$$

Step 13: Calculate the capacity demand ratio

$$C/D = \frac{\Delta_{cap,el}}{\Delta_{dem,el}} = \frac{0.629}{0.681}$$

It can be seen then, that the demand is larger than the capacity and this structure is at high risk of reaching the ultimate limit state. On the other hand. If the calculations are repeated with no corrosion the demand capacity ratio is less than one and appears to be safe. The results highlight the necessity to incorporate the current state of the structure in the assessment of structures. These results are shown graphically in Fig. 6.17.

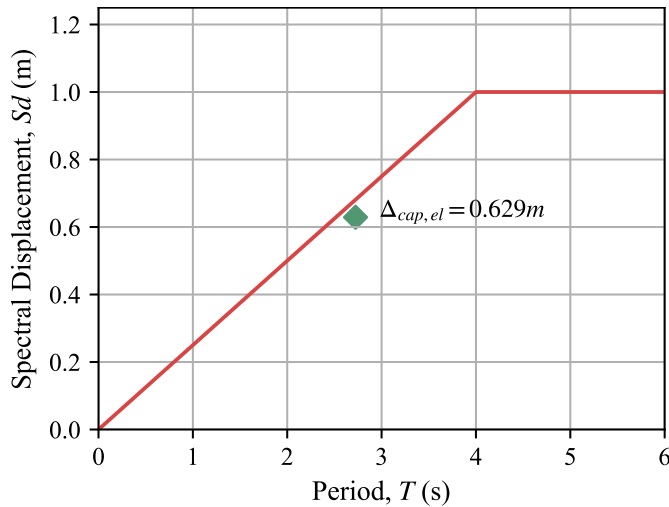


Figure 6.17 Spectral displacement Demands versus displacement capacity of coulumn

6.3 Discussion of results

This chapter showed the versatility of designing and assessing structures using the methodology here proposed. For design, the practicing engineer can readily select the design displacement for the desired level of performance, should the ultimate limit state be too low, the designer can then change the properties of the structure by making the size of the elements larger.

In the case of assessment it was clear that the methodology shows that the structure with corrosion is at risk of sustaining the ultimate limit state for the assessment displacement spectrum.

6.4 Future Work

While the results shown here are preliminary, they present the possibilities of developing a performance based design methodology that directly accounts for the aging conditions of the structure. More experimental results from physical tests performed on corroded RC columns are needed to determine if there are significant changes on the performance limit states such as serviceability and damage control.

Chapter 7

Conclusions and recommendations

The research described in this dissertation aimed to develop the Condition Dependent Performance-Based Design methodology. First, an experimental program was conducted in which the stress-strain behavior and maximum bending strain of corroded reinforcing steel were obtained. The analytical program was then developed based on the outcomes of this experimental program. Second, in the analytical program, an SDOF cantilever column was developed using the open-source structural software OpenSeesPy [79], in which the influence of corrosion level on the performance of the column was investigated. Finally, the results obtained from the experimental program and the analytical program were combined in a design and assessment example. The following sections summarize each phase of this research and highlight key observations. The final section outlines recommendations for future research related to this topic.

7.1 Conclusions

7.1.1 Experimental Program

- The results obtained from tension tests performed on corroded reinforcing steel showed the effect corrosion has on the effective mechanical properties of the corroded reinforcing steel. The specimens were prepared by first developing the passive layer and later corroded to the specified corrosion level.
- The effective mechanical properties of the corroded reinforcing steel can be expressed here:

$$f_{y,CL} = f_{y,o}(1 - 0.0075CL) \quad (7.1)$$

$$f_{u,CL} = f_{u,o}(1 - 0.0075CL) \quad (7.2)$$

- The buckled bar tension tests developed in this research showed that as the corrosion level increases, the maximum bending strain decreases substantially, as can be observed in Fig. 7.1.

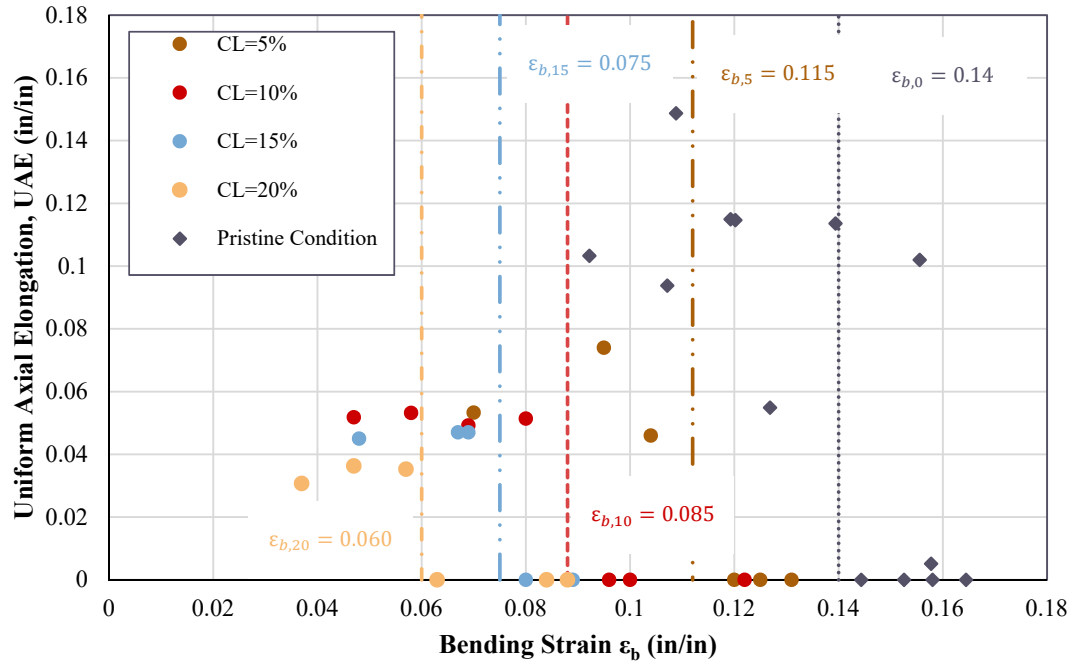


Figure 7.1 Bending strain at different corrosion levels

The expression that relates corrosion level and maximum bending strain is shown here:

$$\epsilon_b(CL) = \epsilon_o - 0.0045CL \quad (7.3)$$

- The SEM observations showed that chloride attack did not onset the fracture of rebars. As the tests on bars with removed imperfections confirmed, the geometrical imperfections caused by corrosion affect the observed behavior on the corroded reinforcing steel. The results from the tension tests on uncorroded reinforcing steel are shown below

7.1.2 Analytical Program

- The analytical program showed that at corrosion level beyond 10% increases the likelihood that a structure will achieve a limit state, as shown in Fig. 7.4.
- As a result of this analysis, recommendations for the design and assessment of a structure

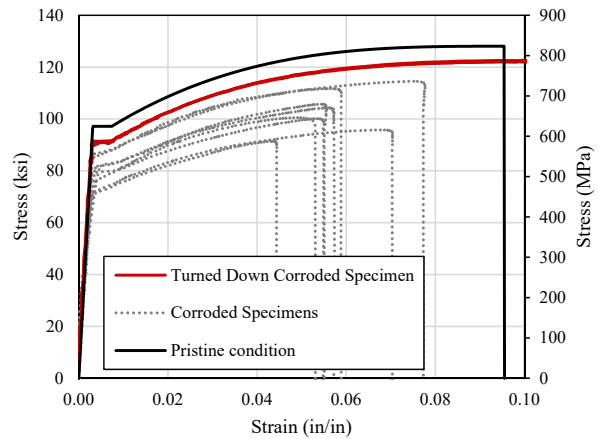


Figure 7.2 Tension tests on turned down specimens

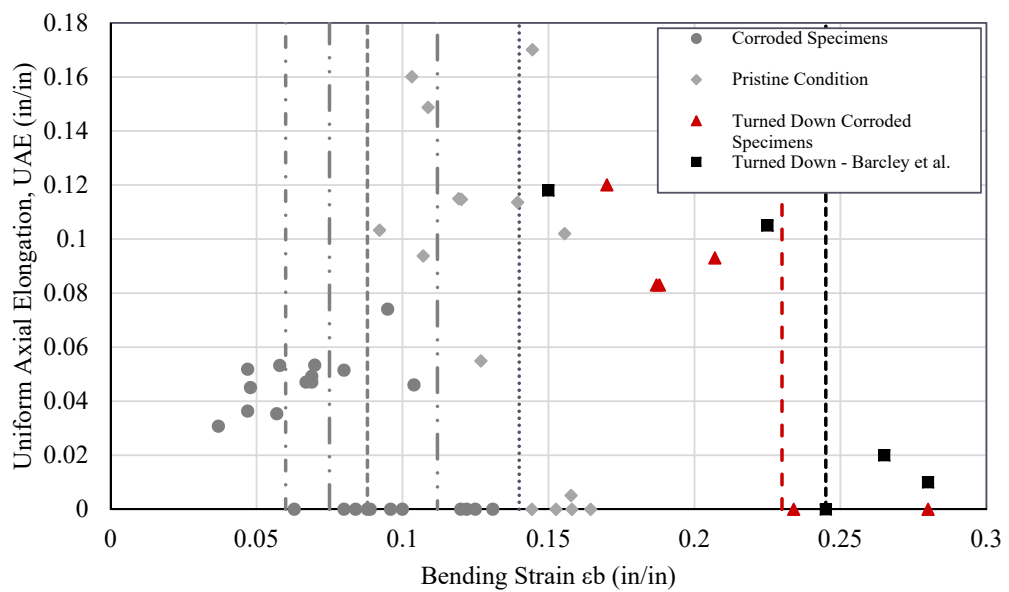


Figure 7.3 BBT tests on turned down specimens

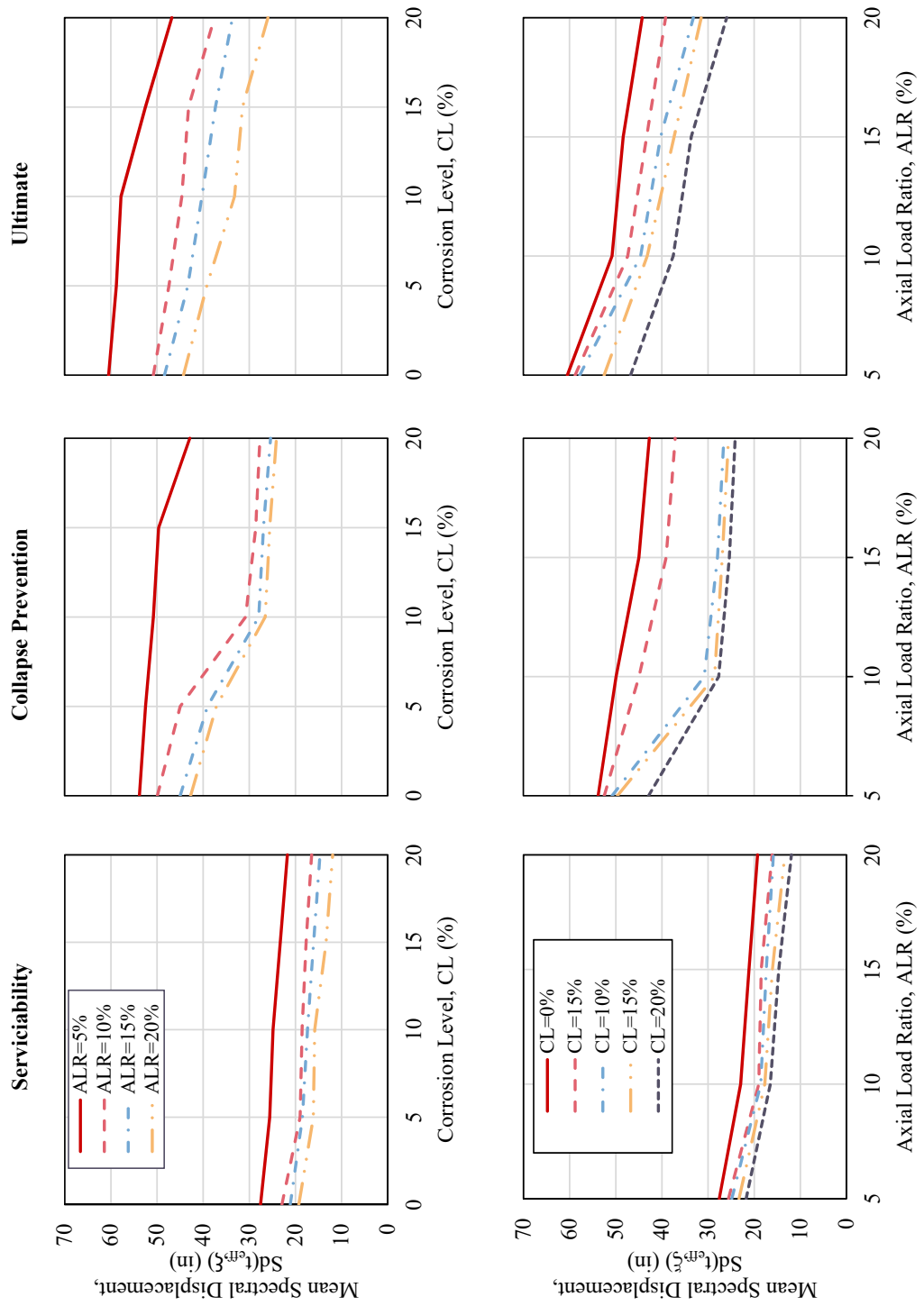


Figure 7.4 Analysis of mean values ($P = 0.5$) for performance limit states

are made: For the design of new structures, the corrosion level of a structure during the life service should not exceed 10%. Similarly, for the assessment of existing structures, the DDBA methodology explained in this research can be used for corrosion levels of 10% or lower. If an existing structure has a value of corrosion level greater than 10%, a more refined procedure such as NLTHA is recommended.

7.1.3 Condition Dependent Performance-Based Design and Assessment

- Although there are tools that allow the design of new structures to reduce the likelihood of corrosion occurring. The approach proposed in this research shows a simple method in which corrosion can be included to check that the structure will remain safe even as it corrodes.
- Similarly, the application of the findings from the experimental program showed that including the effect of corrosion in the assessment of bridges is feasible by including the effective mechanical properties of the reinforcing steel.

7.2 Recommendations

While this research shows that it is possible to design and assess structures to the effect of aging conditions, it is also clear that there is a need to understand the effect of aging on existing structures.

In addition, this research performed tests at the material level only. Therefore large-scale tests on corroded RC columns are necessary to verify the limit state expressions used for the design and assessment of structures.

Another possible avenue of research is to perform large-scale tests that simulate aging conditions with materials related to different eras, i.e., structures with detailing and materials for the 1910-1950, 1950-1970, 1980-present.

Finally, it is essential to understand at the regional level the effect these structures from different eras of design will have on the resiliency of cities across the United States as structures continue to age and new hazards such as climate change increase the threat of structural deterioration in combination with seismic, wind, and other types of loading.

BIBLIOGRAPHY

- [1] Amato, A., Azzara, R., Chiarabba, C., Cimini, G. B., Cocco, M., Di Bona, M., Margheriti, L., Mazza, S., Mele, F., Selvaggi, G., Basili, A., Boschi, E., Courboulex, F., Deschamps, A., Gaffet, S., Bittarelli, G., Chiaraluce, L., Piccinini, D. & Ripepe, M., "The 1997 Umbria-Marche, Italy, earthquake sequence: A first look at the main shocks and aftershocks," *Geophysical Research Letters*, **25**, no. 15, pp. 2861–2864, 1998.
- [2] American Society of Civil Engineers, A., *ASCE 41-17: Seismic Evaluation and Retrofit of Existing Buildings*. 2017.
- [3] Ancheta, T. D., Darragh, R. B., Stewart, J. P., Seyhan, E., Silva, W. J., S-J Chiou, B., Wooddell, K. E., Graves, R. W., Kottke, A. R., Boore, D. M., Kishida, T. & Donahue, J. L., "NGA-West2 Database," 2014.
- [4] Andersson, K., Allard, B., Bengtsson, M. & Magnusson, B., "Chemical composition of cement pore solutions," *Cement and Concrete Research*, **19**, no. 3, pp. 327–332, 1989.
- [5] Baker, J. W., "Efficient analytical fragility function fitting using dynamic structural analysis," *Earthquake Spectra*, **31**, no. 1, pp. 579–599, 2015.
- [6] Barcley, L., "Seismic Performance of A706-80 Reinforced Concrete Columns and Critical Bending Strain of Longitudinal Reinforcement," PhD thesis, North Carolina State University, 2018.
- [7] Barcley, L. & Kowalsky, M., "Critical Bending Strain of Reinforcing Steel and Buckled Bar Tension Test," *ACI Materials Journal*, **116**, no. 3, 2019.
- [8] Bentz, E. C., "Probabilistic Modeling of Service Life for Structures Subjected to Chlorides," *ACI Materials Journal*, pp. 391–397, 2003.
- [9] Bradley, B. A. & Cubrinovski, M., "NEAR-SOURCE STRONG GROUND MOTIONS OBSERVED IN THE 22 FEBRUARY 2011 CHRISTCHURCH EARTHQUAKE," Tech. Rep.
- [10] Calabrese, A., Almeida, J. P. & Pinho, R., "Numerical issues in distributed inelasticity modeling of rc frame elements for seismic analysis," *Journal of Earthquake Engineering*, **14**, no. sup1, pp. 38–68, 2010.
- [11] Choe, D.-E., Gardoni, P., Rosowsky, D. & Haukaas, T., "Probabilistic capacity models and seismic fragility estimates for RC columns subject to corrosion," *Reliability Engineering & System Safety*, **93**, no. 3, pp. 383–393, 2008.
- [12] Comité Euro-International du Betón, *CEB-FIP Model Code 90*, 1st. London, 1993.
- [13] Dawn Marcotte, T., "Characterization of Chloride-Induced Corrosion Products that form in Steel-Reinforced Cementitious Materials," PhD thesis, University of Waterloo, 2001.

- [14] Du, Y. G., Clark, L. A. & Chan, A. H. C., “Residual Capacity of Corroded Reinforcing Bars,” *Magazine of Concrete Research*, **57**, no. 3, pp. 135–147, 2005.
- [15] Du, Y. G., Clark, L. A. & Chan, A. H., “Effect of corrosion on ductility of reinforcing bars,” *Magazine of Concrete Research*, **57**, no. 7, pp. 407–419, 2005.
- [16] Enright, M. P. & Frangopol, D. M., “Probabilistic analysis of resistance degradation of reinforced concrete bridge beams under corrosion,” *Engineering Structures*, **20**, no. 11, pp. 960–971, 1998.
- [17] Fajfar, P., “Equivalent ductility factors, taking into account low-cycle fatigue,” *Earthquake Engineering & Structural Dynamics*, **21**, no. 10, pp. 837–848, 1992.
- [18] FARO Technologies Inc., *FaroArm and FARO Laser ScanArm Quantum Max User Manual*, 2022.
- [19] FEMA, “Prestandard and Commentary for the Seismic Rehabilitation of Buildings,” *Rehabilitation Requirements*, no. 1, pp. 1–518, 2000.
- [20] Filippou, F. C., Popov, E. & Bertero, V., “Effects of bond deterioration on hysteretic behavior of reinforce concrete coint,” Tech. Rep. August, 1983, p. 212.
- [21] Ghods, P., Isgor, O. B., McRae, G. & Miller, T., “The effect of concrete pore solution composition on the quality of passive oxide films on black steel reinforcement,” *Cement and Concrete Composites*, **31**, no. 1, pp. 2–11, 2009.
- [22] Ghods, P., Isgor, O. B., McRae, G. A. & Gu, G. P., “Electrochemical investigation of chloride-induced depassivation of black steel rebar under simulated service conditions,” *Corrosion Science*, **52**, no. 5, pp. 1649–1659, 2010.
- [23] Ghosh, J. & Padgett, J. E., “Aging Considerations in the Development of Time-Dependent Seismic Fragility Curves,” *Journal of Structural Engineering*, **136**, no. 12, pp. 1497–1511, 2010.
- [24] Ghosh, J., Padgett, J. E. & Sánchez-Silva, M., “Seismic Damage Accumulation in Highway Bridges in Earthquake-Prone Regions,” *Earthquake Spectra*, **31**, no. 1, pp. 115–135, 2015.
- [25] Goodnight, J. C., Kowalsky, M. J. & Nau, J., “Strain limit states for circular rc bridge columns,” *Earthquake Spectra*, **32**, no. 3, pp. 1627–1652, 2016.
- [26] Goodnight, J. C., Kowalsky, M. J. & Nau, J. M., “Effect of load history on performance limit states of circular bridge columns,” *Journal of Bridge Engineering*, **18**, no. 12, pp. 1383–1396, 2013.
- [27] Hatzigeorgiou, G. D. & Beskos, D. E., “Inelastic displacement ratios for SDOF structures subjected to repeated earthquakes,” *Engineering Structures*, **31**, pp. 2744–2755, 2009.

- [28] Hosseini, S., Heidarpour, A., Collins, F. & Hutchinson, C. R., “Effect of strain ageing on the mechanical properties of partially damaged structural mild steel,” *Construction and Building Materials*, **77**, pp. 83–93, 2015.
- [29] Jensen, O. M., Hansen, P. F., Coats, A. M. & Glasser, F. P., “Chloride ingress in cement paste and mortar,” *Cement and Concrete Research*, **29**, no. 9, pp. 1497–1504, 1999.
- [30] Khashaee, P. & Eeri, M, “Damage-based Seismic Design of Structures,” *Earthquake Spectra*, **21**, no. 2, pp. 371–387, 2005.
- [31] Krawinkler, H., “Performance Assessment of Steel Component,” *Earthquake Spectra*, **3**, no. 1, pp. 27–41, 1987.
- [32] Krish, Z. F., “Rapid Repair of Reinforced Concrete Bridge Columns Subjected to Seismic Loading via Plastic Hinge Relocation,” PhD thesis, North Carolina State University, 2018.
- [33] Kunnath, S. K., Reinhorn, A. M. & Lobo, R. F., “IDARC Version 3.0: A Program for the Inelastic Damage Analysis of RC Structures,” **818**, no. 1992, pp. 1–20, 1992.
- [34] Ma, G., Li, H. & Hwang, H. J., “Seismic behavior of low-corroded reinforced concrete short columns in an over 20-year building structure,” *Soil Dynamics and Earthquake Engineering*, **106**, no. 2018, pp. 90–100, 2018.
- [35] Ma, Y., Che, Y. & Gong, J., “Behavior of corrosion damaged circular reinforced concrete columns under cyclic loading,” *Construction and Building Materials*, **29**, pp. 548–556, 2012.
- [36] Mackie, K. R. & Stojadinović, B., “Performance-based seismic bridge design for damage and loss limit states,” *Earthquake Engineering & Structural Dynamics*, **36**, no. 13, pp. 1953–1971, 2007.
- [37] Mackie, K. R. & Stojadinović, B., “Seismic demands for performance based design of bridges,” *Pacific Earthquake Engineering Research Center, PEER Repor*, no. August, p. 156, 2003.
- [38] Manafpour, A. R. & Kamrani Moghaddam, P., “Performance capacity of damaged RC SDOF systems under multiple far- and near-field earthquakes,” *Soil Dynamics and Earthquake Engineering*, **116**, pp. 164–173, 2019.
- [39] Mander, J. B., Priestley, M. J. N. & Park, R., “Theoretical stress-strain model for confined concrete,” *Journal of Structural Engineering*, **114**, no. 8, pp. 1804–1826, 1988.
- [40] McKenna, F., Scott, M. H. & Fenves, G. L., “Nonlinear finite-element analysis software architecture using object composition,” *Journal of Computing in Civil Engineering*, **24**, no. 1, pp. 95–107, 2010.

- [41] Meda, A., Mostosi, S., Rinaldi, Z. & Riva, P., “Experimental evaluation of the corrosion influence on the cyclic behaviour of RC columns,” *Engineering Structures*, **76**, pp. 112–123, 2014.
- [42] Mehta, P. K. & Monteiro, P. J. M., *Concrete: Microstructure, Properties, and Materials*, 4th ed. McGraw Hill, 2014.
- [43] Miranda, E., Archbold, J., Heresi, P., Messina, A., Rosa, I., Robertson, I., Mosalam, K., Kijewski-Correa, T., Prevatt, D. & Roueche, D., “PRJ-2712 — StEER - Puerto Rico Earthquake Sequence December 2019 to January 2020: Field Assessment Structural Team (FAST) Early Access Reconnaissance Report (EARR),” Structural Extreme Events Reconnaissance, Tech. Rep., 2020, p. 173.
- [44] Momtahan, A., Dhakal, R. P. & Rieder, A., “Effects of strain-ageing on New Zealand reinforcing steel bars,” *Bulletin of the New Zealand Society for Earthquake Engineering*, **42**, no. 3, pp. 179–186, 2009.
- [45] Montejo, L. A. & Kowalsky, M. J., “CFL Technical Rep. No.IS-07-01: Set of codes for the analysis of reinforced concrete members.,” North Carolina State University, Tech. Rep., 2007.
- [46] Moragues, A., Macias, A. & Andrade, C., “Equilibria of the chemical composition of the concrete pore solution. Part I: Comparative study of synthetic and extracted solutions,” *Cement and Concrete Research*, **17**, no. 2, pp. 173–182, 1987.
- [47] National Cooperative Highway Research Program, *Proposed AASHTO Guidelines for Performance-Based Seismic Bridge Design*. 2020.
- [48] New Zealand Society for Earthquake Engineering, “The Sismic Assessment of Existing Buildings: Technical Guidelines for Engineering Assessments,” Tech. Rep., 2019, p. 98.
- [49] NIED K-NET KiK-net, *K-NET, KiK-net*, 2019.
- [50] Northern Digital Inc., *OPTOTRAK Certus HD dynamic measuring machine*, 2020.
- [51] Overby, D., “Stress-Strain Behavior of ASTM A706 Grade 80 Reinforcement,” PhD thesis, North Carolina State University, 2016.
- [52] Overby, D., Kowalsky, M. & Seracino, R., “Stress-strain response of A706 grade 80 reinforcing steel,” *Construction and Building Materials*, **145**, pp. 292–302, 2017.
- [53] Padgett, J. E. & Desroches, R., “Bridge Functionality Relationships for Improved Seismic Risk Assessment of Transportation Networks,” *Earthquake Spectra*, **23**, no. 1, pp. 115–130, 2007.
- [54] Page, C. L. & Vennesland, “Pore solution composition and chloride binding capacity of silica-fume cement pastes,” *Matériaux et Constructions*, **16**, no. 1, pp. 19–25, 1983.

- [55] Priestley, M., Calvi, G. M. & Kowalsky, M. J., *Displacement-Based Seismic Design of Structures*, 1st. Pavia, Italy: IUSS Press, 2007.
- [56] Raghunandan, M., Liel, A. B. & Luco, N., “Aftershock collapse vulnerability assessment of reinforced concrete frame structures,” *Earthquake Engineering & Structural Dynamics*, **44**, no. 3, pp. 419–439, 2015.
- [57] Restrepo-Posada, J., Dodd, L. L., Park, R & Cooke, N, “Variables Affecting Cyclic Behavior of Reinforcing Steel,” *Journal of Structural Engineering*, **120**, no. 11, pp. 3178–3196, 1994.
- [58] Roufaiel, M. S. L. & Meyer, C., “Analytical modeling of hysteretic behavior of r/c frames,” Tech. Rep.
- [59] Ruiz-Garcia, J., Moreno, J. Y. & Maldonado, I. a., “Evaluation of existing Mexican Highway Bridges Under Mainshock-Aftershock Seismic Sequences,” *Proceedings of the 14th World Conference on Earthquake Engineering*, no. January 2008, 2008.
- [60] Ruiz-García, J. & Negrete-Manriquez, J. C., “Evaluation of drift demands in existing steel frames under as-recorded far-field and near-fault mainshock–aftershock seismic sequences,” *Engineering Structures*, **33**, pp. 621–634, 2011.
- [61] Scott, M. H. & Fenves, G. L., “Plastic Hinge Integration Methods for Force-Based Beam-Column Elements,” *Journal of Structural Engineering*, **132**, no. 2, pp. 244–252, 2006.
- [62] Second Strategic Highway Research Program (SHRP2), “Service Life Design for Bridges,” Tech. Rep., 2019.
- [63] Shearer, P. M., *Introduction to seismology*, 2nd editio. Cambridge: Cambridge University Press, 2009, pp. 301–320.
- [64] Shekhar, S., Ghosh, J. & Padgett, J. E., “Seismic life-cycle cost analysis of ageing highway bridges under chloride exposure conditions: modelling and recommendations,” *Structure and Infrastructure Engineering*, **14**, no. 7, pp. 941–966, 2018.
- [65] Stewart, M. G. & Rosowsky, D. V., “Time-dependent reliability of deteriorating reinforced concrete bridge decks,” *Structural Safety*, **20**, no. 1, pp. 91–109, 1998.
- [66] Sunasaka, Y. & Kiremidjian, A. S., “A method for structural safety evaluation under mainshock-aftershock earthquake sequences,” Stanford University, Tech. Rep., 1993.
- [67] Tesfamariam, S., Goda, K. & Mondal, G., “Seismic Vulnerability of Reinforced Concrete Frame with Unreinforced Masonry Infill Due to Main Shock-Aftershock Earthquake Sequences,” *Earthquake Spectra*, **31**, no. 3, pp. 1427–1449, 2015.

- [68] Thoft-Christensen, P., “Corrosion and Cracking of Reinforced Concrete,” *Life-Cycle Performance of Deteriorating Structures: Assessment, Design and Management*, 2003, pp. 26–36.
- [69] Vamvatsikos, D. & Allin Cornell, C., “Incremental dynamic analysis,” *Earthquake Engineering and Structural Dynamics*, **31**, no. 3, pp. 491–514, 2002.
- [70] Vu, K. A. T. & Stewart, M. G., “Structural reliability of concrete bridges including improved chloride-induced corrosion models,” *Structural Safety*, **22**, no. 4, pp. 313–333, 2000.
- [71] Weyers, R. E., Fitch, M. G., Larsen, E. P., Al-Qadi, I. L., Chamberlin Albany, W. P., York, N. & Hoffman, P. C., “Service Life Estimates,” Strategic Highway Research Program, Washington DC, Tech. Rep., 1994.
- [72] Williams, M. S. & Sexsmith, R. G., “Seismic Damage Indices for Concrete Structures: A State-of-the-Art Review,” *Earthquake Spectra*, **11**, no. 02, pp. 319–349, 1995.
- [73] Y. Liu & R. E. Weyers, “Modeling the Time to Corrosion Cracking in Chloride contaminated Reinforced Concrete Structures,” *ACI Materials Journal*, **95**, no. 6, pp. 675–680, 1998.
- [74] Yang, S.-Y., Song, X.-B., Jia, H.-X., Chen, X. & Liu, X.-L., “Experimental research on hysteretic behaviors of corroded reinforced concrete columns with different maximum amounts of corrosion of rebar,” *Construction and Building Materials*, **121**, pp. 319–327, 2016.
- [75] Young-Ji Park, B., H-S Ang, A. & Asce, F., “Mechanistic seismic damage model for reinforced concrete,” *Journal of Structural Engineering*, **111**, no. 4, pp. 722–739, 1985.
- [76] Yuan, Z., Fang, C., Parsaeimaram, M. & Yang, S., “Cyclic Behavior of Corroded Reinforced Concrete Bridge Piers,” *Journal of Bridge Engineering*, **22**, no. 7, 2017.
- [77] Zhai, C. H., Wen, W. P., Li, S., Chen, Z. Q., Chang, Z. & Xie, L. L., “The damage investigation of inelastic SDOF structure under the mainshock–aftershock sequence-type ground motions,” *Soil Dynamics and Earthquake Engineering*, **59**, pp. 30–41, 2014.
- [78] Zhao, J. & Sritharan, S., “Modeling of strain penetration effects in fiber-based analysis of reinforced concrete structures,” *ACI Structural Journal*, **104**, no. 2, pp. 133–141, 2007. arXiv: [arXiv:1011.1669v3](https://arxiv.org/abs/1011.1669v3).
- [79] Zhu, M., McKenna, F. & Scott, M. H., “OpenSeesPy: Python library for the OpenSees finite element framework,” *SoftwareX*, **7**, pp. 6–11, 2018.

APPENDICES

Appendix A

Standard Operation Procedure for Accelerated Corrosion

Accelerated Corrosion Procedure: Specimen Preparation

Procedure title	Accelerated corrosion for Reinforcing Bars	
Author	Victor Alejandro Calderon	
Date of creation/revision	Date Created: 05/06/2021	Date last revised: 05/06/2021
Principal Investigator	Mervyn J Kowalsky	
Location	Building and room number	
1.	This standard operating procedure (SOP) is for	

Specific laboratory procedure or experiment

This document outlines the procedure to perform the generation of the passive layer in reinforcing steel bars. These documents assume that the specimen is already inside the container where the specimens will develop the passive layer. The passive layer is generated by using a saturated pore solution of calcium hydroxide. The solution concentrations were obtained from the study by Ghods et al. [1]

- [1] P. Ghods, O. B. Isgor, G. McRae, and T. Miller, "The effect of concrete pore solution composition on the quality of passive oxide films on black steel reinforcement," *Cem. Concr. Compos.*, 2009.

2. Process or experiment description

The reinforcing steel bars are placed in an airtight container and are submerged in a calcium chloride saturated solution.

The required chemicals are listed below:

- Sodium hydroxide
- Potassium hydroxide
- Calcium sulfate dehydrate
- Calcium hydroxide
- Distilled water

Other equipment:

- Beaker 500 ml
- Glass mixing rod
- Disposable 1 gal bucket or equivalent glass container
- Measuring scale
- Spoon for the handling of chemicals, paper sheets for spills, and funnel

3.	Hazard and risk assessment.																
<p>Physical hazard: The user must be careful of puncturing edges and tools. For example, the edges of the stainless steel mesh can cut through skin, therefore, the user should wear puncture-resistant gloves for the handling of metals. The user must be careful with the use of tools such as saws.</p> <p>The user should be careful to not breathe PVC dust and residues.</p>																	
4.	Safety equipment <i>Specify all equipment needed to perform procedures safely and to respond to emergencies.</i>																
4.a.	Engineering / ventilation controls N/A																
4.b.	Personal protective equipment <ul style="list-style-type: none"> • Safety glasses/goggles • Puncture-resistant gloves • Lab coat • N95 mask 																
4.c.	Location of nearest emergency safety equipment																
<table border="1" style="width: 100%; border-collapse: collapse;"> <thead> <tr> <th style="text-align: left; padding: 2px;">Item</th><th style="text-align: left; padding: 2px;">Location</th></tr> </thead> <tbody> <tr> <td style="padding: 2px;">Eyewash/safety shower</td><td style="padding: 2px;">See laboratory map</td></tr> <tr> <td style="padding: 2px;">First aid kit</td><td style="padding: 2px;">Safety box</td></tr> <tr> <td style="padding: 2px;">Chemical spill kit</td><td style="padding: 2px;">Contact lab manager</td></tr> <tr> <td style="padding: 2px;">Fire extinguisher</td><td style="padding: 2px;">See laboratory map</td></tr> <tr> <td style="padding: 2px;">Fire alarm manual pull station</td><td style="padding: 2px;">See laboratory map</td></tr> <tr> <td style="padding: 2px;">Telephone</td><td style="padding: 2px;">(919) 515-3000</td></tr> <tr> <td style="padding: 2px;">Other</td><td style="padding: 2px;"></td></tr> </tbody> </table>		Item	Location	Eyewash/safety shower	See laboratory map	First aid kit	Safety box	Chemical spill kit	Contact lab manager	Fire extinguisher	See laboratory map	Fire alarm manual pull station	See laboratory map	Telephone	(919) 515-3000	Other	
Item	Location																
Eyewash/safety shower	See laboratory map																
First aid kit	Safety box																
Chemical spill kit	Contact lab manager																
Fire extinguisher	See laboratory map																
Fire alarm manual pull station	See laboratory map																
Telephone	(919) 515-3000																
Other																	
5.	Step-by-step methodology <i>The methodology explained below is made for 1L of saturated solution. If required multiply the concentrations below by the desired volume.</i>																
<p>Step 1: Cut PVC to the desired length in this examples the PVC is cut to 50 inches</p> <p>Step 2: Cut rebars to specimen length</p> <p>Step 3: Cut stainless steel mesh with sufficient length and width to fit inside the PVC pipes</p>																	



Step 4: Weld or mechanically attach stainless steel wires to the reinforcing steel bar and the stainless steel mesh



Step 5: Mark dimension of grip areas

Step 6: Place 2-part epoxy on the grip areas of the reinforcing steel bars. Wait for the epoxy to cure (see product manual for curing times)



Step 7: Place electroplater tape in the grip areas



Step 8: Place shrink tube around grip areas. Use the heat gun to shrink the tube closer to the surface of the reinforcing steel bars



Step 9: Place stainless steel mesh inside the PVC pipe

Step 10: Place reinforcing steel bars inside the PVC pipe with the plastic wheel chairs as shown below



Step 11: Prepare the connection to the 90-degree elbow. Using primer and the cement glue the PVC elbows on both sides of the PVC pipes.



Step 12: Start procedure to generate passive layer

6.	Designated area
----	------------------------

Room temperature area.

7.	Special handling procedures, transport, and storage requirements <i>Describe special handling and storage requirements for hazardous chemicals used in this procedure, especially those that are highly reactive/ unstable, flammable toxic and corrosive. Describe secondary containment requirements for transport between laboratory rooms.</i>
8	Waste disposal Identify and list all hazardous waste to be generated and appropriate disposal procedures. Include liquid and solid waste.
9.	Emergency procedures Life-threatening emergencies (for example, medical event, fire, explosion, large-scale spill or release, toxic or flammable gas leak, valve failure) <ul style="list-style-type: none"> • Call 911. Provide dispatch the following information: your name and call back number, location of incident, material released, if known, if there are any injured person and their location. • Pull the nearest fire alarm. • Exit the building using the nearest stairway. • Proceed to designated assembly area. • Provide information to emergency responders as able. Chemical spills <ol style="list-style-type: none"> 1. Determine if it is a “major” or “minor” spill. Minor spills are well contained, able to be cleaned using the spill kit at hand and clean-up would not require special PPE such as a respirator. 2. Assist anyone who may have been contaminated or injured during the spill. 3. Clean up minor spills using appropriate spill control equipment. 4. Call 911, NCSU Police ((919) 515-3000) and EHS ((919) 515-7915) for all major spills. 5. Contain major spill with appropriate absorbent only if trained to do so and your safety is not compromised. 6. Post “DO NOT ENTER” on entrance door and evacuate the area. <p style="text-align: center;">Do not re-enter until Emergency Responders have cleaned up the spill and declare the area safe for reentry.</p> If personnel are exposed to chemicals <ol style="list-style-type: none"> 1. Call 911 to seek emergency medical help. 2. Assist exposed person away from incident or source of exposure, to the emergency shower or eyewash. Do this only if able and personal safety is not compromised. The exposed person decontaminates using the nearest emergency shower or eyewash. <ul style="list-style-type: none"> 2.1. Pull the safety shower lever to start the water flowing (or push the eyewash lever to start the water flowing). 2.2 To wash off chemicals from your eyes, hold your eyes open to get the water under your eyelids. 2.3 Remove all contaminated clothing and shoes to effectively wash chemicals off your body. 2.4 Stay under the water for at least 15 minutes to wash all the chemicals off. 3. Report the incident 4. Seek follow-up medical treatment. Building maintenance emergencies (for example, power outages, plumbing leaks, fume hood malfunction) Call (919) 515-2991 to report a facility emergency.

10.

Training requirements

List the general and laboratory-specific training required for authorized users of this SOP

- EHS Chemical and Lab Safety Training
- EHS Hazardous Waste Training
- CFL Safety Training

Accelerated Corrosion on Reinforcing Steel Bars Procedure: Passive Layer Generation

Procedure title	Accelerated Corrosion on Reinforcing Steel Bars Procedure: Passive Layer Generation	
Author	Victor Alejandro Calderon	
Date of creation/revision	Date Created: 05/06/2021	Date last revised: 05/06/2021
Principal Investigator	Mervyn J Kowalsky	
Location	Building and room number	
1.	This standard operating procedure (SOP) is for	

Specific laboratory procedure or experiment

This document outlines the procedure to perform the generation of the passive layer in reinforcing steel bars. This document assumes that the specimen is already inside the container where the specimens will develop the passive layer. The passive layer is generated by using a saturated pore solution of calcium hydroxide. The solution concentrations were obtained from the study by Ghods et al. [1]

- [1] P. Ghods, O. B. Isgor, G. McRae, and T. Miller, "The effect of concrete pore solution composition on the quality of passive oxide films on black steel reinforcement," *Cem. Concr. Compos.*, 2009.

2. Process or experiment description

The reinforcing steel bars are placed in an airtight container and are submerged in a calcium chloride saturated solution.

The required chemicals are listed below:

- Sodium hydroxide
- Potassium hydroxide
- Calcium sulfate dehydrate
- Calcium hydroxide
- Distilled water

Other equipment:

- Beaker 500 ml
- Glass mixing rod
- Disposable 1 gal bucket or equivalent glass container
- Measuring scale
- Spoon for the handling of chemicals
- Paper sheets for spills
- Funnel

3.	Hazard and risk assessment.																
Chemical hazard: All the chemicals in this procedure are irritants and eye hazard.																	
 Irritant Skin irritation, category 2 Specific target organ toxicity following single exposure, category 3																	
 Corrosive Serious eye damage, category 1																	
Skin Irritation 2 Eye Damage 1 Specific Target Organ Toxicity, Single Exposure (respiratory) 3																	
4.	Safety equipment <i>Specify all equipment needed to perform the procedure safely and to respond to emergencies.</i>																
4.a.	Engineering / ventilation controls N/A																
4.b.	Personal protective equipment <ul style="list-style-type: none"> • Safety glasses/goggles • Nitrile gloves with puncture resistance • Lab coat • N95 mask • Chemical spill kit 																
4.c.	Location of nearest emergency safety equipment																
<table border="1" style="width: 100%; border-collapse: collapse;"> <thead> <tr> <th style="text-align: left; padding: 2px;">Item</th> <th style="text-align: left; padding: 2px;">Location</th> </tr> </thead> <tbody> <tr> <td style="padding: 2px;">Eyewash/safety shower</td> <td style="padding: 2px;">See laboratory floor plan</td> </tr> <tr> <td style="padding: 2px;">First aid kit</td> <td style="padding: 2px;">Safety box</td> </tr> <tr> <td style="padding: 2px;">Chemical spill kit</td> <td style="padding: 2px;">Contact lab manager</td> </tr> <tr> <td style="padding: 2px;">Fire extinguisher</td> <td style="padding: 2px;">See laboratory floor plan</td> </tr> <tr> <td style="padding: 2px;">Fire alarm manual pull station</td> <td style="padding: 2px;">See laboratory floor plan</td> </tr> <tr> <td style="padding: 2px;">Telephone</td> <td style="padding: 2px;">(919) 515-3000</td> </tr> <tr> <td style="padding: 2px;">Other</td> <td style="padding: 2px;"></td> </tr> </tbody> </table>		Item	Location	Eyewash/safety shower	See laboratory floor plan	First aid kit	Safety box	Chemical spill kit	Contact lab manager	Fire extinguisher	See laboratory floor plan	Fire alarm manual pull station	See laboratory floor plan	Telephone	(919) 515-3000	Other	
Item	Location																
Eyewash/safety shower	See laboratory floor plan																
First aid kit	Safety box																
Chemical spill kit	Contact lab manager																
Fire extinguisher	See laboratory floor plan																
Fire alarm manual pull station	See laboratory floor plan																
Telephone	(919) 515-3000																
Other																	
5.	Step-by-step methodology <i>The methodology explained below is made for 1 liter (L) of saturated solution. If required multiply the concentrations below by the desired volume.</i>																
Step 1: Prepare the work area, place shipping paper on counter or table of specimen preparation. Place underneath each specimen containers. Step 2: Turn on scale and ensure the scale is level. In the 1 gal container measure the following masses for each of the components:																	

- Saturated calcium hydroxide ($\text{Ca}(\text{OH})_2$) (approximately 1.8 g)
- 4 g Sodium hydroxide ($\text{Na}(\text{OH})$),
- 11.22 g potassium hydroxide (KOH)
- 13.77 g of calcium sulfate dehydrate ($\text{Ca}(\text{SO}_4)_2 \cdot 2\text{H}_2\text{O}$)
- 1 L distilled water

Step 3: Saturate the water with calcium hydroxide, mixing thoroughly with the glass rod until no lumps are left. Mix in the remaining chemical agents.

Step 4: Using a funnel saturate the rebar specimen with the solution. Repeat the process until the specimen is completely covered with the saturated solution.

Step 5: Close the airtight container. The container must be airtight, failure to do so the calcium hydroxide will carbonate and the passive layer will not be generated. Label the chemical contents of the container. Place a transparent tape on top the label. This must be done per Fire Marshall requirements.

Step 6: Wait for a minimum of 8 days for the passive layer to develop on the surface of the specimen.

Step 7: Open the container and start the unwanted material disposal procedure for the solution.

Step 8: Continue with the accelerated corrosion process.

6.	Designated area
	Room temperature area.
7.	Special handling procedures, transport, and storage requirements <i>Describe special handling and storage requirements for hazardous chemicals used in this procedure, especially those that are highly reactive/ unstable, flammable toxic and corrosive. Describe secondary containment requirements for transport between laboratory rooms.</i>
	The disposal of the solution should be performed as follows. Step 1: In a container such as a bucket, slowly pour the solution in the bucket making sure to not spill the solution. Step 2: Pour the solution in the cement waste designated container. Step 3: Clean any droplets in the working area.
8	Unwanted material disposal Identify and list all hazardous waste to be generated and appropriate disposal procedures. Include liquid and solid waste.
	The procedures outlined by EHS should be followed. The unwanted material generated in this process is the calcium hydroxide solution. A waste accumulation label should be obtained and correctly disposed after the passive layer generation process is performed.
9.	Emergency procedures
	Life-threatening emergencies (for example, medical event, fire, explosion, large-scale spill or release, toxic or flammable gas leak, valve failure) <ul style="list-style-type: none"> • Call 911. Provide dispatch the following information: your name and call back number, location of the incident, material released, if known, if there are any injured persons, and their location. • Pull the nearest fire alarm. • Exit the building using the nearest stairway. • Proceed to the designated assembly area. • Provide information to emergency responders as able.

Chemical spills

1. Determine if it is a "major" or "minor" spill. Minor spills are well contained, able to be cleaned using the spill kit at hand and clean-up would not require special PPE such as a respirator.
2. Assist anyone who may have been contaminated or injured during the spill.
3. Clean up minor spills using appropriate spill control equipment.
4. Call 911, NCSU Police ([\(919\) 515-3000](tel:(919)515-3000)) and EHS ([\(919\) 515-7915](tel:(919)515-7915)) for all major spills.
5. Contain major spill with appropriate absorbent only if trained to do so and your safety is not compromised.
6. Post "DO NOT ENTER" on entrance door and evacuate the area.

Do not re-enter until Emergency Responders have cleaned up the spill and declare the area safe for reentry.

If personnel exposed to chemicals

1. Call 911 to seek emergency medical help.
2. Assist exposed person away from incident or source of exposure, to the emergency shower or eyewash. Do this only if able and personal safety is not compromised. Exposed person decontaminates using the nearest emergency shower or eyewash.
 - 2.1. Pull the safety shower lever to start the water flowing (or push the eyewash lever to start the water flowing).
 - 2.2 To wash off chemicals from your eyes, hold your eyes open to get the water under your eyelids.
 - 2.3 Remove all contaminated clothing and shoes to effectively wash chemicals off your body.
 - 2.4 Stay under the water for at least 15 minutes to wash all the chemicals off.
3. Report incident
4. Seek follow-up medical treatment.

Building maintenance emergencies (for example, power outages, plumbing leaks, fume hood malfunction)

Call [\(919\) 515-2991](tel:(919)515-2991) to report facility emergency.

10.

Training requirements

List the general and laboratory-specific training required for authorized users of this SOP

- EHSA Chemical and Lab Safety Training
 CFL Safety Training
 Laboratory Unwanted Material Management Training

Accelerated Corrosion on Reinforcing Steel Bars

Procedure: Accelerated Corrosion

Procedure title	Accelerated Corrosion on Reinforcing Steel Bars Procedure: Accelerated Corrosion	
Author	Victor Alejandro Calderon	
Date of creation / revision	Date Created: 05/06/2021	Date last revised: 05/06/2021
Principal Investigator	Mervyn J Kowalsky	
Location	Building and room number	
1.	This standard operating procedure (SOP) is for	

Specific laboratory procedure or experiment

This document outlines the procedure to perform the accelerated corrosion process on reinforcing steel bars. This process uses an electrolytic process to accelerate corrosion in reinforcing steel bars. The setup consists in providing an anode (stainless steel), cathode (reinforcing steel bar), and an electrolytic connection Sodium Chloride solution at 0.3M concentration (1.75% NaCl solution), and a current to accelerate the oxidation process. The process uses Faraday's law to calculate the amount of time the current must be sustained to obtain a prescribed level of corrosion.

2. Process or experiment description

The reinforcing steel bars are placed in an airtight container and are submerged in a calcium chloride saturated solution.

The required chemicals are listed below:

- Sodium chloride
- Distilled water

Other equipment:

- Beaker 500 ml
- Glass mixing rod
- Disposable 1 gal bucket or equivalent glass container
- Measuring scale
- Spoon for handling of chemicals
- Paper sheets for spills
- Funnel
- Power supply
- Resistor
- Copper cable
- Terminal block
- Screw driver

3.	Hazard and risk assessment.																
The chemicals used are not considered hazardous. No other source of considerable hazard is known.																	
4.	Safety equipment <i>Specify all equipment needed to perform procedure safely and to respond to emergencies.</i>																
4.a.	Engineering / ventilation controls N/A																
4.b.	Personal protective equipment <ul style="list-style-type: none"> • Safety glasses/goggles • Nitrile gloves with puncture resistance • Lab coat 																
4.c.	Location of nearest emergency safety equipment																
<table border="1" style="width: 100%; border-collapse: collapse;"> <thead> <tr> <th style="text-align: left; padding: 2px;">Item</th> <th style="text-align: left; padding: 2px;">Location</th> </tr> </thead> <tbody> <tr> <td style="padding: 2px;">Eyewash / safety shower</td> <td style="padding: 2px;">See laboratory floor plan</td> </tr> <tr> <td style="padding: 2px;">First aid kit</td> <td style="padding: 2px;">Safety box</td> </tr> <tr> <td style="padding: 2px;">Chemical spill kit</td> <td style="padding: 2px;">Contact lab manager</td> </tr> <tr> <td style="padding: 2px;">Fire extinguisher</td> <td style="padding: 2px;">See laboratory floor plan</td> </tr> <tr> <td style="padding: 2px;">Fire alarm manual pull station</td> <td style="padding: 2px;">See laboratory floor plan</td> </tr> <tr> <td style="padding: 2px;">Telephone</td> <td style="padding: 2px;">(919) 515-3000</td> </tr> <tr> <td style="padding: 2px;">Other</td> <td style="padding: 2px;"></td> </tr> </tbody> </table>		Item	Location	Eyewash / safety shower	See laboratory floor plan	First aid kit	Safety box	Chemical spill kit	Contact lab manager	Fire extinguisher	See laboratory floor plan	Fire alarm manual pull station	See laboratory floor plan	Telephone	(919) 515-3000	Other	
Item	Location																
Eyewash / safety shower	See laboratory floor plan																
First aid kit	Safety box																
Chemical spill kit	Contact lab manager																
Fire extinguisher	See laboratory floor plan																
Fire alarm manual pull station	See laboratory floor plan																
Telephone	(919) 515-3000																
Other																	
5.	Step-by-step methodology <i>The methodology explained below is made for 1 liter (L) of saturated solution. If required multiply the concentrations below by the desired volume.</i>																
<p>Step 1: With the desired density current, calculate the amount of current needed for the test set up. Low-density currents are preferred. With the current and the voltage output the resistor resistance can be calculated:</p> <p>For example for a current density of $470 \frac{\mu A}{cm^2}$, and a current of 150 mA and a 3V output, the resistor is calculated as follows:</p> $J = 470 \frac{\mu A}{cm^2}; i = 150 mA; V = 3 V$ $V = iR$ $R = \frac{V}{i} = \frac{3 V}{0.15 A} = 20 \Omega$ <p>Checking the power in the resistor is at most half of the rated power. In this example the rated power is 1 Watt</p> $P = i^2 R = 0.15^2 * 20 = 0.45 Watts$ <p>Therefore, we have a factor of safety of approximately 2. If the power is less than the rating or close to the rated power, there is a high chance of the resistor burning, thus the current will not be maintained in the circuit.</p>																	

Step 2: Prepare the work area: put packing paper on counter or table of specimen preparation. Place underneath each specimen container.

Step 3: Turn on scale and ensure the scale is level. In the 1 gal container measure 0.3M of NaCl (17.5 g per L of water)

- 17.5 g of sodium chloride (NaCl)
- 1 L distilled water

Step 4: Saturate the assembly with Sodium Chloride solution.

Step 5: Connect the resistor to the terminal block. Connect the rebar wire to the terminal block. The positive current is connected to the resistor wire. The negative pole is connected to the stainless steel mesh wire.



a) Connection of resistor and stainless steel wire in terminal block. Also shown connection to positive pole

b) Connect negative pole to stainless steel mesh wire

Figure 1 Connections for test setup



Figure 2 Final accelerated corrosion setup

Step 6: Turn on the power supply. Set the current and the voltage according to the values used to calculate the desired level of corrosion.

Step 7: Start the current.

Step 8: If necessary, adjust the voltage to maintain the desired current.

Step 9: Wait the amount of time calculated using Faraday's Equation for the desired level of corrosion.

Step 10: Continue with cleaning of the corrosion cleaning procedure

6.	Designated area Room temperature area.
7.	Special handling procedures, transport, and storage requirements <i>Describe special handling and storage requirements for hazardous chemicals used in this procedure, especially those that are highly reactive/ unstable, flammable toxic and corrosive. Describe secondary containment requirements for transport between laboratory rooms.</i>
	The disposal of the solution should be performed as follows. Step 1: In a container such as a bucket, slowly pour the solution in the bucket making sure to not spill the solution. Step 2: Pour the solution in the cement waste designated container. Step 3: Clean any droplets in the working area.
8	Unwanted material disposal Identify and list all hazardous waste to be generated and appropriate disposal procedures. Include liquid and solid waste.
	The procedures outlined by EHS should be followed. The unwanted material generated in this process is the calcium hydroxide solution. A waste accumulation label should be obtained and correctly disposed after the passive layer generation process is performed.
9.	Emergency procedures Life-threatening emergencies (for example, medical event, fire, explosion, large-scale spill or release, toxic or flammable gas leak, valve failure) <ul style="list-style-type: none">• Call 911. Provide dispatch the following information: your name and call back number, location of incident, material released, if known, if there are any injured person and their location.• Pull the nearest fire alarm.• Exit the building using the nearest stairway.• Proceed to designated assembly area.• Provide information to emergency responders as able. Chemical spills <ol style="list-style-type: none">1. Determine if it is a "major" or "minor" spill. Minor spills are well contained, able to be cleaned using the spill kit at hand and clean-up would not require special PPE such as a respirator.2. Assist anyone who may have been contaminated or injured during the spill.3. Clean up minor spills using appropriate spill control equipment.4. Call 911, NCSU Police ((919) 515-3000) and EHS ((919) 515-7915) for all major spills.

5. Contain major spill with appropriate absorbent only if trained to do so and your safety is not compromised.

6. Post "DO NOT ENTER" on entrance door and evacuate the area.

Do not re-enter until Emergency Responders have cleaned up the spill and declare the area safe for reentry.

If personnel exposed to chemicals

1. Call 911 to seek emergency medical help.
2. Assist exposed person away from incident or source of exposure, to the emergency shower or eyewash. Do this only if able and personal safety is not compromised. Exposed person decontaminates using the nearest emergency shower or eyewash.
 - 2.1. Pull the safety shower lever to start the water flowing (or push the eyewash lever to start the water flowing).
 - 2.2 To wash off chemicals from your eyes, hold your eyes open to get the water under your eyelids.
 - 2.3 Remove all contaminated clothing and shoes to effectively wash chemicals off your body.
 - 2.4 Stay under the water for at least 15 minutes to wash all the chemicals off.
3. Report the incident
4. Seek follow-up medical treatment.

Building maintenance emergencies (for example, power outages, plumbing leaks, fume hood malfunction)

Call **(919) 515-2991** to report facility emergency.

10.

Training requirements

List the general and laboratory-specific training required for authorized users of this SOP

- EHSA Chemical and Lab Safety Training
 CFL Safety Training
 Laboratory Unwanted Material Management Training



Accelerated Corrosion on Reinforcing Steel Bars

Procedure: Cleaning Corrosion

Procedure title	Accelerated Corrosion on Reinforcing Steel Bars Procedure: Passive Layer Generation	
Author	Victor Alejandro Calderon	
Date of creation / revision	Date Created: 05/06/2021	Date last revised: 05/06/2021
Principal Investigator	Mervyn J Kowalsky	
Location	Building and room number	
1.	This standard operating procedure (SOP) is for	
<input type="checkbox"/> Specific laboratory procedure or experiment This document outlines the procedure to safely remove the corrosion products in reinforcing steel bars. This procedure uses hydrochloric acid to remove the iron oxides from the surface of the reinforcing steel. Since this procedure uses hydrochloric acid, the user must understand the hazards, and procedure to safely handle this chemical. Under no circumstances should this procedure be performed without the knowledge of your PI, lab manager or any other person in the laboratory. Do not attempt to perform this procedure outside operating hours or without the presences of someone in the laboratory. The reasoning behind this is that there should be someone to assist you in case you need assistance. Please refer to the training section before attempting to perform this procedure.		
2.	Process or experiment description	
The reinforcing steel bars are placed in an airtight container and are submerged in a calcium chloride saturated solution. The required chemicals are listed below: <ul style="list-style-type: none">• Hydrochloric acid• Acetone• Distilled water Other equipment: <ul style="list-style-type: none">• Beaker 500 ml• Steel brush• Clean rags• Plastic tray to catch hydrochloric acid		

3.	Hazard and risk assessment.								
Chemical hazard:									
Hydrochloric Acid									
The hydrochloric acid is a corrosive chemical and must be handled carefully.									
<p>Signal Word: Danger</p> <p>Pictograms(s):</p>									
Hazard Statements									
<table style="width: 100%; border-collapse: collapse;"> <tr> <td style="width: 30%;">H290</td> <td>May be corrosive to metals.</td> </tr> <tr> <td>H314</td> <td>Causes severe skin burns and eye damage.</td> </tr> <tr> <td>H318</td> <td>Causes serious eye damage.</td> </tr> <tr> <td>H335</td> <td>May cause respiratory irritation.</td> </tr> </table>		H290	May be corrosive to metals.	H314	Causes severe skin burns and eye damage.	H318	Causes serious eye damage.	H335	May cause respiratory irritation.
H290	May be corrosive to metals.								
H314	Causes severe skin burns and eye damage.								
H318	Causes serious eye damage.								
H335	May cause respiratory irritation.								
Acetone									
The acetone is a flammable solvent and should be kept away from heat and fire sources.									
<p>Hazard pictograms (GHS US)</p>									
<p>Signal word (GHS US)</p> <p>Hazard statements (GHS US)</p>									
<table style="width: 100%; border-collapse: collapse;"> <tr> <td style="width: 30%;">Signal word (GHS US)</td> <td>: Danger</td> </tr> <tr> <td>Hazard statements (GHS US)</td> <td>: H225 - Highly flammable liquid and vapour H319 - Causes serious eye irritation H336 - May cause drowsiness or dizziness</td> </tr> </table>		Signal word (GHS US)	: Danger	Hazard statements (GHS US)	: H225 - Highly flammable liquid and vapour H319 - Causes serious eye irritation H336 - May cause drowsiness or dizziness				
Signal word (GHS US)	: Danger								
Hazard statements (GHS US)	: H225 - Highly flammable liquid and vapour H319 - Causes serious eye irritation H336 - May cause drowsiness or dizziness								
4.	Safety equipment <i>Specify all equipment needed to perform procedure safely and to respond to emergencies.</i>								
4.a.	Engineering / ventilation controls If available use vapor vent								
4.b.	Personal protective equipment <ul style="list-style-type: none"> • Nitrile gloves with puncture and chemical resistance • Hazmat suit covering the head, skin, clothes. • Googles • Face shield • Boots with steel toes • Respirator • Chemical spill kit 								

4.c.	Location of nearest emergency safety equipment
Item	Location
Eyewash / safety shower	See laboratory floor plan
First aid kit	Safety box
Chemical spill kit	Contact lab manager
Fire extinguisher	See laboratory floor plan
Fire alarm manual pull station	See laboratory floor plan
Telephone	(919) 515-3000
Other	
5.	<p>Step-by-step methodology</p> <p><i>The methodology explained below is made for 1 liter (L) of saturated solution. If required multiply the concentrations below by the desired volume.</i></p> <p>Step 1: Ensure that there is adequate ventilation for the hydrochloric acid. If vapor ventilator is not available, consider performing this procedure outside with enough ventilation room.</p> <p>Step 2: Place the specimen in the tray and pour the hydrochloric acid on the reinforcing steel bar. The acid will immediately react with the iron oxide. Brush off any residue with the steel brush.</p> 
	<p>Figure 1 Apply hydrochloric acid to reinforcing steel bar.</p>



Figure 2 Brush any corrosion product off the reinforcing steel bar

Step 3: Clean the specimen with abundant distilled water.

Step 5: Dry the surface of the specimen with a clean cloth.

Step 6: Apply acetone to the reinforcing steel bar to dry the surface. Repeat steps 5 and 6 as necessary.

Step 7: Store the specimen in an airtight container

6.	Designated area Outside of the lab or in a vapor-vented designated area of the laboratory.
7.	Special handling procedures, transport, and storage requirements <i>Describe special handling and storage requirements for hazardous chemicals used in this procedure, especially those that are highly reactive/ unstable, flammable toxic, and corrosive. Describe secondary containment requirements for transport between laboratory rooms.</i>
The disposal of the solution should be performed as follows. Step 1: Thoroughly clean the tray with water in the cement waste area. If the procedure is performed inside the lab, the unwanted waste material must be stored per EHS regulations and disposed of correspondingly.	
8	Unwanted material disposal Identify and list all hazardous waste to be generated and appropriate disposal procedures. Include liquid and solid waste.
The procedures outlined by EHS should be followed. The unwanted material generated in this process is the calcium hydroxide solution. A waste accumulation label should be obtained and correctly disposed of after the passive layer generation process is performed.	
9.	Emergency procedures Life-threatening emergencies (for example, medical event, fire, explosion, large-scale spill or release, toxic or flammable gas leak, valve failure)

- Call 911. Provide dispatch the following information: your name and call back number, location of incident, material released, if known, if there are any injured person and their location.
- Pull the nearest fire alarm.
- Exit the building using the nearest stairway.
- Proceed to designated assembly area.
- Provide information to emergency responders as able.

Chemical spills

1. Determine if it is a “major” or “minor” spill. Minor spills are well contained, able to be cleaned using the spill kit at hand and clean-up would not require special PPE such as a respirator.
2. Assist anyone who may have been contaminated or injured during the spill.
3. Clean up minor spills using appropriate spill control equipment.
4. Call 911, NCSU Police ([\(919\) 515-3000](#)) and EHS ([\(919\) 515-7915](#)) for all major spills.
5. Contain major spill with appropriate absorbent only if trained to do so and your safety is not compromised.
6. Post “DO NOT ENTER” on entrance door and evacuate the area.

Do not re-enter until Emergency Responders have cleaned up the spill and declare the area safe for reentry.

If personnel exposed to chemicals

1. Call 911 to seek emergency medical help.
2. Assist exposed person away from incident or source of exposure, to the emergency shower or eyewash. Do this only if able and personal safety is not compromised. Exposed person decontaminates using the nearest emergency shower or eyewash.
 - 2.1. Pull the safety shower lever to start the water flowing (or push the eyewash lever to start the water flowing).
 - 2.2 To wash off chemicals from your eyes, hold your eyes open to get the water under your eyelids.
 - 2.3 Remove all contaminated clothing and shoes to effectively wash chemicals off your body.
 - 2.4 Stay under the water for at least 15 minutes to wash all the chemicals off.
3. Report incident
4. Seek follow-up medical treatment.

Building maintenance emergencies (for example, power outages, plumbing leaks, fume hood malfunction)

Call [\(919\) 515-2991](#) to report facility emergency.

10.	Training requirements <i>List the general and laboratory-specific training required for authorized users of this SOP</i>
	<input type="checkbox"/> EHSA Chemical and Lab Safety Training <input type="checkbox"/> CFL Safety Training <input type="checkbox"/> Laboratory Unwanted Material Management Training <input type="checkbox"/> Respirator Training

Appendix B

Code for NLTHA

File - C:\ConditionDependentPBEE\NLTHA_ConditionDependentPBEE\MainshocksParallel_2.0.3\main.py

```
1 # -*- coding: utf-8 -*-
2 """
3 Created on Wed Aug 14 16:32:05 2019
4
5 @author: VACALDER
6 """
7
8 # -----
9 # /      PROGRAM TO CHECK TIME DEPENDENT PROPERTIES EFFECTS
10# /          ON STRUCTURES      /
11# /      version: 2.0.2
12# /      Victor A Calderon
13# /      PhD Student/ Research Assistant
14# /      NC STATE UNIVERSITY
15# /      2021 (c)
16# /
17# /
18# -----
19
20
21# -----
22# /          IMPORTS
23# -----
24
25# import the os module
26import pandas as pd
27import time
28
29start_time = time.time()
30import os
31from LibUnitsMUS import *
32import Build_RC_Column
33import Postprocessor_of_data
34import openseespy.opensees as ops
35
36# -----
37# / VARIABLES THAT CHANGE WITH TIME
```

```

38 # -----
39 #
40 #
41 # *cover = Cover of concrete in cm
42 # *Tcorr = Time to corrosion in yrs
43 # *Time = Different times that are being analyzed
44 # *wcr = Water to cement ratio
45 # *dbi = Initial longitudinal bar diameter
46 # *dti = Initial transverse steel diameter
47
48
49 compressive_strength_concrete = 5 * ksi
50 yield_strength_long_steel = 60 * ksi
51 yield_strength_trans_steel = 60 * ksi
52 iShapeFactor = [4,6,8]
53 iCL = [0,5,10,15,20]
54 iCLt = [0]
55 pid = ops.getPID()
56 np = ops.getNP()
57 GM_Path = r'/home/vacalderon/Documents/MainshocksParallel_2
.0.3/GroundMotion_Mainshock_Records'
58 GMListing = os.listdir(GM_Path)
59 rootdir = r'/home/vacalderon/Documents/MainshocksParallel_2
.0.3'
60 iALR = [0.05, 0.10, 0.15, 0.20] # [0.10] #
61 GMDB = pd.read_csv('mainshock_file_database.csv')
62 GeomDB = pd.read_csv('column_database.csv')
63 counter = 0
64 # -----
65 # /                                BATCH RUN
66 #
67
68 for column, Crow in GeomDB.iterrows():
69     D = float(Crow['column_diameter'])
70     dbi = float(Crow['long_bar_diameter'])
71     nbi = float(Crow['number_of_bars_longitudinal'])
72     dti = float(Crow['trans_bar_diameter'])
73     sti = float(Crow['spacing_trans_steel'])
74     rho_l = float(Crow['rho_l'])
75     rho_v = float(Crow['rho_v'])

```

```

76     for shapefactor in iShapeFactor:
77         Height_of_Column = shapefactor * D
78         for ALR in iALR:
79
80             Ag = 0.25 * math.pi * D ** 2
81             AxialLoad = compressive_strength_concrete * Ag
82             * ALR
83
84             for GM, row in GMDB.iterrows():
85                 i = -1
86                 GM_fn = row['horizontal_1_filename']
87                 GM_dt = row['dt_horizontal1']
88                 GM_npt = row['npt_horizontal1']
89                 print('GM = ', GM_fn)
90                 GM_file = GM_Path + '/' + GM_fn
91                 for CL in iCL:
92                     for CLt in iCLt:
93                         if (counter % np) == pid:
94
95                             datadir = rootdir + "/" + "data" + "/" + GM_fn + "/CL" + str(CL) + "/CLt" + str(CLT)
96                             ) + "/D" + str(D) + "/SF" + str(
97                             shapefactor) + "/ALR" +
98                             str(ALR) + "/RhoL" + str(rhol) + "/Rhov" + str(rhov)
99                             if not os.path.exists(datadir):
100
101                             os.makedirs(datadir)
102
103
104             == 60*ksi:
105                 alpha = 0.0075
106             == 80*ksi:
107                 alpha = 0.0075
108
109             dblc = ((1 - CL*0.01) ** 0.5
110             ) * dbi
111             Build_RC_Column.
112             Build_RC_Column(D, Height_of_Column,
113             compressive_strength_concrete,
114             yield_strength_long_steel, yield_strength_trans_steel,
115
116             yield_strength_long_steel, yield_strength_trans_steel,
117

```

File - C:\ConditionDependentPBEE\NLTHA_ConditionDependentPBEE\MainshocksParallel_2.0.3\main.py

```
107     dbi, dti, CL, dblc, nbi, CLt, sti, datadir, AxialLoad,
108     GM_file, GM_dt, GM_npt, ALR, alpha)
109
110             with open(datadir + "/  

111             Conditions.out", 'w') as f:  

112                 f.write("%s \n" % (CL))  

113                 f.close  

114
115             Postprocessor_of_data.  

116             Postprocessor_of_data(GM_fn, CL, CLt, D, shapefactor, ALR  

117             , rhol, rhov)  

118
119             os.remove(datadir + "/  

120             StressStrain.out")  

121             os.remove(datadir + "/  

122             StressStrain2.out")  

123             os.remove(datadir + "/  

124             StressStrain3.out")  

125             os.remove(datadir + "/  

126             StressStrain4.out")  

127             os.remove(datadir + "/  

128             Conditions.out")  

129             os.remove(datadir + "/DFree.  

130             out")  

131             os.remove(datadir + "/mat.out"  

132             )  

133             os.remove(datadir + "/Period.  

134             out")  

135             os.remove(datadir + "/PGA.out"  

136             )  

137             os.remove(datadir + "/RBase.  

138             out")  

139             counter += 1  

140             print("ALL ANALYSIS COMPLETE")  

141             print("--- %s minutes ---" % ((time.time() - start_time  

142             ) / 60))  

143
```

File - C:\ConditionDependentPBEE\NLTHA_ConditionDependentPBEE\MainshocksParallel_2.0.3\Build_RC_Column.py

```
1 # -*- coding: utf-8 -*-
2 """
3 Created on Thu Sep  5 13:23:30 2019
4
5 @author: VACALDER
6 """
7
8 # PROGRAM TO CODE COLUMN NLTHA RUN IN OPENSEESESPY
9 # Victor A Calderon
10 # PhD Student/ Research Assistant
11 # NC STATE UNIVERSITY
12 # 2021 (c)
13 #
14 #
15 # -----
16 # /           IMPORTS
17 # -----
18
19 import numpy as np
20 from LibUnitsMUS import *
21 import ManderCC
22 import openseespy.opensees as ops
23
24
25 def Build_RC_Column(Diameter, Height_of_Column, fPrimeC, fy
26 , fy_transverse, dbi, dti, CL, dblc, nb, CLt, s_tc, datadir
27 ,
28             AxialLoad, GM_file, GM_dt, GM_npt, ALR
29             , alpha):
30
31     #
32     #
33     #
34     #
35     #
36     #
```

File - C:\ConditionDependentPBEE\NLTHA_ConditionDependentPBEE\MainshocksParallel_2.0.3\Build_RC_Column.py

```
37      #   /   /
38      #   /   /
39      # =2=   _/_  ----->X
40      # =1=   ZeroLength
41
42
43      # /           IMPORTS
44
45      ops.wipe()
46
47
48      #           GENERATE GEOMETRY
49
50
51      ops.model('basic', '-ndm', 2, '-ndf', 3)
52      LCol = Height_of_Column * inch # column length
53      Weight = AxialLoad * kip # superstructure weight
54
55      # define section geometry
56      DCol = Diameter * inch # Column Diameterepth
57
58      # Weight = Weight # nodal dead-Load weight per column
59      Mass = Weight / g
60
61      ACol = 0.25 * np.pi * DCol ** 2 # cross-sectional area
, make stiff
62      IzCol = 0.25 * np.pi * DCol ** 4 # Column moment of
inertia
63
64      ops.node(1, 0.0, 0.0)
65      ops.node(2, 0.0, 0.0)
66      ops.node(3, 0.0, LCol)
67      # Node, Dx, Dy, Rz
68      ops.fix(1, 1, 1, 1)
69      ops.fix(2, 1, 0, 0)
```

```

70
71     ops.mass(3, Mass, 1e-9, 0.0)
72
73     # MATERIAL parameters
74     IDconcC = 1 # material ID tag -- confined cover
    concrete
75     IDconcU = 2 # material ID tag -- unconfined cover
    concrete
76     IDreinf = 3 # material ID tag -- reinforcement
77     IDSP = 4 # material ID tag -- Strain Penetration
78     # Define materials for nonlinear columns
79     # -----
80     # Longitudinal steel properties
81     Fy = fy * ksi * (1 - alpha * CL) # STEEL yield stress
82     Fu = 1.375 * Fy # Steel Ultimate Stress
83     Es = 29000.0 * ksi # modulus of steel
84     Bs = 0.012 # strain-hardening ratio
85     R0 = 20.0 # control the transition from elastic to
    plastic branches
86     cR1 = 0.90 # control the transition from elastic to
    plastic branches
87     cR2 = 0.08 # control the transition from elastic to
    plastic branches
88     a1 = 0.039
89     a2 = 1
90     a3 = 0.029
91     a4 = 1.0
92     c = 2 * inch # Column cover to reinforcing steel NA.
93     numBarsSec = nb # number of uniformly-distributed
    longitudinal-reinforcement bars
94     barAreaSec = 0.25 * np.pi * dblc ** 2 # area of
    longitudinal-reinforcement bars
95     dbl = dblc * inch
96
97     # Transverse Steel Properties
98     fyt = fy_transverse * ksi * (1 - alpha * CLt) # Yield
    Stress of Transverse Steel
99     dbt = dti * inch # Diameter of transverse steel
100    st = s_tc * inch # Spacing of spiral
101    Ast = 0.25 * np.pi * (dbt ** 2) # Area of transverse
    steel
102    Dprime = DCol - 2 * c - dti * 0.5 # Inner core
    diameter

```

File - C:\ConditionDependentPBEE\NLTHA_ConditionDependentPBEE\MainshocksParallel_2.0.3\Build_RC_Column.py

```

103     Rbl = Dprime * 0.5 - dti * 0.5 - dbi * 0.5 # Location
104         of Longitudinal bar
105     # nominal concrete compressive strength
106     fpc = fPrimeC * ksi # CONCRETE Compressive Strength,
107         ksi (+Tension, -Compression)
108     Ec = 57.0 * ksi * np.sqrt(fpc / psi) # Concrete
109         Elastic Modulus
110
111     # unconfined concrete
112     fc1U = -fpc # UNCONFINED concrete stress
113     eps1U = -0.003 # strain at maximum strength of
114         unconfined concrete
115     fc2U = 0.2 * fc1U # ultimate stress
116     eps2U = -0.01 # strain at ultimate stress
117     lambdac = 0.1 # ratio between unloading slope at
118         $eps2 and initial slope $Ec
119
120     mand = ManderCC.ManderCC(fpc, Ast, fyt, Dprime, st)
121
122     fc = mand[0]
123     eps1 = mand[1]
124     fc2 = mand[2]
125     eps2 = mand[3]
126
127     # CONCRETE           tag    f'c      ec0    f'
128         cu        ecu
129
130     # Core concrete (confined)
131     ops.uniaxialMaterial('Concrete01', IDconcC, fc, eps1,
132         fc2, eps2)
133
134     # Cover concrete (unconfined)
135     ops.uniaxialMaterial('Concrete01', IDconcU, fc1U,
136         eps1U, fc2U, eps2U)
137
138     # STEEL
139     # Reinforcing steel
140     params = [R0, cR1, cR2]
141     #           tag    fy   E0      b
142     ops.uniaxialMaterial('Steel02', IDreinf, Fy, Es, Bs,
143         R0, cR1, cR2)
144
145     # STRAIN PENETRATION MATERIAL

```

File - C:\ConditionDependentPBEE\NLTHA_ConditionDependentPBEE\MainshocksParallel_2.0.3\Build_RC_Column.py

```
137     SPalpha = 0.4
138     SPsy = 0.1 * ((dbl * Fy) * (2 * SPalpha + 1) / (4000
139             * ((-fc) ** 0.5))) ** (1 / SPalpha) + 0.013
140     SPsu = 35 * SPsy
141     SPb = 0.45
142     SPR = 1.01
143
144     # uniaxialMaterial StrPen01 Tag fy sy fu su b R
145     ops.uniaxialMaterial('Bond_SP01', IDSP, Fy, SPsy, Fu,
146     SPsu, SPb, SPR)
147
148     # Writing Material data to file
149     with open(datadir + "/mat.out", 'w') as matfile:
150         matfile.write("%s %s %s
151             %s %s %s\n" %
152             Fy, fyt, Ast, st, Dprime, Weight, DCol, LCol,
153             barAreaSec, fc, SPsy, SPsu, SPb, SPR, ALR, dbl))
154     matfile.close
155
156     # -----#
157     #-----#
158     #-----#
159     #-----#
160     #-----#
161     #-----#
162     #-----#
163     #-----#
164     #-----#
165     #-----#
166     #-----#
167     #-----#
168     #-----#
169     #-----#
```

```

170     ro = DCol / 2.0
171     nfCoreR = 8
172     nfCoreT = 8
173     nfCoverR = 2
174     nfCoverT = 8
175     rc = ro - c
176     theta = 360.0 / numBarsSec
177
178     ops.section('Fiber', ColSecTag, '-GJ', 1e+10)
179
180     # Create the concrete fibers
181     ops.patch('circ', 1, nfCoreT, nfCoreR, 0.0, 0.0, ri,
182               rc, 0.0, 360.0) # Define the core patch
183     ops.patch('circ', 2, nfCoverT, nfCoverR, 0.0, 0.0, rc
184               , ro, 0.0, 360.0) # Define Cover Patch
185
186     # Create the reinforcing fibers
187     ops.layer('circ', 3, numBarsSec, barAreaSec, 0.0, 0.0
188               , Rbl, theta, 360.0)
189
190     # Set parameters for ZeroLength Element
191
192     SecTag2 = 2
193     ops.section('Fiber', SecTag2, '-GJ', 1e+10)
194
195     # Create the concrete fibers
196     ops.patch('circ', 1, nfCoreT, nfCoreR, 0.0, 0.0, ri,
197               rc, 0.0, 360.0) # Define the core patch
198     ops.patch('circ', 2, nfCoverT, nfCoverR, 0.0, 0.0, rc
199               , ro, 0.0, 360.0) # Define Cover Patch
200
201     # Creating Elements
202
203     ColTransfTag = 1
204     ops.geomTransf('Linear', ColTransfTag)
205     ops.element('zeroLengthSection', ZL_eleTag, 1, 2,
206                 SecTag2, '-orient', 0., 1., 0., 1., 0., 0.)

```

```

206
207     ColeleTag = 2
208
209     # Defining Fiber Elements as ForceBeamColumn
210     # element('nonlinearBeamColumn', eleTag, 1, 2,
211     numIntgrPts, ColSecTag, ColTransfTag)
211     ColIntTag = 1
212     # beamIntegration('Lobatto',ColIntTag,ColSecTag,
213     numIntgrPts)
213     ops.beamIntegration('HingeRadau', ColIntTag, ColSecTag
214     , Lpt, ColSecTag, 1e-10, ColSecTag)
214     ops.element('forceBeamColumn', ColeleTag, 2, 3,
215     ColTransfTag, ColIntTag, '-mass', 0.0)
215
216     # Setting Recorders
217
218     ops.recorder('Node', '-file', datadir + '/DFree.out',
219     '-time', '-node', 3, '-dof', 1, 2, 3, 'disp')
220     ops.recorder('Node', '-file', datadir + '/RBase.out',
221     '-time', '-node', 2, '-dof', 1, 2, 3, 'reaction')
222     ops.recorder('Element', '-file', datadir + '/StressStrain.out',
223     '-time', '-ele', 2, 'section', '1',
224     'fiber',
225             str(Rbl), '0', '3', 'stressStrain') #
226     Rbl,0, IDreinf
227     ops.recorder('Element', '-file', datadir + '/StressStrain4.out',
228     '-time', '-ele', 2, 'section', '1',
229     'fiber',
230             str(-Rbl), '0', '3', 'stressStrain') #
231     Rbl,0, IDreinf
232     ops.recorder('Element', '-file', datadir + '/StressStrain2.out',
233     '-time', '-ele', 2, 'section', '1',
234     'fiber',
235             str(-Dprime), '0.0', '1', 'stressStrain'
236     ) # Rbl,0, IDreinf
237     ops.recorder('Element', '-file', datadir + '/StressStrain3.out',
238     '-time', '-ele', 2, 'section', '1',
239     'fiber',
240             str(-DCol), '0.0', '2', 'stressStrain')
241
242     # -----
243     -----

```

```

230      # /                               NLTHA RUN
231
232      # -----
233
232      dt = GM_dt
233      npt = GM_npt
234      with open(datadir + "/PGA.out", 'w') as PGAfile:
235          accelerations = open(GM_file)
236          linesacc = accelerations.readlines()
237          acc = [line.split() for line in linesacc]
238          flat_list = []
239          for sublist in acc:
240              for item in sublist:
241                  flat_list.append(item)
242
243
244          ACC = [float(i) for i in flat_list]
245          PGA = max(abs(max(ACC)), abs(min(ACC)))
246          PGAfile.write("%s \n" % (PGA))
247          PGAfile.close
248
249      # defining gravity loads
250      ops.timeSeries('Linear', 1)
251      ops.pattern('Plain', 1, 1)
252      ops.load(3, 0.0, -Weight, 0.0)
253
254      Tol = 1e-3 # convergence tolerance for test
255      NstepGravity = 10
256      DGravity = 1 / NstepGravity
257      ops.integrator('LoadControl', DGravity) # determine
the next time step for an analysis
258      ops.numberer('Plain') # renumber dof's to minimize
band-width (optimization), if you want to
259      ops.system('BandGeneral') # how to store and solve
the system of equations in the analysis
260      ops.constraints('Plain') # how it handles boundary
conditions
261      ops.test('NormDispIncr', Tol, 6) # determine if
convergence has been achieved at the end of an iteration
step
262      ops.algorithm('Newton') # use Newton's solution
algorithm: updates tangent stiffness at every iteration
263      ops.analysis('Static') # define type of analysis

```

```

263 static or transient
264     ops.analyze(NstepGravity) # apply gravity
265
266     ops.loadConst('-time', 0.0) # maintain constant
267     gravity loads and reset time to zero
268
269     GMdirection = 1
270     GMfile = GM_file
271     GMfact = 1.0
272
273     Lambda = ops.eigen('-fullGenLapack', 2) # eigenvalue
274     mode 1
275     Omega = math.pow(Lambda[0], 0.5)
276     T1 = 2 * np.pi / Omega
277
278     with open(datadir + "/Period.out", 'w') as Periodfile:
279         Periodfile.write("%s\n" % (T1))
280     Periodfile.close
281
282     xDamp = 0.04 # 4% damping ratio
283     betaKcomm = 2 * (xDamp / Omega)
284     alphaM = 0.0 # M-pr damping; D = alphaM*M
285     betaKcurr = 0.0 # K-proportional damping;      +
286     beatKcurr*KCurrent
287     betaKinit = 0.0 # initial-stiffness proportional
288     damping      +beatKinit*Kini
289
290     ops.rayleigh(alphaM, betaKcurr, betaKinit, betaKcomm
291 ) # RAYLEIGH damping
292
293     # Uniform EXCITATION: acceleration input
294     IDloadTag = 400 # Load tag
295     Dt = dt # time step for input ground motion
296     GMfatt = GMfact * g # data in input file is in g
297     Units -- ACCELERATION TH
298     maxNumIter = 50
299     ops.timeSeries('Path', 2, '-dt', Dt, '-filePath',
300     GMfile, '-factor', GMfatt)
301     ops.pattern('UniformExcitation', IDloadTag,
302     GMdirection, '-accel', 2)
303
304     ops.wipeAnalysis()

```

```

298     ops.constraints('Transformation')
299     ops.numberer('Plain')
300     ops.system('BandGeneral')
301     ops.test('NormUnbalance', Tol, maxNumIter)
302     ops.algorithm('KrylovNewton')
303
304     NewmarkGamma = 0.5
305     NewmarkBeta = 0.25
306     ops.integrator('Newmark', NewmarkGamma, NewmarkBeta)
307     ops.analysis('Transient')
308     analysis_substeps = 100
309
310     DtAnalysis = dt / analysis_substeps
311     TmaxAnalysis = DtAnalysis * analysis_substeps * npt
312
313     Nsteps = int(TmaxAnalysis / DtAnalysis)
314
315     ok = ops.analyze(Nsteps, DtAnalysis)
316
317     tCurrent = ops.getTime()
318
319     # for gravity analysis, load control is fine, 0.1 is
320     # the load factor increment (http://opensees.berkeley.edu/wiki/index.php/Load\_Control)
321
322     Atest = {1: 'NormDispIncr', 2: 'RelativeEnergyIncr', 4:
323             : 'RelativeNormUnbalance', 5: 'RelativeNormDispIncr',
324             6: 'NormUnbalance'}
325     Algorithm = {1: 'KrylovNewton', 2: 'SecantNewton', 4:
326                 'RaphsonNewton', 5: 'PeriodicNewton', 6: 'BFGS', 7: 'Broyden',
327                             8: 'NewtonLineSearch'}
328
329     for i in Atest:
330
331         for j in Algorithm:
332
333             if ok != 0:
334                 if j < 4:
335                     ops.algorithm(Algorithm[j], '-initial'
336 )
337
338             else:

```

File - C:\ConditionDependentPBEE\NLTHA_ConditionDependentPBEE\MainshocksParallel_2.0.3\Build_RC_Column.py

```
335                 ops.algorithm(Algorithm[j])
336
337                 ops.test(Atest[i], Tol, 1000)
338                 ok = ops.analyze(Nsteps, DtAnalysis)
339                 ops.algorithm('ModifiedNewton')
340                 if ok == 0:
341                     print('Analysis successful: ', Atest[i]
342                         , ' ', Algorithm[j], ' OK = ', ok)
343                     break
344                 else:
345                     continue
346
347             print("GroundMotion Done ", ops.getTime())
348
349         ops.wipe()
350
```

File - C:\ConditionDependentPBEE\NLTHA_ConditionDependentPBEE\MainshocksParallel_2.0.3\Postprocessor_of_data.py

```
1 # -*- coding: utf-8 -*-
2 """
3 Created on Thu Sep  5 13:23:30 2019
4
5 @author: VACALDER
6 """
7
8 # PROGRAM TO ANALYZE DATA FROM BATCH RUN of NLTHA FOR
# TDPBEE
9 # Victor A Calderon
10 # PhD Student/ Research Assistant
11 # NC STATE UNIVERSITY
12 # 2021 (c)
13 #
14 #
15 # -----
16 # /           IMPORTS
17 # -----
18
19 import time
20
21 start_time = time.time()
22 import numpy as np
23 import pandas as pd
24 from LibUnitsMUS import *
25
26
27 # -----
28
29 def Postprocessor_of_data(GM_fn, CL, CLt, D, SF, ALR, rhoL,
, rhoV):
30     # 1. Opening folder to access data
31
32     SpectrumDir = r'/home/vacalderon/Documents/
MainshocksParallel_2.0.3/ResponseSpectrumAnalysis'
33     rootdir = r'/home/vacalderon/Documents/
MainshocksParallel_2.0.3/data'
34
35     Es = 29000
36     earthquake = []
```

```
37     PGA_MS = []
38     covers = []
39     times = []
40     WaterCement_Ratios = []
41     CorrosionLvs_Long = []
42     CorrosionLvs_Trans = []
43     Steel_Strains = []
44     CConc_Strains = []
45     UConc_Strains = []
46     YieldStresses = []
47     YieldStressesTrans = []
48     AreaOfSteels = []
49     spacings = []
50     CoreDiameters = []
51     AxialLoads = []
52     Diameters = []
53     AreaRebars = []
54     BarDiameters = []
55     CompStrength = []
56     LS_ConcCover = []
57     LS_SteelBB = []
58     LS_ConfYield = []
59     FirstPeriods = []
60     EffectivePeriods = []
61     Forces = []
62     Displacements = []
63     SpectralDisplacement_Results = []
64     PGD_Results = []
65     Rho_ls = []
66     Rho_vs = []
67     Heights = []
68     AxialLoadRatios = []
69     SpectralDisplacement_Teff_xi = []
70     LSs = []
71     LSc = []
72     DCs = []
73     DCc = []
74     Us = []
75     Ductilities = []
76     datadir = rootdir + '/' + GM_fn + "/CL" + str(CL) + "/"
77     CLt" + str(CLt) + "/D" + str(D) + "/SF" + str(SF) + "/ALR"
+ str(
    ALR) + "/RhoL" + str(rhol) + "/Rhov" + str(rhov)
```

```

78
79      # 2. Read Conditions
80      groundmotion = GM_fn
81      with open(datadir + "/PGA.out") as pgafile:
82          linespgafile = pgafile.readline()
83          pga = float(linespgafile.split()[0])
84      with open(datadir + "/Conditions.out") as conditions:
85          linesconditions = conditions.readline()
86
87      CLL = float(linesconditions.split()[0])
88
89      # 3. Read Period of the Structure
90      with open(datadir + "/Period.out") as Period_01:
91          lines_Period_01 = Period_01.readline()
92          T1 = float(lines_Period_01.split()[0])
93
94      # 4. Read Material Properties for run
95
96      with open(datadir + "/mat.out") as material_prop:
97          lines_material_prop = material_prop.readline()
98
99      YieldStress_Long = float(lines_material_prop.split()[0]
100     ])
100     YieldStress_Trans = float(lines_material_prop.split()[1])
101     AreaOfSteel = float(lines_material_prop.split()[2])
102     spacing_of_steel = float(lines_material_prop.split()[3]
103     ])
103     CoreDiameter = float(lines_material_prop.split()[4])
104     AxialLoad = float(lines_material_prop.split()[5])
105     Diameter = float(lines_material_prop.split()[6])
106     Height = float(lines_material_prop.split()[7])
107     AreaRebar = float(lines_material_prop.split()[8])
108     CompStrengths = float(lines_material_prop.split()[9])
109     AxialLoadRatio = float(lines_material_prop.split()[14
110     ])
110     dbl = float(lines_material_prop.split()[15])
111     ros = (4 * AreaOfSteel) / (CoreDiameter *
112         spacing_of_steel)
112     Ag = 0.25 * math.pi * Diameter ** 2
113     e_ss = 0.015
114     e_ccc = 0.004
115     e_bb = 0.03 + 700 * ros * YieldStress_Trans / Es - 0.1

```

```

115 * AxialLoad / (CompStrengths * Ag)
116     e_csy = 0.009 - 0.3 * AreaRebar / Ag + 3.9 *
YieldStress_Trans / Es
117
118     e_cbs = 0.14-0.0045*CL
119     e_bb_barclay = np.log(e_cbs/0.001)/(300*ALR+0.7/rhov)
120
121     # 5. Force Displacement Plot
122
123     with open(datadir + "/DFree.out") as d:
124         linesd = d.readlines()
125     with open(datadir + "/RBase.out") as F:
126         linesf = F.readlines()
127
128     x = [line.split()[1] for line in linesd[:-1]]
129     y = [line.split()[1] for line in linesf[:-1]]
130
131     X = [float(i) for i in x]
132     Y = [-float(i) for i in y]
133     maxDisp = max(X)
134     minDisp = min(X)
135     if maxDisp > abs(minDisp):
136         AbsMaxDisp = maxDisp
137     elif maxDisp < abs(minDisp):
138         AbsMaxDisp = minDisp
139     maxDispPoss = X.index(AbsMaxDisp)
140     maxForce_at_maxDisp = Y[maxDispPoss]
141     Keff = abs(maxForce_at_maxDisp) / abs(AbsMaxDisp)
142     meff = AxialLoad * kip / g
143     Teff = (2 * math.pi) * (math.sqrt((meff / Keff)))
144     Lsp = 0.15 * YieldStress_Long * dbl
145     e_steele_yield = YieldStress_Long/Es
146     phi_y = 2.25 * e_steele_yield/Diameter
147     delta_y = phi_y * (Height + Lsp) ** 2 / 3
148     delta_u = AbsMaxDisp
149     mu = abs(delta_u) / delta_y
150
151
152     # 6. Steel Stress Strain Analysis
153     with open(datadir + "/StressStrain.out") as
SteelStressStrain1:
154         linesSteelStressStrain1 = SteelStressStrain1.
readlines()

```

```

155     StlStress1 = [line.split()[1] for line in
156         linesSteelStressStrain1]
157     StlStrain1 = [line.split()[-1] for line in
158         linesSteelStressStrain1]
159     siGM_fnaStl1 = [float(i) for i in StlStress1]
160     epsilonStl1 = [float(i) for i in StlStrain1[:-1]]
161
162     with open(datadir + "/StressStrain4.out") as
163         SteelStressStrain2:
164             linesSteelStressStrain2 = SteelStressStrain2.
165             readlines()
166             StlStress2 = [line.split()[1] for line in
167                 linesSteelStressStrain2]
168             StlStrain2 = [line.split()[-1] for line in
169                 linesSteelStressStrain2]
170             siGM_fnaStl2 = [float(i) for i in StlStress2]
171             epsilonStl2 = [float(i) for i in StlStrain2[:-1]]
172
173     # 7. Confined Concrete Stress Strain Analysis
174     with open(datadir + "/StressStrain2.out") as
175         CConcStressStrain:
176             linesCConcStressStrain = CConcStressStrain.
177             readlines()
178             CConcStress = [line.split()[1] for line in
179                 linesCConcStressStrain]
180             CConcStrain = [line.split()[2] for line in
181                 linesCConcStressStrain]
182             siGM_fnaCConc = [float(i) for i in CConcStress]
183             epsilonCConc = [float(i) for i in CConcStrain[:-1]]
184
185     # 8. UncConfined Concrete Stress Strain Analysis
186     with open(datadir + "/StressStrain3.out") as
187         UnConcStressStrain:
188             linesUnConcStressStrain = UnConcStressStrain.
189             readlines()
190             UnConcStress = [line.split()[1] for line in
191                 linesUnConcStressStrain]
192             UnConcStrain = [line.split()[2] for line in
193                 linesUnConcStressStrain]
194             siGM_fnaUnConc = [float(i) for i in UnConcStress]
195             epsilonUnConc = [float(i) for i in UnConcStrain[:-1]]
196
197     # 9. Writing SD_teff

```

```

184     SpectrumFile = open(SpectrumDir + '/' + groundmotion
185     + '.csv')
186     SpectrumContent = SpectrumFile.readlines()
187     SDC = SpectrumContent[12:109]
188     SDC_cols = ['Period', 'SD', 'PSV', 'PSA']
189     SDC_Data = [line.split(',') for line in SDC[:]]
190     SDC_DF = pd.DataFrame(columns=SDC_cols, data=SDC_Data)
191     PeriodStringList = list(SDC_DF['Period'])
192     SpectralDisplacementStringList = list(SDC_DF['SD'])
193     PGD = float(SpectralDisplacementStringList[-1])
194     T = [float(i) for i in PeriodStringList]
195     SpectralDisplacementList = list(SDC_DF['SD'])
196     SD_Float = [float(i) for i in SpectralDisplacementList
197 ]
198     SD_at_Teff = np.interp(Teff, T, SD_Float)
199
200     if mu > 1:
201         xi_eq = 0.05 + 0.565 * (mu - 1) / (mu * np.pi)
202         DF = np.sqrt((0.07) / (0.05 + xi_eq))
203         SD_Teff_xi_eq = DF * SD_at_Teff
204
205
206
207     #10. Collapse analysis for strains
208     e_steele_max = max(max(max(epsilonSt11), max(
209         epsilonSt12)), abs(min(min(epsilonSt11), min(epsilonSt12
210         ))))
211     e_concrete_max = -min(epsilonCConc)
212     #10.1 Steel Serviciability
213     if e_steele_max < e_ss:
214         steel_serviciability = 0
215     elif e_steele_max > e_ss:
216         steel_serviciability = 1
217     #10.2 Concrete Serviciability
218     if e_concrete_max < e_ccc:
219         concrete_serviciability = 0
220     elif e_concrete_max > e_ccc:
221         concrete_serviciability = 1
222     #10.3 Concrete Damage Control
223     if e_concrete_max < e_csy:
224         concrete_damage = 0

```

```

223     elif e_concrete_max > e_csy:
224         concrete_damage = 1
225     #10.4 Steel Damage Control
226     if e_steele_max < e_bb:
227         steel_damage = 0
228     elif e_steele_max > e_bb:
229         steel_damage = 1
230     #10.5 Steel Ultimate (Barcley)
231     if e_steele_max < e_bb_barclay:
232         steel_ultimate = 0
233     elif e_steele_max > e_bb_barclay:
234         steel_ultimate = 1
235
236 # 11. Writing data to variables
237
238     earthquake.append(groundmotion)
239     PGA_MS.append(pga)
240     CorrosionLvls_Long.append(CL1)
241     CorrosionLvls_Trans.append(CLt)
242     Steel_Strains.append(max(max(max(epsilonStl1), max(
243         epsilonStl2)), abs(min(min(epsilonStl1), min(epsilonStl2
244         )))))
245     CConc_Strains.append(-min(epsilonCConc))
246     UConc_Strains.append(-min(epsilonUnConc))
247     YieldStresses.append(YieldStress_Long)
248     YieldStressesTrans.append(YieldStress_Trans)
249     AreaOfSteels.append(AreaOfSteel)
250     spacings.append(spacing_of_steel)
251     CoreDiameters.append(CoreDiameter)
252     AxialLoads.append(AxialLoad)
253     Diameters.append(Diameter)
254     AreaRebars.append(AreaRebar)
255     BarDiameters.append(db1)
256     CompStrength.append(-CompStrengths)
257     LS_ConcCover.append(e_ccc)
258     LS_ConfYield.append(e_csy)
259     LS_SteelBB.append(e_bb)
260     FirstPeriods.append(T1)
261     EffectivePeriods.append(Teff)
262     Forces.append(maxForce_at_maxDisp)
263     Displacements.append(AbsMaxDisp)
264     SpectralDisplacement_Results.append(SD_at_Teff)
265     PGD_Results.append(PGD)

```

```

264     Rho_ls.append(rhol)
265     Rho_vs.append(rhov)
266     Heights.append(Height)
267     AxialLoadRatios.append(AxialLoadRatio)
268     LSs.append(steel_serviability)
269     LSc.append(concrete_serviability)
270     DCs.append(steel_damage)
271     DCc.append(concrete_damage)
272     Us.append(steel_ultimate)
273     SpectralDisplacement_Teff_xi.append(SD_Teff_xi_eq)
274     Ductilities.append(mu)
275
276     # 10. Preparing dictionary to wirte output database
277
278     dataDict = {'earthquake': earthquake,
279                 'pga_(g)': PGA_MS,
280                 'CorrosionLvl_Long': CorrosionLvs_Long,
281                 'CorrosionLvl_Trans': CorrosionLvs_Trans,
282                 'First_Period_s': FirstPeriods,
283                 'Steel_Strain': Steel_Strains,
284                 'Conf_Conc_Strain': CConc_Strains,
285                 'Unc_Conc_srain': UConc_Strains,
286                 'Fy_ksi': YieldStresses,
287                 'fyt_ksi': YielStressesTrans,
288                 'Ast_in2': AreaOfSteels,
289                 'st_in': spacings,
290                 'Dprime_in': CoreDiameters,
291                 'PCol_kip': AxialLoads,
292                 'DCol_in': Diameters,
293                 'barAreaSec_in2': AreaRebars,
294                 'fc_ksi': CompStrength,
295                 'LimitState_ConcreteCoverCrushing':
296                 LS_ConcCover,
297                 'ConfinementSteelYielding': LS_ConfYield,
298                 'LongitudinalSteelBuckling': LS_SteelBB,
299                 'Effective period, Teff': EffectivePeriods
300                 ,
301                 'Force': Forces,
302                 'MaxDisplacement at MaxForce':
303                 Displacements,
304                 'SD_at_Teff': SpectralDisplacement_Results
305                 ,
306                 'SD_Teff_xi':SpectralDisplacement_Teff_xi,

```

```
303             'rho_l': Rho_ls,
304             'rho_v': Rho_vs,
305             'ALR': AxialLoadRatios,
306             'height_of_col': Heights,
307             'long_bar_diameter': BarDiameters,
308             'ServciabilitySteel': LSs,
309             'ServiciabilityConcrete': LSc,
310             'DamageControlSteel': DCs,
311             'DamageControlConcrete': DCC,
312             'UltimateSteel': Us,
313             'Ductility': Ductilities}
314
315     # 11. Generating data frame to write data to csv file
316
317     DataFrame_Out = pd.DataFrame(dataDict)
318
319     # 12. Writing CSV File
320     DataFrame_Out.to_csv('/home/vacalderon/Documents/
321                         MainshocksParallel_2.0.3/results/PosprocData.csv', mode='a'
322                         ,
323                         header=False)
324
325     # Output to show in console
326     print(
327         '-----')
328     print("POSTPROCESSING COMPLETE")
329     print(
330         '-----')
331     print("--- %s minutes ---" % ((time.time() -
332         start_time) / 60))
333
334
```

Appendix C

Records of Mainshocks used for NLTHA

RSN	Earthquake Name	Earthquake	Rrup	PGA	PGD
		Magnitude			
		(Mw)	(Km)	(g)	(cm)
1004	Northridge-01	6.69	8.48	0.75	17.20
1547	Chi-Chi, Taiwan-01	7.62	33.80	0.15	30.90
1197	Chi-Chi, Taiwan-01	7.62	32.67	0.77	24.00
620	Whittier Narrows-01	5.99	21.73	0.23	1.08
1245	Chi-Chi, Taiwan-01	7.62	70.48	0.05	4.77
695	Whittier Narrows-01	5.99	36.68	0.20	1.11
1209	Chi-Chi, Taiwan-01	7.62	54.93	0.18	12.20
1205	Chi-Chi, Taiwan-01	7.62	51.15	0.50	8.58
598	Whittier Narrows-01	5.99	29.49	0.17	0.39
1500	Chi-Chi, Taiwan-01	7.62	42.05	0.14	34.00
599	Whittier Narrows-01	5.99	22.61	0.11	1.47
1231	Chi-Chi, Taiwan-01	7.62	31.65	0.83	27.40
1530	Chi-Chi, Taiwan-01	7.62	52.43	0.16	50.60
1504	Chi-Chi, Taiwan-01	7.62	28.70	0.43	78.70
1194	Chi-Chi, Taiwan-01	7.62	32.15	0.16	29.50
983	Northridge-01	6.69	13.00	0.76	31.60
1193	Chi-Chi, Taiwan-01	7.62	24.10	0.23	42.30
1195	Chi-Chi, Taiwan-01	7.62	41.99	0.07	27.70
1509	Chi-Chi, Taiwan-01	7.62	19.08	0.49	18.50
982	Northridge-01	6.69	12.97	0.52	33.80
1503	Chi-Chi, Taiwan-01	7.62	26.67	0.69	81.80
1193	Chi-Chi, Taiwan-01	7.62	24.10	0.23	42.30
1492	Chi-Chi, Taiwan-01	7.62	39.58	0.40	221.00
1505	Chi-Chi, Taiwan-01	7.62	47.86	0.47	366.00
1517	Chi-Chi, Taiwan-01	7.62	8.91	0.74	28.30
1529	Chi-Chi, Taiwan-01	7.62	45.56	0.27	75.30
1605	Duzce, Turkey-01	7.14	1.61	0.43	48.70
545	Chalfant Valley-01	5.77	17.22	0.07	2.65
368	Coalinga-01	6.36	9.98	0.52	15.80
289	Irpinia, Italy-01	6.90	15.04	0.14	4.96
231	Mammoth Lakes-01	6.06	12.65	0.37	5.57
214	Livermore-01	5.80	17.13	0.12	4.27
95	Managua, Nicaragua-01	6.24	5.68	0.35	6.10
698	Whittier Narrows-01	5.99	45.44	0.06	0.71
699	Whittier Narrows-01	5.99	43.47	0.05	0.51
700	Whittier Narrows-01	5.99	43.52	0.59	1.86
705	Whittier Narrows-01	5.99	12.00	0.15	2.31
718	Superstition Hills-01	6.22	24.79	0.13	5.02
942	Northridge-01	6.69	40.15	0.09	1.80
948	Northridge-01	6.69	48.42	0.11	1.73

RSN	Earthquake Name	Earthquake Magnitude	Rrup	PGA	PGD
		(Mw)	(Km)	(g)	(cm)
949	Northridge-01	6.69	11.10	0.33	9.50
950	Northridge-01	6.69	54.68	0.13	1.36
951	Northridge-01	6.69	45.26	0.08	1.89
954	Northridge-01	6.69	31.55	0.21	1.36
956	Northridge-01	6.69	63.53	0.12	2.52
962	Northridge-01	6.69	50.30	0.09	2.19
963	Northridge-01	6.69	40.68	0.51	13.60
964	Northridge-01	6.69	47.47	0.10	2.69
966	Northridge-01	6.69	60.30	0.09	1.41
967	Northridge-01	6.69	49.88	0.15	1.56
968	Northridge-01	6.69	47.48	0.22	2.11
970	Northridge-01	6.69	50.83	0.15	3.61
974	Northridge-01	6.69	29.72	0.26	1.00